A Multiple Sensor System For Quality Inspection of Onions and Investigation of Onion Optical Properties

by

Weilin Wang

(Under the Direction of Changying Li)

Abstract

Onion is one of the three most important U.S. fresh vegetables in terms of the production value. Postharvest quality inspection and grading is essential for ensuring the quality of onions and reducing the production losses in the postharvest handling. This dissertation work focused on designing and developing a novel multimodal system to enhance postharvest quality inspection of onions in packinghouses, and addressing major needs and challenges facing the development of the system.

In this study, the optical properties (light absorption and scattering coefficients) of onion tissues were studied to guide the selection of sensing techniques. The optical properties of dry skin, wet skin, flesh of red, Vidalia sweet, white, and yellow onions were measured at the wavelength 633 nm. The optical properties of dry skin and flesh of healthy onions, onions with sour skin, and onions with neck rot were also investigated in the spectral regions of 550-880 nm and 950-1650 nm. The results of these studies provide in-depth understanding of the optical properties of onion tissues and the light propagation in onion bulbs.

A novel multisensor system was designed and implemented for quality inspection and grading of onions, which integrated color, RGB-depth, hyperspectral, and X-ray imaging

technologies. A LabVIEW program was developed to control and synchronize the hardware devices to acquire the data. Based on the spatial, spectral, and radiographic images acquired by the system, image processing and machine learning algorithms were developed to measure quality factors of onions collectively and nondestructively. The results of the validation tests showed that the multisensor system is capable of nondestructively evaluating key onion quality factors (size, weight, volume, density, and defect) accurately and effectively. The proposed system and methods can potentially be extended for quality inspection of other agricultural products.

INDEX WORDS: Imaging, Hyperspectral Imaging, X-ray, 3-D, Spectroscopy, Data Fusion, Depth Imaging, Sensor Fusion, Optical Properties, Scattering, Food Quality, Food Safety, Fruits and Vegetables, Onion, Automation, Classification, Postharvest.

A Multiple Sensor System For Quality Inspection of Onions and Investigation of Onion Optical Properties

BY

Weilin Wang

B.S., China Agricultural University, 2002

M.S., University of Georgia, 2010

A Dissertation Submitted to the Graduate Faculty of The University of Georgia in Partial Fulfillment of the Requirements for the Degree

Doctor of Philosophy

Athens, Georgia

2013

A MULTIPLE SENSOR SYSTEM FOR QUALITY INSPECTION OF ONIONS AND INVESTIGATION OF ONION OPTICAL PROPERTIES

BY

WEILIN WANG

Major Professor:	Changying Li
Committee:	Ernest W. Tollner Glen C. Rains Mark Haidekker Ronald D. Gitaitis

Electronic Version Approved:

Maureen Grasso
Dean of the Graduate School
The University of Georgia
December 2013

DEDICATION

To my wife and my daughter.

ACKNOWLEDGEMENTS

I would like to sincerely thank my major advisor Dr. Changying Li for his support, guidance, encouragement, and trust. Without his immeasurable effort, this work and any of my accomplishments in my graduate study would not have been possible. I would also like to extend my appreciation to Dr. Li's family for the kindness they expressed to me and my family in the past five years. I was very fortunate to work together with a knowledgeable, productive, and considerate supervisor.

My profound appreciation goes to members of my advisory committee: Professor Ernest William Tollner, Professor Ronald D. Gitaitis, Professor Glen C. Rains, and Professor Mark Haidekker for their friendly and helpful guidance and support. Moreover, I would like to express my deep gratefulness to many of my friends and lab colleagues such as Dr. Qi Wang, Dr. Herbert Ssegane, Tharun Konduru, and Dr. Adnan Mustafic. Their friendship and encouragement helped me to keep a positive mind during the long course of this work. Particularly, I would like to thank people at the University of Georgia Tifton campus, such as Mr. Duncan Mcclusky, Dr. Xinzhi Ni, and Dr. Georgia Vellidis, for their kindness and hospitality. I would also like to appreciate those who were directly involved in this study: Mr. Anthony Mason Dean, Mr. Paul Glatz, Ms. Delmaries Gonzalez, and Ms. Amber Leigh Stewart for their useful assist in these experiments.

My sincerely gratitude also goes to my family who gave me unwavering support for years. I am deeply indebted to their unconditional love and care.

TABLE OF CONTENTS

Page

LIST OF TABLES

Page

LIST OF FIGURES

Page

CHAPTER 1

INTRODUCTION

1.1 BACKGROUND

In recent years, electronic and computer vision technologies have been increasingly adopted in agriculture to develop robotic systems for various applications. Automation of the harvesting and handling of fresh market fruits and vegetables is of a high priority for agricultural engineers/researchers since this type of task is generally labor intensive, time consuming, and demanding on processing speed and efficiency. Intensive research efforts have been devoted to developing automated and nondestructive harvesting, processing, sorting and grading systems to increase the efficiency and productivity of harvesting and post-harvesting operations of fresh fruits and vegetables (Blasco et al., 2003; Kondo, 2010).

The key reason for the fresh fruit and vegetable industry to adapt latest technologies is the rising awareness and increasing expectations of customers for quality products, in addition to potential higher economic returns. With the ever growing public interest of having clean and high quality food, the safety and quality standards for fresh fruits and vegetables have been increased globally. To provide quality-guaranteed products to customers, producers need to employ effective and consistent methods to monitor and control the quality of their products. However, technologies employed by the current harvesting and post-harvesting systems for fruits and vegetables cannot meet the

increased demand of quality control. Therefore, continuous research efforts are needed to make technological innovations and improvements to enhance the quality control of fruits and vegetables by incorporating advanced machine vision and sensing techniques.

1.2 Statement of the Problem

Onion (*Allium cepa* L.) is one of the three largest fresh vegetables grown in the United States in terms of the production value (U.S. Department of Agriculture, 2013). As an ancient plant, onions have been cultivated throughout the world since at least 3,000 B.C. and are widely used as one of the main food ingredients by human beings. Nowadays, it is well known that characteristic chemical constituents in onions like flavonoids and the alk(en)yl cysteine sulphoxides have biological and pharmacological effects beneficial to consumers, such as antifungal, antibacterial, antitumor, and anti-inflammatory (Corzo-Martinez et al., 2007). Partly due to the consumer's increased awareness of healthy benefits of onions, the U.S. onion production and consumption has significantly increased in the past decade, resulting in an annual farm gate value of more than one billion dollars (U.S. Department of Agriculture, 2011, 2013).

Similar to other fresh fruits and vegetables, onions are susceptible to postharvest diseases, such as neck rot (*Botrytis allii/Botrytis aclada*) and sour skin (*Burkholderia cepacia)* (Schwartz and Mohan, 2008a). In the U.S. onion industry, postharvest diseases cause very significant losses in both field production and storage. With multilayered heterogeneous dry skins, diseased onions can easily bypass human inspectors and go into onion packages or storage rooms. The existence of onions with diseases can affect other disease-free onions, resulting in subsequent storage loss. For instance, neck rot by itself has reportedly caused storage losses of 20-30% in Colorado, 50% in Idaho, and 60% in

Europe (Schwartz, 2011). Besides economic losses and reduced profit, the occurrence of diseased onions can also affect the health of consumers and thus damage the reputation of onion brand owners. Therefore, ensuring the product quality is one of the most essential and challenging tasks in the postharvest handling of onions.

The U.S. onion industry has learned to utilize cold and controlled atmosphere (CA) rooms to reduce the rate of decay and spread of onion diseases in storage. Another effective disease control approach is to identify diseased and defective onions and divert them from being stored. This approach can decrease the initial quantity of pathogen in the storage room and thus reduce the overall storage loss. In practice, some large U.S. onion packers often use a semi-automated approach to control the quality of onions in the postharvest handling by: applying automated sorting systems using grayscale or color imaging techniques to grade onions based on size, and employing human visual inspection (HVI) to discover and remove diseased and defective onions from sorting lines. This approach, however, is not sufficient enough for onion quality inspection since current grading systems using grayscale/color imaging techniques and HVI mainly evaluate the surface conditions of onions. Mature onion bulbs usually have about 8-10 layers of fleshy scales and several layers of dry skin. Since most onion diseases start at the inner layers, the multilayered structure of onion scales and the presence of outer dry skins makes the quality inspection of onions very difficult. In addition, HVI not only requires a lot of seasonal labor but is also prone to human subjectivity and inconsistency.

To achieve effective and consistent quality inspection of onions, more advanced nondestructive inspection techniques are highly desired to automatically evaluate onion quality on the onion packing line. Since onion disease infections can occur at both outer

and internal scales, an ideal inspection system should be able to check both internal and external diseases and defects of onions.

1.3 OBJECTIVES

The main purpose of the dissertation research was to design and implement a multimodal machine vision system to nondestructively evaluate both external and internal quality of onions. The prototype system was expected to have a quality inspection capability superior to those classification and grading systems currently used in the U.S. onion industry. The research projects were targeted at evaluating and addressing theoretical and technical needs for developing such a system.

To achieve a comprehensive assessment of onion quality, a multiple sensor system was desirable since onions have various key quality factors in different aspects, which are difficult to be accurately evaluated by applying a single sensing technique. By taking into account the key demands of an online classification system for onions (such as the sensing capability, speed, and cost), multiple nondestructive imaging and sensing technologies should be selected and integrated appropriately.

An in-depth understanding of the fundamental physical and chemical properties of onions was also needed for the development of the system. Particularly, the effectiveness of many sensing techniques such as imaging and spectroscopic methods is highly associated with the optical properties of the test object. To apply these techniques appropriately for onion quality inspection, it is essential to understand the key optical properties of onion tissues, such as the light absorption coefficient and light scattering coefficient. Nevertheless, the optical properties of onion tissues were seldom studied and

reported before this study. Thus, another important task of this work was to investigate the key optical properties of onion tissues.

In summary, the dissertation work addresses the following main issues:

1. Studying the fundamental optical properties of biological tissues of onions to understand the light-onion interaction and provide theoretical support for the selection of sensing techniques.

2. Designing and implementing a hardware platform to integrate multiple imaging and sensing techniques selected for onion quality inspection, and developing a software program with graphic user interface to integrate the hardware devices for data acquisition.

3. Using the selected imaging/sensing techniques and the developed system, to develop image processing algorithms to measure the key quality parameters of onions, and distinguish defective onions from healthy ones for onion postharvest quality inspection and grading.

1.4 Overview of the Dissertation Chapters

In this dissertation, Chapter 1 states the background and purpose of this study, defines the objectives of the research projects, and provides an overview of the subsequent chapters. Chapter 2 reviews fundamental properties of onions and provides a synthesis of basic principles of machine vision and sensing technologies for quality inspection of agricultural products, particularly for fresh fruits and vegetables.

Chapter 3 studies the fundamental optical properties (the light absorption coefficient, scattering coefficient, scattering anisotropy, and refractive index) of onion dry skins and flesh for four common types of onions (red, yellow, sweet, and white) at 633 nm. Chapter

4 reports a study that investigated the optical properties of the dry skin and flesh of healthy, sour skin-infected, and neck rot-infected onions in the spectral region of 550-1650 nm.

Chapter 5 demonstrates the use of a low-cost RGB-depth sensor to measure the physical characteristics of onions, including the maximum diameter, volume, and density. Chapter 6 introduces the design and implementation of a multimodal sensing system for onion quality inspection, integrating hyperspectral, X-ray, color, and depth imaging techniques. The sensing capability of the proposed system was demonstrated by a validation test in which key quality parameters of onions were accurately measured and defective onions were effectively distinguished from healthy onions.

Chapter 7 summarizes the key findings and contributions of this work. The chapter also discusses the limitations of this work and proposes research topics for further study.

CHAPTER 2

LITERATURE REVIEW

2.1 PROPERTIES AND QUALITY PARAMETERS OF ONIONS

Nowadays, the usage of mature onions (*Allium cepa* L.) is very versatile. Fresh onions are food and medicinal materials commonly accepted by almost all traditions and cultures worldwide (Griffiths et al., 2002). Onions are dehydrated to make onion powders and other health products. Onion dry skin, traditionally used to make natural food color additives (Block, 2010), has been found to be a good source for making food by-products, such as flavonoids (Ko et al., 2011). Depending on the cultivar and growing conditions of onions, the chemical and physical properties of onions such as shape, color, dry matter content, and pungency can be greatly different.

In general, the main chemical content of fresh onion is water (89-95%). The major fraction (60-80%) of the non-water part (onion dry matter) consists of non-structural and soluble carbohydrates, including glucose, fructose, sucrose, and fructans (Brewster, 2008). The rest of the onion dry matter is comprised of protein, minerals, dietary fiber, vitamins, etc. Although fresh onion is a good source of certain vitamins and minerals, the most beneficial nutritional part of an onion is the non-structural and soluble carbohydrates which have characteristic biological and medical functions for human health (Corzo-Martinez et al., 2007). The content of dry matter and nonstructural carbohydrates of onions can vary among different cultivars. For instance, the dry matter content of onions grown for dehydration can be 20% and higher, while some types of sweet onions may only be about 7% (Brewster, 2008). Onion dry matter content is usually

measured by directly drying them in an oven, or indirectly by using a refractometer to determine soluble solids content (SSC) in onion juice since these two parameters are correlated. Near-infrared spectroscopy method can also be used to predict dry matter content of onions nondestructively (Birth et al., 1985).

The outer dry skins of onions have very different physical and chemical properties from onion flesh. Essentially, onion dry skins are dried onion flesh scales comprised of dead onion cells. During the process of dehydration, the physical and chemical properties of the scale change gradually and the concentration of the pigment increases, resulting in a significant change of color. Pigments of onions include mainly two groups of flavonoids: flavonols (brown/yellow color) and anthocyanins (red/purple color) (Brandwein, 1965; Griffiths et al., 2002).

Depending on the daylight length need to develop bulbs, U.S. onion cultivars can be classified as short-day or long-day onions (Brewster, 2008). Onions begin to form a bulb when the temperature and the day length reach certain levels. Short-day onions develop bulbs in days of no more than 14 hours of daylight, while long-day onions begin to form a bulb when the day length is 14-16 hours. In the U.S., northern onion growers plant long-day onions while southern growers often plant short-day onions. Based on the level of pungency, onion cultivars can be as grouped as pungent onions or sweet onions. The onion growers in the southern U.S. produce large amounts of sweet onions, such as Vidalia sweet onions. The mildness of sweet onions is attributable to their low sulfur content, high sugar content, and high water content compared to pungent onion varieties.

In the postharvest handling, detailed requirements were documented to assure the safety and quality of fresh onions supplied to the consumer. According to the United States standards for grades of onions (U.S. Department of Agriculture, 1995), onions sold in fresh market have to

meet certain minimum requirements such as: (a) be larger than 1.5 inches; (b) have the same general color category; (c) be mature and no soft or spongy; (d) free from decay and wet sunscald; (e) free from serious damage or defects. To reach the U.S. No. 1 onion grade, onions have to fulfill many additional requirements, such as being dorminant, fairly firm, well shaped, and being free from defects and damages caused by diseases. To meet these requirements, a number of key quality factors of onions, such as size, shape, color, disease, defect, consistency, and firmness, have to be examined in sorting and grading.

2.2 Basic Concepts of Optical Properties of Biological Tissues

Optical imaging is a widely accepted nondestructive quality inspection method in the food industry since light photons provide nonionizing and safe radiation. Light has particle and wave properties and the energy of a light particle (a photon) is the combination of these two properties, which is defined as:

$$E_t = \frac{hc}{\lambda} \tag{2.1}$$

in which E_t represents the energy, h is Planck's constant, c is the velocity of light in a vacuum, and λ refers to the wavelength of the light.

When a light beam interacts with a biological tissue of a fruit or vegetable (Figure 2.1), basic propagation for light photons include reflection, scattering, absorption, and transmission.

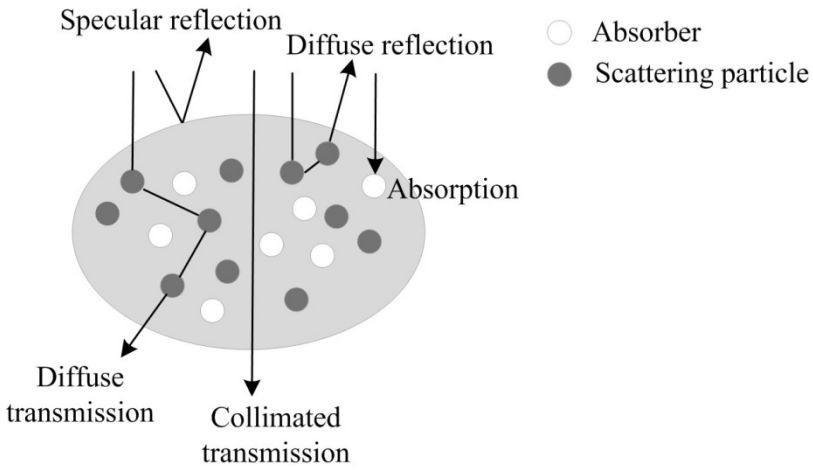

Figure 2.1. Illustration of light interactions with a fruit or vegetable.

Specular reflection is the case where the photon is directly reflected back when it hits the surface (the optical boundary between two media) of the object. The direction of the reflection is defined by Snell's Law:

$$(\sin\theta_i)n_1 = (\sin\theta_r)n_2 \tag{2.2}$$

in which θ_i is the angle of incidence ray, θ_r is the angle of reflection, n_1 and n_2 is the refractive index of medium 1 and medium 2. The refractive index n is a dimensionless number describing how light propagates in media, defined as the ratio of the light velocity in vacuum (c) to the light velocity in the sample (v):

$$n = \frac{c}{v} \tag{2.3}$$

When photons enter the object, they could be absorbed (absorption) or scattered (scattering) by the particles in the material. In absorption, photons lose their kinetic energy in the tissue due to the electrical transition and the vibrational overtones of molecules, a process called energy coupling. The energy coupling is selective: the molecule only absorbs light with a energy level

corresponding to the difference between two vibrational states of itself. The ability of a molecule to absorb a photon of a particular energy level is defined as absorption cross section (N_a).

The light absorption capability of a medium is described by the absorption coefficient μ_a, defined as:

$$\mu_a = N_a \sigma_a \tag{2.4}$$

in which σ_a indicates the geometric absorption cross-sectional area of the medium.

In scattering, the light radiation (photons) entering a particle is diffracted by the electron cloud of the molecules, and reflected from internal surface of the particles, or partially absorbed while it transverses the particles. The ability of a single scatter causing scattering of a photon is defined as the scattering cross section (N_s). The light scattering coefficient of the medium is defined as:

$$\mu_s = N_s \sigma_s \tag{2.5}$$

in which σ_s indicates the geometric scattering cross-sectional area of the medium. The reciprocal of μ_s is also called the scattering mean free path.

After the propagation in the object, light moving through the object is called transmittance. For an absorbing-only medium, the energy of the transmittance light (I) has a relationship to the original incident light (I_0) and the thickness of the medium (x), described by the Beer-Lambert law:

$$I(x) = I_0 \exp(-\mu_a x) \tag{2.6}$$

The propagation of a constant continuous light wave in a biological tissue can be mathematically described by the steady-state radiative transfer equation (RTE) (Tuchin, 2007b):

$$\frac{\partial \mathrm{I}(\mathrm{r},\hat{\mathrm{s}})}{\partial \mathrm{s}} = -(\mu_{\mathrm{a}} + \mu_{\mathrm{s}})\mathrm{I}(\mathrm{r},\hat{\mathrm{s}}) + \frac{\mu_{\mathrm{s}}}{4\pi}\int_{4\pi} \mathrm{f}(\mathrm{s},\hat{\mathrm{s}})\mathrm{I}(\mathrm{r},\hat{\mathrm{s}})\mathrm{d}\omega \tag{2.7}$$

The RTE model describes the change of the radiance $I(r, \hat{s})$ at the point r along the direction $\hat{s}$ in the tissue. In this model, the optical characteristics of the tissue are described using three parameters: the absorption coefficient μ_a, the scattering coefficient μ_s, and the scattering phase function $f(s,\hat{s})$.

The μ_a describes the probability that photons lose their kinetic energy in the tissue due to the electrical transition and the vibrational molecular overtones of molecules. The μ_s represents the probability that photons encounter the mismatches of the refractive indices at microscopic boundaries.

The scattering phase function $f(s,\hat{s})$ is often expressed as a function of the cosine of the scattering angle ($f(\cos\theta)$). The mean cosine of the scattering angle is defined as the scattering anisotropy factor g and a positive/negative g refers to a forward/backward light scattering, respectively. Two scattering parameters μ_s and g, in practice, are often combined into one parameter called the reduced scattering coefficient, defined as:

$$\mu_s' = \mu_s \times (1 - g) \tag{2.8}$$

It is well-known that μ_a is associated with the chemical constituents of the product and μ_s is related to the physical characteristics of cell structure, such as tissue density and firmness (Lu, 2008). In conventional optical methods applied to fruits and vegetables, such as visible and near-infrared (NIR) spectroscopy or spectral imaging, the light absorption and scattering effects are often considered together by correlating the quality factors of the product to its light reflectance or transmittance spectral data. To more accurately correlate the light-tissue interactions with the specific physical or chemical attribute of the product, it's necessary to evaluate the light absorption and scattering properties of the product separately.

Various methods have been reported for measuring the optical properties of biological tissues (Tuchin, 2007a; Wang and Wu, 2007). These methods can be classified into "*ex vivo*" and "*in vivo*" categories in terms of the way of the sample preparation (Kim and Wilson, 2011). The *ex vivo* method, which requires samples in certain shapes and sizes, is often based on the transmittance and reflectance measurements. Then, the optical properties of the measured tissue can be estimated by using computational methods such as the adding-doubling (Prahl et al., 1993a) or Monte Carlo (Wang et al., 1995) in their inverse forms. The *in vivo* method is often based on the approximations of the radiative transport theory by using the diffuse reflectance or backscattering measurements directly made on the sample in the spatial, temporal, or frequency domains (Kim and Wilson, 2011).

The μ_a and the μ_s of some fruits and vegetables have been studied and reported in the past decade. Cubeddu et al. (2001) applied the time-resolved reflectance spectroscopy to monitor the μ_a and μ_s of apples. Fraser et al. (2003) presented a NIR laser-based system to measure the absorption and scattering parameters of the skin and flesh of mandarins. Saeys et al. (2008) measured the μ_a and μ_s of the apple skin and flesh from 350 to 2200 nm using the inverse adding doubling method (Prahl et al., 1993b). Qin and Lu (2007, 2008) presented a spatially resolved technique applying the hyperspectral diffuse reflectance to estimate the absorption and scattering characteristics of milk, fruit juices, and a number of fruits and vegetables. Similar spatially resolved approaches were applied to study the scattering characteristics of normal and bruised apples (Lu et al., 2010) and pickling cucumbers (Lu et al., 2011). Generally, the *ex vivo* method is used to obtain knowledge of the optical properties of a food product, while the *in vivo* method is more suitable to be used for online inspection of food quality.

2.3 Nondestructive Imaging/Sensing Techniques for Quality Inspection of Fruits and Vegetables

Optical sensing methods including spectroscopy and imaging techniques have been proven to be successful for online measurements of agro-food products (Brosnan and Sun, 2004; Zude, 2008). These techniques are appealing for nondestructive quality and safety inspection of agricultural products since they are fast, low cost, and flexible for sample preparation.

Spectroscopy, particularly near-infrared (NIR) spectroscopy, has been accepted as a standard nondestructive analytical instrument for testing the chemical properties of agricultural products (Wang and Paliwal, 2007; Williams and Norris, 2001). The fundamental principle of spectroscopy is that chemical bonds between atoms in a molecule vibrate in a simple harmonic motion. When the frequency of the radiation of the light matches the vibrating molecule, energy of the radiation at that frequency (wavelength) will be transferred to (absorbed by) the molecule. By examining the absorption, reflection, and emission of energy over the test frequencies, a plot of energy versus wavelength can be obtained, called a spectrum. The spectrum can be used to quantitatively characterize the chemical and physical properties of the test object after chemometric analysis (Figure 2.2).

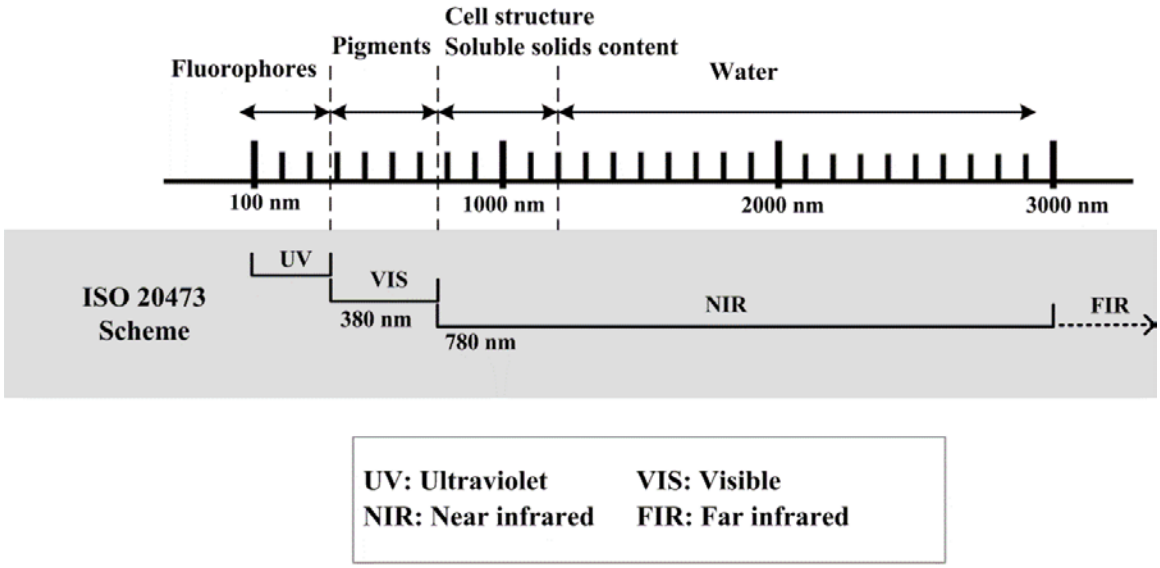

Figure 2.2. Common spectral range for spectroscopic measurements of fruits and vegetables.

Machine vision techniques such as monochrome/color imaging capture the spatial light pattern of a two-dimensional scene. The light radiation reflected, emitted, or transmitted from the test scene is converted into electrical signal by area array or linear array sensors such as a charge-coupled device (CCD). The electrical signals are digitalized to numerical values and saved as an image following its spatial distribution. Monochrome/color imaging technologies have been widely used to recognize the size, color, shape, and texture information of agro-food products (Abbott, 1999; Brosnan and Sun, 2004; Moreda et al., 2009). The advances in this branch were mainly achieved in imaging processing methods and algorithms, especially with the use of novel pattern recognition and machine learning techniques.

In recent years, a new trend for nondestructive quality and safety inspection of agro-food products is the hyperspectral imaging (Gowen et al., 2007). Spectral imaging (including

hyperspectral and multispectral imaging) combines the advantages of traditional spectroscopy and imaging to acquire spatial and spectral information of the test object simultaneously. A hyperspectral image can be interpreted as a three dimensional image cube including successive spatially-aligned images taken at a number of wavelengths. For each spatial pixel in a hyperspectral image, there is a corresponding spectrum at the spectral axis. The integrated spectral-spatial data collected by spectral imaging provide a strong sensing capability to examine the spatial distribution of certain chemical compositions in agricultural products (Lu, 2008). Depending on the mode of scanning, hyperspectral and multispectral imaging can be grouped as two categories: line scan and area scan (Qin et al., 2013). Line scan mode is mainly applied in hyperspectral imaging systems, which uses an imaging spectrograph to disperse broadband light at a line into an area where different wavelengths are spatially distributed at many parallels lines. Area scan mode is used by both hyperspectral imaging and multispectral imaging. Area scan hyperspectral imaging mainly uses electronically tunable filters to select specific narrowband wavelengths, while area scan multispectral imaging often uses a beam splitting device to divide the light (scene) into different parts, and redirect each part of light to a narrowband pass filter to get monochromic images at selected wavelengths.

As an optical method with strong nondestructive sensing capability, spectral imaging is favored by researchers and engineers in food inspection. In the past five years, the number of reported applications of using spectral imaging for quality inspection of fruits and vegetables has increased rapidly (Gowen et al., 2007; Sun, 2010). Wang et al. (2011) used hyperspectral reflectance imaging (400-720 nm) to detect external insect infestation in jujube fruit. Wang et al. (2012a) applied LCTF-based NIR hyperspectral reflectance imaging (950-1650 nm) to distinguish sour skin-infected onions and healthy onions. Qin et al. (2009) reported a study of

using hyperspectral reflectance imaging in 450-930 nm to detect citrus canker. Lorente et al. (2013) applied hyperspectral imaging in 400-1100 nm to detect citrus fruits with fungi-induced decay.

In addition to surface blemish and diseases, hyperspectral imaging has been increasingly used to assess internal and intrinsic quality factors of fruits and vegetables. Qin and Lu (2008) proposed a spatially resolved method to measure the optical properties of fruits and vegetables using hyperspectral diffuse reflectance imaging. Rajkumar et al. (2012) used hyperspectral imaging to predict the maturity stages of banana. Wang et al. (2013) proposed a method to predict the soluble solids content and dry matter content of onions using hyperspectral reflectance, transmittance, and interactance imaging in 400-1000 nm. Particularly, many recent applications were reported to apply hyperspectral scattering technique to predict the firmness of fruits and vegetables (Lu et al., 2011; Mendoza et al., 2011; Qing et al., 2008).

Hyperspectral imaging for food and agricultural products is a fast growing research area. Lorente et al. (2012) and Wu and Sun (2013) summarized the recent hyperspectral imaging applications for food quality and safety inspection, which included several hundred applications in total. Also, several relatively new techniques such as microscope hyperspectral imaging (Park et al., 2011), fluorescence hyperspectral imaging (Noh et al., 2007; Yang et al., 2012), and Raman imaging (Qin et al., 2011) were proposed and studied in recent years. Undoubtedly, these trends, including the continuous and rapid development of hyperspectral imaging technique and the boom of hyperspectral imaging applications, will continue in the foreseeable future.

Thermal (infrared) imaging is another electromagnetic radiation-based non-contact measuring method used in safety and quality inspection of food (Gowen et al., 2010). Thermal imaging measures the infrared radiation emitted by the material and maps it to an image. Typical

off-the-shelf thermal imaging detectors are in the spectral region of 3-15 μm. Unlike spectral imaging systems, a typical thermal imaging system does not require an illumination system since it directly measures the radiation emitted by the sample. However, it often requires cooling or heating treatments to increase the temperature contrast of the test object. Several applications (Baranowski et al., 2008; Baranowski et al., 2009; Veraverbeke et al., 2006) using thermal imaging to assess the quality factors (i.e. bruising, watercore) of apples have been reported, which showed that thermal imaging is a potential nondestructive technique for quality inspection of fruits and vegetables. Generally, although thermal imaging has gained more attention in food quality inspection, it is still quite difficult to apply it in real production environment due to several big limitations, including the high cost of IR detector and the difficulty to cool or heat the sample (Gowen et al., 2010).

Aforementioned nondestructive measuring techniques are electromagnetic radiation-based methods, which mainly observe the surface of the test object. To look more in depth within the object, a number of other non-contact sensing techniques with stronger penetration capability have been widely studied in food quality inspection, such as X-ray imaging, computed tomography (CT), and magnetic resonance imaging (MRI).

X-ray imaging uses X-rays to check the uniformity of the density of the test material. X-ray photons have much higher energy than regular light photons, giving X-ray imaging has a distinct advantage in assessing the interior situation of the test object. As an "old" technology, X-ray imaging has been widely adopted as a nondestructive testing method in various areas, including the food industry (Haff and Toyofuku, 2008). X-ray imaging techniques have been traditionally used to identify foreign matters in food products.

With the technical advances of X-ray generator and detectors, X-ray imaging has been increasingly investigated for safety and quality assessment of fruits and vegetables in the past two decades. For instance, Tollner et al. (2005) employed commercial X-ray machine to check internal defects of onions by detecting lines in onion X-ray images. Mendoza et al. (2010) used X-ray imaging to study the pore-size distribution in three varieties of apple tissues. A recent review of X-ray applications in agricultural products was given by Mathanker et al. (2013). Overall, line scan X-ray imaging has been proved to be a promising non-contact inspection technique for many food items. On the other hand, a big safety concern of using X-ray technique in online food inspection is that X-ray inspection system could hurt the health of operators and induce radioactivity in food. This disadvantage, however, now is overcome by using low-energy soft X-ray (photon energy small than 10 keV) inspection systems (Kotwaliwale et al., 2007; Neethirajan et al., 2007), which are safer for use in the food industry than regular industrial X-ray imaging devices.

CT imaging is a radiographic method extending regular X-ray imaging to 3-D image by using tomography technique, which takes many slices of X-ray images at different angles to form a 3-D image. CT imaging provides a better observation of the test object but is more time-consuming with a higher cost. Thus, in food safety and quality area, CT imaging was mainly used in lab conditions (Barcelon et al., 1999; Van Dyck et al., 2014). X-ray fluorescence (XRF) is another X-ray related nondestructive measuring method. The XRF is a technique similar to fluorescence imaging, but it uses x-rays instead of light rays to induce fluorescence. XRF has been applied to detect certain chemical elements in food samples under lab conditions (Jastrzębska et al., 2003; Noda et al., 2006).

Nuclear magnetic resonance (NMR) and magnetic resonance imaging (MRI) are another branch of nondestructive techniques for internal quality inspection of food products in research and industry (Marcone et al., 2013). The basic principle of NMR is that nuclei absorb and re-emit electromagnetic radiation in an external magnetic field at a specific resonance frequency that matches the energy difference between their nuclear spin levels. In food processing and quality assessment, the most common NMR technique is proton NMR imaging (^{1}H MRI), which maps the mobile molecules containing hydrogen in the test object into an image by detecting radio frequency signal emitted by excited hydrogen atoms. The contrast of MRI image is also related with the speed of excited hydrogen atoms returning to the equilibrium state (relaxation). Similar to CT, ^{1}H MRI is used to get 3-D anatomy of the test object by taking images from multiple angles. ^{1}H MRI technique has been proven to be useful tool to track the changes of intrinsic quality factors of some food products, such as tomato (Musse et al., 2009), onion (Gonzalez et al., 2010), rice (Kasai et al., 2007), and cheese (Altan et al., 2011). Nevertheless, due to relatively high cost and the speed limitation, the MRI technique is currently used mainly as an analytical tool in lab environment.

CHAPTER 3

MEASUREMENT OF THE LIGHT ABSORPTION AND SCATTERING PROPERTIES OF ONION SKIN AND FLESH AT 633 NM[1]

[1] Weilin Wang and Changying Li. Postharvest Biology and Technology 86 (2013) 494–501

Reprinted here with permission of publisher.

3.1 ABSTRACT

Understanding the optical properties of onion tissues is essential to applying optical methods for onion quality inspection. This study estimated the optical properties of dry skin, wet skin, and flesh of red, Vidalia sweet, white, and yellow onions at the wavelength of 633 nm. The total diffuse reflectance, total transmittance, and collimated transmittance of single-layer onion tissues were measured by spectroscopic systems. Based on the measured data, the absorption coefficient μ_a and reduced scattering coefficient μ_s' of onion tissues were calculated using the inverse adding-doubling method. The results indicated that the dry and wet skins had significantly higher μ_a and μ_s' than the flesh at 633 nm. For both skins and flesh, the μ_a varied between cultivars, while the differences of the μ_s' between cultivars were less profound. All types of onion tissues were high-albedo materials at 633 nm. Using the calculated optical properties, Monte Carlo simulations were performed to model the light propagation in 25 different scenarios of multi-layer onion tissues for four cultivars, respectively. The results showed that the incident light at 633 nm would lose 99% of its energy within 6 layers in any of the simulated scenarios, and the light penetrated more layers in the sweet onions than in the other three cultivars. This work provided fundamental understanding of the optical properties of onion tissues and the light propagation in onion bulbs at 633 nm. The investigation of the onion optical properties will be extended to a broader spectrum in the future.

3.2 INTRODUCTION

Onion (*Allium cepa* L.) is an important fresh vegetable which had an approximate production value of $1 billion in the United States in 2012 (USDA, 2013). Mature onions are well ripened bulbs that have concentric layers of dry skins and flesh scales. The flesh scales of

onions are edible parts while outer dry skins can be used to make natural food color additives (Block, 2010). Onion skins were also found to be good sources of other by-products such as flavonoids (Ko et al., 2011). The health benefits of onion consumption, such as antifungal, antibacterial, antitumor, antiinflammatory, and antithrombotic (Griffiths et al., 2002; Corzo-martíez et al., 2007), have been widely recognized and advertised in recent decades.

Currently, onion buyers have high expectation of quality. In addition to the nutritional value of onions, other factors such as the appearance, flavor, and existence of defects are also important to consumers (Griffiths et al., 2002). Thus, it is critical to monitor all key onion quality factors throughout the onion harvest and marketing chain. Although some onion packing houses have employed automated systems to sort onions based on size or weight, other quality properties such as presence of disease and surface blemishes have to be evaluated by trained human inspectors. This approach is often inefficient and subjective. Particularly, human visual inspection is not capable of evaluating the internal quality attributes of onions. Thus, it is necessary to develop more versatile nondestructive techniques to improve the efficacy and efficiency of onion quality inspection.

Among various sensing techniques, optical methods such as imaging, spectroscopy, and spectral imaging are attractive to food industry because they are fast, safe, nondestructive, and low-cost (Zude, 2008; Cubero et al., 2011). Several optical techniques were reported for onion quality inspection. Birth et al. (1985) applied near-infrared spectroscopy to predict dry matter content of intact onions, and Wang et al. (2012) employed spectral imaging technology to differentiate sour skin-infected onions from healthy ones. The main principle of these techniques was to observe the interaction between the controlled incident light and the onion, which was

determined collectively by the optical properties of onion tissues and the properties of the incident light.

Onions are biological tissues and their key optical properties include: the absorption coefficient (μ_a), scattering anisotropy (g), scattering coefficient (μ_s), and the refractive index (n)(Tuchin, 2007). The g and μ_s could be combined into one parameter called reduced scattering coefficient ($\mu_s' = \mu_s(1-g)$). These optical properties are requisite parameters in the radiative transport equation to describe the light reflection, propagation, and attenuation on/in the onion tissue. If the optical properties of onion tissues are known, mathematical methods (such as Monte Carlo simulations) can be applied to numerically model the light-onion interaction, which could provide useful reference for designing an appropriate optical system to monitor onion quality. In addition, the optical properties of onion tissues could be indicative of their physical/chemical properties. Therefore, to effectively make optical measurements, it is important to understand and quantify the optical properties of the onion tissues. However, although the physical and chemical attributes of onions have been widely investigated (Abhayawick et al., 2002; Maw et al., 1996; Rodríguez Galdón et al., 2009), the key optical properties (μ_a and μ_s) of onion tissues have never been reported.

Various methods have been reported for measuring the optical properties of biological tissues in the biomedical area (Tuchin, 2007). These methods can be classified into "*ex vivo*" and "*in vivo*" categories in terms of the sample preparation (Kim and Wilson, 2011). The *ex vivo* method, which requires samples of certain shapes and sizes, is often based on the transmittance and reflectance measurements. Then, the optical properties of the measured tissue can be estimated by using computational methods such as the adding-doubling (Prahl et al., 1993; Pickering et al.,1993) or Monte Carlo (Wang et al., 1995) in their inverse forms. The *in vivo*

method is often based on approximations of radiative transport theory by using the diffuse reflectance or backscattering measurements directly made on the sample in the spatial, temporal, or frequency domains (Kim and Wilson, 2011). In the past decade, the optical properties of a number of food products have been investigated by using *ex vivo* methods such as the apple (Saeys et al., 2008) and mandarin (Fraser et al., 2003), or by *in vivo* methods, such as milk and juice (Qin and Lu, 2007), apple (Qin and Lu, 2008, 2009), and beef (Xia et al., 2007). Generally, the *ex vivo* method is used to obtain knowledge of the optical properties of a food product due to its good reliability and adaptability, while the *in vivo* method can be used for online inspection of food quality.

Despite the difference, both *ex vivo* and *in vivo* methods require collimated incident light with a very small beam size (Tuchin, 2007). For this reason, the coherent laser has been considered as one of the standard light sources for measuring the optical properties of tissues. As a relatively inexpensive and reliable light source, the laser has short emission time and emits a monochrome light beam with high intensity. Due to these advantages, many laser-based optical systems have been reported to measure the optical properties of food products (Cubeddu et al., 2001; Fraser et al., 2003) or to predict certain quality parameters of food items by measuring their scattering profiles under the laser irradiation (Lu and Peng, 2007; Qing et al., 2008; Romano et al., 2011).

This study was aimed to quantitatively measure the optical properties of the tissues of four common types of onions (red, sweet, white, and yellow) using a coherent laser. Specific objectives of this research were to:

• Estimate the absorption coefficient μ_a, the reduced scattering coefficient μ_s', and the scattering anisotropy g of the onion tissues using laser and integrating sphere based systems.

• Compare the optical properties of the onion skin and flesh.

• Evaluate the differences of the optical properties between four cultivars of onion tissues.

• Model the light propagation in multi-layer onion tissues using the Monte Carlo simulation.

3.3 Materials and Methods

3.3.1 Sample preparation

Onions of four common types: red (cv. Salsa), Vidalia sweet (cv. Century), white (cv. White Cloud), and yellow (cv. Granero) were used in this study. The sweet onions (short-day onions) were harvested from the state of Georgia, USA in May, 2011 and others (long-day onions) were harvested in the state of Idaho, USA in October, 2011. Onions were stored 2-4 months in a cold storage room (2 ± 1 ^{o}C) in the Vidalia Onion Research Lab at the University of Georgia. Onions were taken out from the cold room 2-3 hours prior to the test and a box fan was used to remove the condensed moisture on the onion surface under room temperature (22 ± 1 ^{o}C).

Three types of onion tissues were examined: dry outer skin, wet outer skin, and flesh. The dry outer skin is the onion outer scale(s) dried during harvesting and storage, which protects flesh scales from the pathogens in the surrounding environment. It has to be noted that the drying of the outer scales is a slow process accompanied by the biochemical changes of pigments and carbohydrate compositions of cell walls of onion tissues (Brewster, 2008). Thus, in most cases, there is an onion scale whose status is at the intermediate stage between the dry skin and flesh scale, which is called wet outer skin. For the sake of brevity, we used dry skin to represent the onion dry outer skin, and wet skin to indicate the onion wet outer skin in the following sections of this paper.

In each cultivar, 20 large size onion bulbs (76-102 mm in diameter) were tested. All onions were manually selected and inspected to be disease-free and with intact dry skins. Onion bulbs

were cut in half longitudinally (from the neck to root). In each half of the onion, a set of onion tissues were cut from the equatorial area. At each set of onion tissues, the surface dry skin, the wet skin, the first layer of flesh scale, and the second layer of flesh scale were selected. Two flesh scales instead of one were examined so that the difference between the two layers of scales could be evaluated. Then, selected onion scales were cut into square pieces (30×30 mm) and the flesh samples were shaved to slabs using a razor blade. In total, 640 pieces of onion tissue samples (4 cultivars $\times$ 20 onions $\times$ 2 sample sets $\times$ 4 pieces of tissues) were measured.

3.3.2 Thickness and refractive index of the sample

The thickness (d) of each sample was measured using an electronic micrometer (model 35-025, iGaging, San Clemente, CA, USA) with an accuracy of ± 0.001 mm in the central area of the tissue. For onion flesh samples, two 1-mm thick glass slides were used to sandwich the sample so that the metal tip of the micrometer could not cut into the tissue, and the thickness of the glass slides were deducted from the measurement later. Three replicates were made for each sample and the average value was reported. The refractive indices (n) of samples were measured by a Leica Abbe refractometer (model Abbe Mark II, Reichert, Inc. Depew, NY, USA). For each cultivar, eight pieces of dry skins and eight pieces of flesh tissues were randomly selected and measured. The refractive index of dry skins were measured by directly placing the sample at the prism of the refractometer and using distilled water as the contact liquid. The refractive index of the onion flesh was estimated by testing the onion juice extracted from the tissue. For the dry skin and flesh samples, each of them was measured three times. Then, for each onion group, the mean refractive index was calculated and used in the later calculations.

In practice, it is difficult to measure the refractive index for some wet skin samples by using the Abbe refractometer since they were too thick to be measured as a film but not fleshy enough

to be measured by using its juice. It was also observed that, depending on its moisture content, the refractive index of the wet skin of an onion was either close to the one of its dry skin or close to that of its flesh. Thus, based on their thickness values, the refractive indices of onion wet skins were approximated individually to those of dry skins (thin as dry skin) or those of flesh (thick as flesh).

3.3.3 Reflectance and transmittance measurements

The spectroscopic system (Fig. 3.1 A, B, and C) was assembled to measure the total reflectance, total transmittance, and collimated transmittance spectra of onion samples at 633 nm. The system mainly consisted of an integrating-sphere (model 4P-GPS-060-SF, Labsphere, North Sutton, NH, USA) and a Vis-NIR spectrometer (model USB4000, Ocean Optics, Dunedin, FL, USA). Based on the availability of the device, a low power helium-neon (HeNe) laser (0.8 mW, 633 nm) (model HRP008-1, Thorlabs, Newton, NJ, USA) was used in this study. This type of laser has been widely used for studying the optical properties of biological tissues (Tuchin, 2007; Kim and Wilson, 2011).

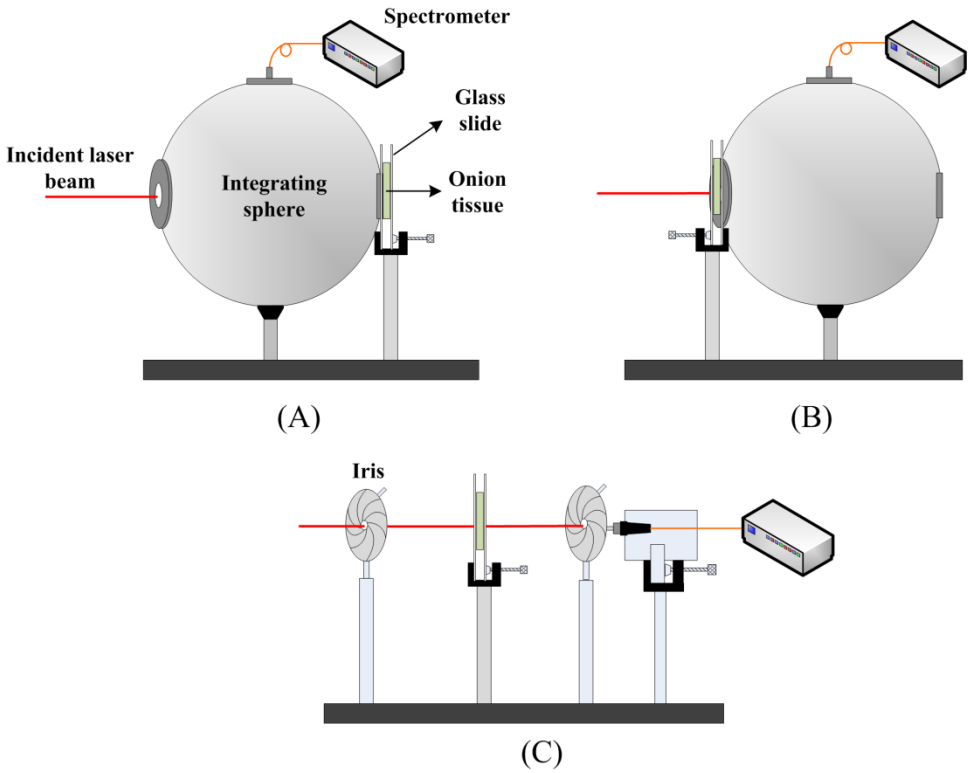

Figure 3.1. The schematic of the system configurations for measuring the total reflectance (A), the total transmittance (B), and the collimated transmittance (C).

The interior wall of the integrating sphere is coated by Spectraflect material that has a reflectivity of 98% at 633 nm. The internal diameter of the sphere is 152.4 mm and it has four ports (25.4 mm in diameter) at 0°, 90°, 180°, and the north pole. The aperture to surface area ratio of the sphere is less than 3%. The ports at 0° and 180° were used as the entrance and exit, respectively. An optical fiber with a diameter of 400 μm and numerical aperture of 0.37 (model M32L02, Thorlabs, Newton, NJ, USA) was used to deliver the light to the spectrometer from the port at 90° of the sphere. The laser head was placed on a kinematic V-clamp mount (model C1503, Thorlabs, Newton, NJ, USA) so that its position can be precisely adjusted at the horizontal and vertical axes. To align the laser and the sphere, two circular cross targets (25.4

mm in diameter) were printed on transparent films and placed on the entrance and the exit ports, respectively. Then, the positions and orientations of the laser head and the integrating sphere were adjusted until the incident laser beam can go through the center spots of both the entrance and the exit ports. The wavelength accuracy of the spectroscopic system was calibrated by using a pencil style krypton calibration lamp (model 6031, Oriel Instruments, Stratford, CT, USA).

To measure the total reflectance, the sample was placed behind the exit port while the entrance port was open (Fig. 3.1 A). To measure the total transmittance, the sample was placed in front of the entrance port and the opposite exit port was blocked by a Spectraflect plug (Fig. 3.1 B). The reference signal (Ref) was measured by using the setup in Fig. 3.2 A, but replacing the onion sample with a certified 99% diffuse reflectance Spectralon target (model AS-00158-060, Labsphere, North Sutton, NH, USA). The dark signal (D) of the system was measured by covering all ports of the integrating sphere. Then, the total diffuse reflectance (R_{raw}) and the total transmittance (T_{raw}) were converted to the relative total reflectance (R) and relative total transmittance (T) by:

$$R = \frac{R_{raw} - D}{Ref - D} \tag{3.1}$$

$$T = \frac{T_{raw} - D}{Ref - D} \tag{3.2}$$

The collimated transmittance was measured following the set-up recommended by Prahl (2011) (Fig. 3.1 C). The laser beam was aligned with the center of the detecting optic fiber. An iris was placed between the laser head and the sample to adjust the intensity of the laser beam to avoid saturations of the spectrometer. Another iris in front of the detector was used to block the

scattered light from entering the detector. The relative collimated transmittance (T_c) was obtained by:

$$T_c = \frac{Tc_{raw} - Dark}{Tc_{ref} - Dark} \tag{3.3}$$

where Tc_{ref} was the original light intensity of the incident laser beam and Tc_{raw} was the intensity of the laser beam transmitted through the onion tissue sample. The dark signal ($Dark$) of the spectrometer was measured when the probe of the spectrometer was covered by a black cap.

In all measurements, the onion tissue was sandwiched by two pieces of $70 \times 70 \times 2$ mm (width $\times$ height $\times$ thick) borosilicate glass slides (model BOROFLOAT 33, SCHOTT North America, Inc. Louisville, KY, USA). BOROFLOAT glass was used because of its good homogeneity and high transmittance (>90%) at the visible range. The refractive index of the BOROFLOAT 33 glass is 1.47 at 633 nm. A U-shape clamp and a C-shape clamp were used to apply slight pressure on the glass slides so that the onion tissue formed a flat slab. The whole system was enclosed in a dark chamber covered by a black cloth. All measurements were performed at room temperature (22 ± 1 ^{o}C).

3.3.4 Estimating the absorption and scattering coefficients

The inverse adding-doubling (IAD) program provided by Prahl (2011) was used to calculate the absorption and scattering coefficients for each onion tissue sample. The IAD method has been widely used for estimating the optical properties of biological tissues due to its flexibility and reliability in measuring tissues with various albedos and optical depths (Tuchin, 2007). The fundamental principle of the IAD method is to iteratively solve the stationary (steady-state) radiative transfer equation based on the measured reflection and transmittance values of the

sample (Prahl et al., 1993). As the mathematical description of continuous wave light propagation in a medium, the stationary radiative transfer equation (Tuchin, 2007) can be described as:

$$\frac{\partial I(r,\hat{s})}{\partial s} = -(\mu_a + \mu_s) I(r,\hat{s}) + \frac{\mu_s}{4\pi} \int_{4\pi} p(s,\hat{s}) I(r,\hat{s}) \mathrm{d}\Omega \qquad (3.4)$$

Where the μ_a is the absorption coefficient, μ_s is the scattering coefficient, $I(r,\hat{s})$ is the average flux density at the point *r* along the direction $\hat{s}$, $\mathrm{d}\Omega$ is the unit solid angle for the direction $\hat{s}$, $p(s,\hat{s})$ is the phase function of the angular distribution of the scattered light, which describes the probability of the polar deflection angle of the photon after each scattering event. The phase function used in all IAD calculations was Henyey-Greenstein (HG) phase function (Prahl et al., 1993), described as $\rho(\theta) = \frac{1}{4\pi} \frac{1-g^2}{(1+g^2-2g\cos\theta)^{3/2}}$. The HG phase function approximates the angular distribution of scattering in biological tissues depending on the mean cosine of scattering angle (the scattering anisotropy coefficient g = $<\cos\theta>$) (Tuchin, 2007).

Using the IAD program, μ_a and μ_s' can be calculated from the measured R and T values, with a fixed g value. The g value can also be estimated by the IAD method when the collimated transmittance T_c is included. In our work, since the anisotropy of onion tissues was unknown before this study, it was first estimated by using the IAD program with three inputs: T, R, and T_c. A small part of data sets (42 out of 640) were removed because of the invalidity of T_c (either T_c was greater than T or the sum of T_c and R was equal to or greater than 1). When the g had been estimated, the IAD program with two inputs of T and R were used to calculate μ_a and μ_s' again. Once g, μ_a, and μ_s' were estimated, μ_s was calculated by $\mu_s = \frac{\mu_s'}{1-g}$.

It should be noted that the IAD program is often prone to error in estimating the anisotropy due to the difficulty of measuring T_c accurately (Prahl, 2011). In this study, to compensate the individual bias in the estimated g values, the mean g of for each group of onion tissues was calculated and then was used for all samples in the group in later calculations. The more accurate quantifications of anisotropies of onion tissues could be made by using other specific measuring approaches in the future, such as measuring the angular distribution of the scattered light by rotating a collimated detector around the sample enclosed in a cylinder tank with index-matching liquid (Kim and Wilson, 2011).

Analysis of variance (ANOVA) was used to evaluate the differences between four types of onion tissues and between different onion cultivars. The significance of the differences between the means of the measured optical properties of different groups were evaluated by using Tukey's HSD (honest significant difference) tests at the significance level of 0.05. All ANOVA tests were conducted by using the GLM (general linear models) procedure in SAS (v9.2, SAS Institute Inc. Cary, NC, USA).

3.3.5 Validation procedure

The system was verified by using the phantoms made from a standard scattering material (Intralipid-20%, Sigma Aldrich, St. Louis, Missouri, USA) and two absorption dyes (Nigrosin and Naphthol Green B, Sigma Aldrich, St. Louis, Missouri, USA). In the validation test, the Intralipid-20% was first diluted to one percent by distilled water, and then the absorbers were added to make three different types of liquid solutions. Liquid solutions were added into a quartz glass cuvette with a 10 mm light path to make the phantoms. The cuvette had 40×40 mm side walls which can cover the entire sampling port of the integrating sphere. The T and R of the phantom were measured by the system respectively (5 replicates for each type of phantom).

Then, the μ_a and μ_s' of the phantoms were estimated by the IAD program using g=0.73, in which the g was calculated by using the empirical equation ($g(\lambda)=1.1-0.58\lambda$) established by Staveren et al. (1991). The estimated values were compared with each other and with the values reported by Ninni et al. (2011).

3.3.6 Monte Carlo simulation of light propagation in multi-layer onion tissues

Monte Carlo simulations were performed to model the light propagation in multi-layer onion tissues. The "MCML" program provided by Wang et al. (1995) was used for the simulation. Typically, a mature onion bulb has 1-3 layers of dry skins, one layer of wet skin, and a number of flesh scales. Thus, onion models with multiple layers were simulated with the presence of 0-3 layers of dry skins. All examined scenarios had one layer of wet skin and 1-6 flesh scales, which were gradually included in the model. The simulations were stopped at the seventh layer since light rarely can penetrate deeper than that. In each Monte Carlo simulation, 500,000 photons were launched, and the spatial resolution of radial distance and tissue depth was 0.01 mm. The number of grids for the radial and tissue depth was 1000. To simplify the simulation, the onion scales were assumed to be slabs with the mean thickness value listed in Table 3.1 and the tiny gaps between the inside scales of onions were ignored.

3.4 RESULTS

3.4.1 Thickness and refractive indices of onion scales

The thickness of most onion dry skins tested in this study was 0.07-0.09 mm and the thickness of onion flesh tissue was 3-5 mm (Table 3.1). As expected, the average thickness values of onion wet skins (0.391-0.827 mm) were in-between those of the dry skin (0.071-0.087 mm) and the flesh (2.833-4.049 mm). On average, the dry skins of the tested red onions were

about 15% thinner than those of other cultivars, and the flesh scales of red and yellow onions were about 15-20% thinner than those of sweet and white onions.

Generally, the measured refractive indices of onion flesh (1.341-1.345) were in agreement with the values (1.343-1.351) reported by Foskett and Peterson (1950). For either the onion dry skin or onion flesh, the ratio of SD to mean of the refractive index was very small ($< 0.5\%$). No statistical difference was observed in flesh or dry skin between cultivars in their refractive indices with the exception of red onion flesh. Since the difference was minute (≈0.003), it was ignored. The averaged values (1.335 for dry skin and 1.342 for flesh) were used as universal values for all samples. A threshold value 0.5 mm was arbitrarily selected based on the histogram of the thickness values of the tested wet skins. If a wet skin was thicker than 0.5 mm, the refractive index value for the flesh (1.342) was used for it; otherwise, the value of dry skin (1.335) was used.

3.4.2 System validation

On average, the estimated μ_s' of the phantom showed 3.1% difference to the μ_s' value of Intralipid 20% reported by Ninni et al. (2011). The results of the validation tests showed that the system successfully separated the μ_a and the μ_s' for the three types of phantoms. The estimations of the μ_a and μ_s' for each type of phantom had standard deviations of 1.6-6.7% (on average 3.2%). Based on the two tailed t-tests at the significance level of 0.05, the mean μ_s' of three types of phantoms were not significantly different from each other, while their mean μ_a were significantly different ($p<0.001$). Overall, the accuracy of the system in estimating the μ_a and μ_s' was comparable to other reported studies (Pickering et al., 1993). As discussed by

Pickering et al. (1993), the error of the IAD estimation could be caused by the light loss at the rim of the sample and by the interference between the glass slides.

3.4.3 Scattering anisotropy

The estimated anisotropies of onion tissues at 633 nm (Table 3.2) varied from 0.35 to 0.73 in different groups, which were smaller than those of regular human tissues (0.8-1) (Tuchin, 2007) and close to those of apples (0.6-0.8) (Saeys et al., 2008). The anisotropies of onion dry skins were lower than those of flesh, except for yellow onions. No significant difference was found between the first and the second flesh scales. The onion wet skins did not show consistent patterns in different cultivars. For red and white onions, the anisotropies of their wet skins were significantly higher than those of dry skins, while not significantly different from those of flesh scales. For sweet and yellow onions, however, the differences between the anisotropies of the wet skins and the dry skins and flesh were not distinctive. This inconsistency can be explained by the data shown in Table 3.1: the wet skins of red and white onions were thicker than those of sweet and yellow onions, which indicated that the physical characteristics of their wet skins could be more similar to those of the flesh scales than those of sweet and yellow onions. These results indicated that the anisotropies of onion tissues could be significantly different between cultivars and between different types of tissues. Therefore, the mean anisotropy of each type of onion tissue in each cultivar was computed and used in later calculations. Since the anisotropies of the first and second flesh scales were not significantly different, they were averaged and used in later computations.

3.4.4 The absorption and reduced scattering coefficients

Table 3.3 shows the means and standard deviations of the estimated μ_a and μ_s' values of onion tissues. Onion dry skins had strongest light absorption at 633 nm in red onions (μ_a =1.97

$\times 10^3\ m^{-1}$), which was significantly higher than those of the other cultivars. The colorless dry skins of white onions showed the lowest μ_a value ($0.5\times 10^3\ m^{-1}$), which was significantly lower than that of yellow onions. The difference between the μ_a of sweet and white onions was not statistically significant. The average μ_s' of dry skins were from $18.53\times 10^3\ m^{-1}$ (white onion) to $22.47\times 10^3\ m^{-1}$ (yellow onion) at 633 nm. The μ_s' of the dry skin of red, sweet, white, and yellow onions were about 10, 25, 37, and 16 times of their corresponding μ_a, respectively. No significant difference was observed between the μ_s' of different cultivars.

As illustrated in Table 3.3, the μ_a and μ_s' of the onion wet skins were in-between those of dry skins and flesh, respectively. The average μ_a of wet skins were about 20-60% of those of the corresponding dry skins, and 5-10 times higher than those of flesh. The average μ_s' of wet skins was about 10-25% of that of dry skins, and 2-18 times higher than that of flesh. Statistical data suggested that the onion wet skin had distinct optical properties from the dry skin and the flesh scale in all cultivars. Thus, it should be considered as a separate type of medium in optical models of onions.

The average estimated μ_s' values of onion flesh were from $0.032\times 10^3\ m^{-1}$ to $0.117\times 10^3\ m^{-1}$, which were significantly smaller (13-41 times) than those of the dry skin. The average μ_a of the flesh scale of red onions was significantly higher than that of the other three cultivars, while no significant difference was found between the other three cultivars. Statistical tests did not reveal any significant difference between the first and the second flesh scales of the μ_a in all examined cultivars. The average μ_s' values of onion flesh were from $0.15\times 10^3\ m^{-1}$ to 0.66

$\times 10^3\ m^{-1}$. The μ_s' of the flesh of red, white, and yellow onions were quite close, which were significantly higher than those of sweet onions. The mean μ_s' of the flesh of red, white, and yellow onions were about 30 times smaller than those of their dry skins, and the mean μ_s' of sweet onions was about 120 times smaller than that of their dry skins. Similar to the μ_a, no significant difference was presented between the mean μ_s' of the first and the second flesh scales of onions.

3.5 DISCUSSION

3.5.1 Optical properties of single layer onion tissues at 633 nm

It is well known that for fruits and vegetables, their scattering coefficients (μ_s or μ_s') are mainly determined by the cellular structure of their tissues, and the absorption coefficients are related to their chemical compounds (Zude, 2008). In this study, the tissues of the four tested onion cultivars did not statistically differ from each other in terms of the μ_s' of their dry skins, but had significant difference between the dry skins of red, yellow, and other onions. In this regard, the results suggested that the dry skins of four onion cultivars had similar cellular structures but had different contents of chemical compounds. As for the onion flesh, it is observed that red onions showed higher μ_a than other cultivars and the μ_s' of sweet onions illustrated significant difference from those of other cultivars at 633 nm. In summary, the optical properties of onion dry skin and flesh could be different between certain cultivars.

Results of this study (Table 3.4) showed that onion dry skins have greater μ_a and μ_s' than flesh. Onion flesh consists of high percentage of moisture ($>90\%$), glucose, fructose, sucrose, protein, ash, etc (Brewster, 2008). All these major chemical compounds in onion flesh do not

have strong absorption at 633 nm. Also, it is known that the absolute content of pigments decreases from outer scales to inner scales in onions (Pérez-Gregorio et al., 2010; Takahama and Hirota, 2000). During the dehydration process of an onion flesh scale to dry skin, with respect to the decrease of its moisture content, the concentration of the pigment in the scale increases (Takahama and Hirota, 2000) and other physical properties such as the density of the scale also change (Hole et al., 2000). Thus, it is reasonable that the dry skin has higher μ_a and μ_s' than the flesh, since it has greater content of pigments and denser cell structure than the flesh scale.

Compared to the onion dry skin and onion flesh, the onion wet skin showed higher standard errors in their μ_a and μ_s' values. The relative standard error of the μ_a and μ_s' of onion wet skins were 30-100% higher than those of onion dry skins or flesh. This can be explained by the physiological process of onion wet skins in drying. The formation of an onion skin is a slow process affected by many conditions such as the storage time and the relative humidity of the environment. As a result, the physical and chemical properties of onion wet skin could be very different at different stages of drying. Therefore, the optical properties of onion wet skins, intermediate between those of onion dry skins and flesh scales, could have large variations. For this reason, although in this study the μ_a and μ_s' were significantly different between certain tested cultivars, it might not be conclusive that the optical properties of the wet skins of these cultivars are significantly different. The μ_a and μ_s' of onion wet skins reported in this article could only represent the situations of the onions tested in this study.

Overall, the estimated μ_a (0.5×10^3 - $1.97\times10^3\ m^{-1}$) of onion dry skins were at the same magnitude as those of apple skins ($<2\times10^3\ m^{-1}$) reported by Saeys et al. (2008) at 633 nm. The estimated mean μ_s' of onion dry skins (18.48×10^3-$22.48\times10^3\ m^{-1}$) were several times higher

than those of apple skins (about 3.5×10^{3}-4×10^{3} m^{-1}). The μ_a and μ_s' of onion flesh at 633 nm were at the same order of magnitude with those of other fruits and vegetables (kiwifruit, peach, pear, plum) presented by Qin and Lu (2008).

Similar to other biological tissues, onion dry skins and flesh are high-albedo biological media (albedo is defined as $\frac{\mu_s'}{\mu_a+\mu_s'}$) at 633 nm. It is known that the biological materials must be scattering dominated to apply the diffusion theory to estimate their optical properties nondestructively (Zude, 2008). Thus, our results supported the feasibility of nondestructively measuring the optical properties of onions at 633 nm by using the diffusion theory, such as the diffuse reflectance or backscattering.

The variances shown in the results of this study were most probably caused by the biological variations (moisture content, pigment content, firmness, etc) of the samples. There were a few other factors that could affect the accuracy of this study. First is the systematic error introduced by the spectroscopic system and the IAD algorithm. In addition, based on our validation tests, the intensity of the laser beam presented a 2.1% deviation in 100 measurements, which could be another error source. Moreover, real onion tissues, particularly onion dry skins, are heterogeneous media with distinguishable textures. However, as a general rule in tissue optics, in this study the onion tissues were assumed being homogeneous to apply the IAD estimation.

Based on the measured optical properties of onion tissues, the light loss caused by absorption and scattering in single layer onion tissues could be estimated. For instance, assuming onion dry skins are pure absorption material (ignoring any scattering effect), based on the definition of μ_a, the probability for photons at 633 nm to survive after traveling 1 mm in the dry skin of red onions and white onions would be 13.81% ($e^{-\mu_a*d}=e^{-1.98*1}$) and 60% ($e^{-0.5*1}$),

respectively. Onion bulbs often have 1-3 layers of 0.02-0.1 mm thick dry skins (Brewster, 2008). Thus, for μ_a at this level (0.5×10^3-2×10^3 m^{-1}), the light loss in the dry skins of an onion could approximately be about 1% ($1-e^{-0.5*0.02}$) to 45% ($1-e^{-1.98*0.3}$) depending on its cultivar and the number and thickness of its dry skins. Similarly, if only considering the scattering, using an anisotropy value of 0.5, even in a thin (0.02 mm) dry skin, the approximate light loss caused by the scattering at 633 nm could be higher than 50% ($1-e^{-\frac{\mu_s'}{1-g}*d} = 1-e^{-\frac{18.53}{1-0.5}*0.02} = 0.52$). Considering the thickness of the onion, the light absorption and scattering effects at 633 nm in single layer onion tissues can be indicated by their optical depths ($\tau = (\mu_a + \mu_s)\times d$) (Table 3.4).

3.5.2 Light propagation in multi-layer onion tissue at 633 nm

Results of the Monte Carlo simulations revealed that the laser light had different transmission rates in different onion cultivars at 633 nm. Based on the definition of the penetration depth of 1% light transmittance (Fraser et al., 2001), the laser light beam generally penetrated the deepest in Vidalia sweet onions and the least in red onions, while the light transmission in white and yellow onions were in-between (Fig. 3.2). Overall, the laser beam was not able to penetrate more than 6 onion layers regardless of onion cultivar and layer type. It should be noted that the transmission rate was not only determined by the attenuation factor (combination of absorption and scattering coefficients), but also affected by the thickness of each layer in each cultivar.

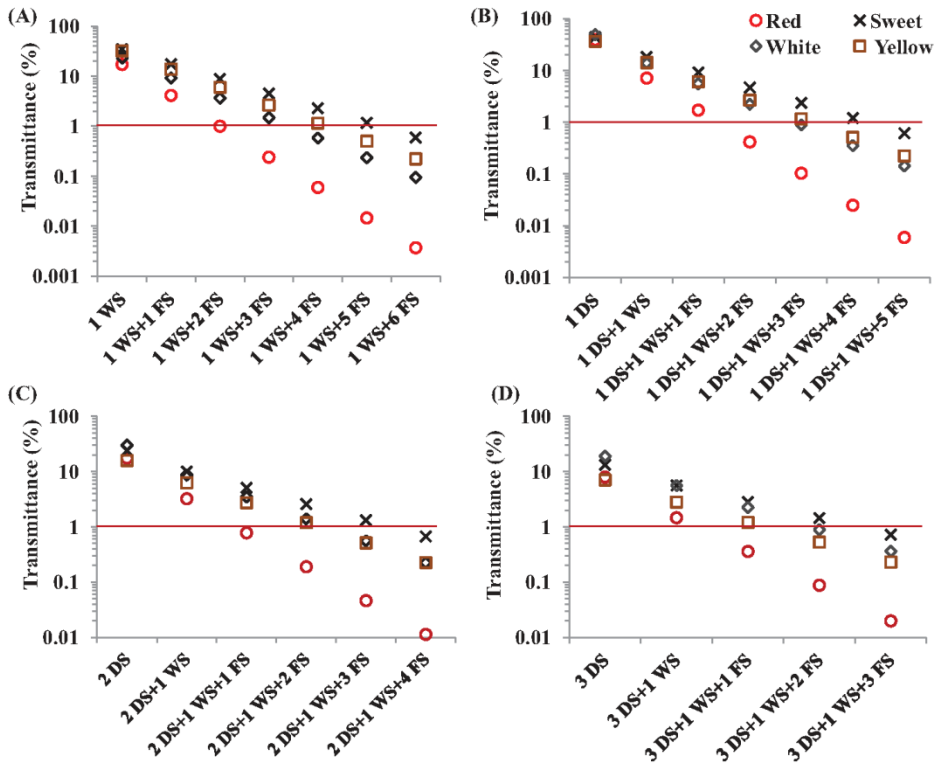

Figure 3.2. The relative transmittance of the light propagation (at 633 nm) in multi-layer onion tissues in the scenarios of: no dry skin (A), 1 layer of dry skin (B), 2 layers of dry skins (C), and 3 layers of dry skins (D). The meaning of the labels on the horizontal axis: DS - outer dry skin, WS - wet skin, and FS - flesh scale.

The onion dry skin greatly attenuated the propagation of the light in onion tissues in all cultivars. Although onion dry skins were much thinner than flesh scales, the attenuation effect of light from the dry skin was comparable to that from a flesh scale since the dry skin has greater absorption and scattering coefficients than the flesh, which were in accordance with our experimental observations in the total transmittance and collimated transmittance measurements. According to the results of simulations, by adding one, two, and three layers of dry skin(s) to the baseline scenario (one wet skin and one flesh scale) in red onions, the transmission rate of light was reduced from 4.1% to 1.7%, 0.8%, and 0.4%, respectively. After passing three dry skin

layers and one wet skin layer of red onions, the light lost 99% of its energy and only a few photons could reach the flesh scales. Thus, in the optical measurements of onions, the onion dry skin should be considered and handled appropriately.

It should be noted that no air gap between onion scales was considered in our simulations. In practice, for some onions, there could be thin air gaps between onion scales. For instance, if the outermost dry skin of the onion bulb is loose, there could be a layer of air between the outermost dry skin and the scale beneath it. The additional air layer could reduce the penetration depth. For example, in the last multi-layer onion model shown in Fig. 3.2 D, when a thin layer of air (d =0.036, $\mu_s = 10 \times 10^{-6}\ m^{-1}$, $\mu_a = 0.5 \times 10^{-6}\ m^{-1}$) was included between the first and second dry skins, the total diffuse reflectance increased 2.37%, the total absorption and transmission decreased 2.37% and 0.003% (of the overall energy of the initial light), respectively. Therefore, the results of our models could have overestimated the light penetration depth for those onions with air gaps.

3.6 CONCLUSIONS

Our study revealed that onion dry skin and wet skin had significantly higher absorption and reduced scattering coefficients than onion flesh at 633 nm. Different cultivars of onions could be significantly different in terms of the μ_s' of the flesh and the μ_a of both the flesh and dry skin. Our data also indicated that onion tissues are scattering dominated (high-albedo) biological materials. Monte Carlo simulations of light propagation in multi-layer onion tissues showed that the low power laser at 633 nm would lose 99% of its energy within 6 layers of onion tissues in any of the 25 simulated scenarios because of the substantial light absorption and scattering in onion tissues. The results suggested that the transmittance measurement at 633 nm of an intact onion is not likely and the reflectance or interactance measurements could be more suitable. For

the applications that intend to measure the characteristics of onion flesh by using optical methods, it is important to handle onion outer skins properly.

This study is the first effort to measure the light absorption and scattering characteristics of onion tissues, which provides quantitative evidences to better design the optical systems for onion quality evaluation. However, this study only investigated the optical properties of onion tissues at one wavelength and future research is needed to expand our understanding to a wider spectral range.

3.7 Acknowledgements

This work was funded by the USDA NIFA Specialty Crop Research Initiative (Award No. 2009-51181-06010). The authors also gratefully acknowledge Dr. Ron Gitaitis, Dr. Howard Schwartz, and Dr. Krishna S. Mohan for offering onion samples, Dr. Elizabeth L. Andress for providing the Abbe Refractometer to this study. The assistance from Mr. Anthony M. Dean during data collection was also sincerely appreciated.

Table 3.1. The thickness and refractive indices (mean ± SD) of onion tissues in four cultivars.

	Tissue Type	Red Onion	Sweet Onion	White Onion	Yellow Onion
Thickness (mm)	Dry skin	0.071 ± 0.019	0.087 ± 0.033	0.083 ± 0.025	0.083 ± 0.023
	Wet skin	0.827 ± 0.566	0.468 ± 0.517	0.638 ± 0.802	0.391 ± 0.489
	First flesh	2.833 ± 0.554	3.941 ± 0.734	3.708 ± 0.984	2.962 ± 0.684
	Second flesh	3.317 ± 0.398	3.995 ± 1.109	4.049 ± 0.745	3.392 ± 0.833
Refractive index (n)	Dry skin	1.3345 ± 0.0006	1.3371 ± 0.0074	1.3345 ± 0.0004	1.3337 ± 0.0005
	Flesh	1.3450 ± 0.0007	1.3410 ± 0.0011	1.3413 ± 0.0003	1.3413 ± 0.0015

Table 3.2. The means and standard deviations of the estimated anisotropies of onion tissues at 633 nm.

	Tissue Type	Red Onion	Sweet Onion	White Onion	Yellow Onion
g	Dry skin	$0.589 \pm 0.023^{A,b}$	$0.474 \pm 0.034^{B,b}$	$0.371 \pm 0.035^{B,b}$	$0.545 \pm 0.046^{AB,a}$
	Wet skin	$0.720 \pm 0.025^{A,a}$	$0.589 \pm 0.045^{AB,ab}$	$0.509 \pm 0.032^{BC,a}$	$0.421 \pm 0.047^{C,ab}$
	First flesh	$0.686 \pm 0.015^{A,a}$	$0.727 \pm 0.036^{A,a}$	$0.511 \pm 0.025^{B,a}$	$0.499 \pm 0.045^{B,ab}$
	Second flesh	$0.691 \pm 0.016^{A,a}$	$0.599 \pm 0.042^{AB,ab}$	$0.560 \pm 0.028^{B,a}$	$0.354 \pm 0.037^{C,b}$

Upper case letters in the superscripts indicate the significant differences between the four onion cultivars ($p<0.05$), and lower case letters indicate the significant differences between the four types of onion tissues ($p<0.05$).

Table 3.3 The means and standard deviations of the absorption coefficients and the reduced scattering coefficients of onion tissues at 633 nm.

	Tissue Type	Red Onion	Sweet Onion	White Onion	Yellow Onion
μ_a ($\times 10^3$ m^{-1})	Dry skin	$1.974\pm0.819^{A,a}$	$0.760\pm0.460^{C,a}$	$0.501\pm0.485^{C,a}$	$1.371\pm1.107^{B,a}$
	Wet skin	$0.599\pm0.841^{A,b}$	$0.305\pm0.316^{AB,b}$	$0.284\pm0.378^{B,b}$	$0.325\pm0.375^{AB,b}$
	First flesh	$0.117\pm0.051^{A,c}$	$0.043\pm0.020^{B,c}$	$0.036\pm0.018^{B,c}$	$0.033\pm0.022^{B,b}$
	Second flesh	$0.093\pm0.028^{A,c}$	$0.044\pm0.023^{B,c}$	$0.032\pm0.010^{B,c}$	$0.033\pm0.023^{B,b}$
μ_s' ($\times 10^3$ m^{-1})	Dry skin	$19.733\pm8.396^{A,a}$	$19.075\pm8.326^{A,a}$	$18.480\pm7.524^{A,a}$	$22.476\pm15.81^{A,a}$
	Wet skin	$1.988\pm2.829^{B,b}$	$3.756\pm3.994^{AB,b}$	$4.424\pm4.39^{A,b}$	$5.573\pm4.044^{A,b}$
	First flesh	$0.616\pm0.194^{A,b}$	$0.152\pm0.155^{B,c}$	$0.579\pm0.319^{A,c}$	$0.659\pm0.270^{A,c}$
	Second flesh	$0.600\pm0.194^{AB,b}$	$0.253\pm0.164^{C,c}$	$0.479\pm0.247^{B,c}$	$0.657\pm0.300^{A,c}$

Upper case letters in the superscripts indicate the significant differences between the four onion cultivars (p<0.05), and lower case letters indicate the significant differences between the four types of onion tissues (p<0.05).

Table 3.4 The average absorption coefficient (μ_a), scattering coefficient (μ_s), anisotropy (g), thickness (d), refractive index (n), and optical depth (τ) of the single-layer onion tissues of red, Vidalia sweet, white, and yellow onions.

Cultivar	Tissue Type	μ_a ($\times 10^3$ m^{-1})	μ_s ($\times 10^3$ m^{-1})	g	d (mm)	n	τ
Red	Dry skin	1.974	47.987	0.589	0.071	1.335	3.547
	Wet skin	0.599	7.104	0.72	0.827	1.335	6.370
	Flesh	0.105	1.9505	0.688	3.075	1.342	6.321
Sweet	Dry skin	0.76	36.243	0.474	0.087	1.335	3.219
	Wet skin	0.305	9.137	0.589	0.468	1.335	4.419
	Flesh	0.044	0.593	0.663	3.968	1.342	2.526
White	Dry skin	0.501	29.385	0.371	0.083	1.335	2.481
	Wet skin	0.284	9.014	0.509	0.638	1.335	5.932
	Flesh	0.034	1.137	0.536	3.879	1.342	4.542
Yellow	Dry skin	1.371	49.355	0.545	0.083	1.335	4.210
	Wet skin	0.325	9.617	0.421	0.391	1.335	3.887
	Flesh	0.033	1.166	0.427	3.177	1.342	3.809

CHAPTER 4

QUANTIFICATION OF THE OPTICAL PROPERTIES OF HEALTHY AND DISEASED ONION TISSUES IN THE VISIBLE AND NEAR-INFRARED SPECTRAL REGION[2]

[2] Weilin Wang, Changying Li, and Ronald D. Gitaitis. To be submitted to Transactions of the ASABE.

4.1 ABSTRACT

Modern optical techniques such as spectroscopy and hyperspectral imaging are promising tools for the nondestructive inspection of onions for the purpose of safety and quality control. To apply these optical techniques appropriately, it is important to understand the fundamental optical properties of onion tissues. In this study, the light absorption coefficient (μ_a), reduced scattering coefficient (μ_s'), and scattering anisotropy (g) of onion tissues were estimated in the wavelength range of 550-880 nm and 950-1650 nm. Dry skin and flesh samples of healthy, *Burkholderia cepacia*-infected (causing sour skin), and *Botrytis aclada*-infected (causing neck rot) onions were tested. The total diffuse reflectance, total transmittance, and collimated transmittance spectra of the samples were collected using spectroscopic systems that mainly consisted of the integrating sphere, fiber guide, and spectrometers. Based on the collected spectra, the μ_a, μ_s', and g of the onion tissues were calculated using the inverse adding-doubling method. The results indicated that onion dry skins and flesh were scattering dominated biological tissues in the wavelengths below 1300 nm. The μ_a values of the dry skin of onions with sour skin were significantly greater than those of healthy onions in the near-infrared region. Dry skins from onions with neck rot were statistically different from those of healthy ones in terms of the μ_a in 550-750 nm and the μ_s' in 550-1650 nm. The flesh of onions with sour skin or neck rot were significantly different from those of healthy ones with regard to the μ_s' in 550-1650 nm, and in terms of the absorption coefficient in 550-1100 nm. This study demonstrates the feasibility of detecting diseased onions by investigating their optical characteristics. The measured optical properties of healthy and diseased onion tissues can be used in the theoretical modeling and simulations of the light-onion interactions for various onion quality inspection systems.

4.2 INTRODUCTION

Optical techniques have been widely studied and used in quality control and food safety programs for fruits and vegetables. These techniques have the advantage of being non-invasive and relatively inexpensive (Zude, 2008). To using optical sensing techniques effectively, the optical properties of the product should be evaluated since they could be used as indicators of its quality attributes. For instance, the refractive indices (n) of fruit and vegetable juices can be precisely correlated to their soluble solids contents (SSC), and this principle has been used to develop the handheld refractometer used to measure the SSC of fruits and vegetables (Zude, 2008).

Three fundamental optical properties of fruits and vegetables are the light absorption coefficient (μ_a), scattering coefficient (μ_s), and scattering anisotropy factor (g), which collectively define the light propagation in the product. For fruits and vegetables, it is well known that the μ_a is associated with the chemical constituents of the product and the μ_s is related to the physical characteristics of cell structure, such as tissue density and firmness (Lu, 2008). The two scattering related coefficients μ_s and g are often combined as one parameter called the reduced scattering coefficient $\mu_s' = \mu_s \times (1 - g)$. In conventional optical methods applied to fruits and vegetables, such as visible/near-infrared (NIR) spectroscopy or spectral imaging, the light absorption and scattering effects are often considered together by correlating the quality factors of the product to its light reflectance or transmittance spectral data. To more accurately correlate the light-tissue interactions with the specific physical or chemical attribute of the product, it's necessary to separately evaluate the light absorption and scattering properties of the product.

A number of techniques have been reported for measuring the μ_a and the μ_s of fruits and vegetables separately. Cubeddu et al. (2001) applied the time-resolved reflectance spectroscopy

to determine the μ_a and μ_s of apples. Fraser et al. (2003) presented a NIR laser-based system to measure the absorption and scattering parameters of the skin and flesh of mandarins. Saeys et al. (2008) measured the μ_a and μ_s of the apple skin and flesh from 350 to 2200 nm using the inverse adding doubling method (Prahl et al., 1993b). Qin and Lu (2007, 2008) presented a spatially resolved technique based on the hyperspectral diffuse reflectance to estimate the absorption and scattering characteristics of milk, fruit juices, and a number of fruits and vegetables. Similar spatially resolved approaches were used to study the scattering characteristics of normal and bruised apples (Lu et al., 2010) and pickling cucumbers (Lu et al., 2011).

Onion is one of the top three largest fresh vegetables of the U.S. in terms of the production value (United States Department of Agriculture, 2013). However, grading and monitoring onion quality using automated methods remains a big challenge for the onion industry. The main reason is that onions have multilayer flesh scales covered by heterogeneous dry skins. Conventional color imaging based sorting systems are ineffective for onion quality inspection since the surface color or texture information of onions is not indicative of their quality factors. As a result, there is intensive use of human labor and reliance on visual inspection for onion grading and inspection. Thus, more capable and non-destructive automated sensing techniques are greatly needed. Recently, our group explored the potential of applying spectral imaging to detect onions with sour skin (Wang et al., 2012a; Wang et al., 2012d) and predict the onion's internal quality (Wang et al., 2013). During these trials, it became apparent that greater understanding of the optical properties of healthy and diseased onion tissues was needed so that light propagation in onion tissues could be understood and the most indicative optical features of onion tissues could be identified. Once understood, threshold values could be established for these properties and used to develop an onion quality inspection system. In addition, if the

optical properties of onion tissues are known, the light-onion tissue interactions could be simulated based on theoretical models and simulation tools, which leads to the possibility of numerically evaluating and optimizing the system design.

The objectives of this study were to measure the light absorption and scattering properties of onion dry skins and flesh in the broad visible and NIR spectral regions, and evaluate the potential of distinguishing between healthy and disease-infected onion tissues via their optical properties. Specific objectives were to: (1) build and calibrate integrating sphere-based spectroscopic systems to measure the total reflectance, total transmittance, and collimated transmittance spectra of onion dry skins and flesh in 550-1650 nm; (2) use the collected spectra to calculate the μ_a, μ_s', and g of onion dry skins and flesh using the inversing adding doubling method; and (3) compare the optical properties between tissues of healthy onions and onions with sour skin or neck rot.

4.3 Materials and Methods

4.3.1 Plant materials and sample preparation

Pungent Spanish yellow onions (produced in Mexico) were purchased from the local grocery store in Tifton, Georgia, USA. Sixty jumbo size, disease-free onions were visually inspected and selected. Onions were randomly divided into three groups (20 per group). Onions in the first group, treated as healthy onions, were stored in a refrigerator (6 ±1°C) for 6-8 days before testing. Onions in the second and third groups were inoculated with *Burkholderia cepacia* (bacterium) and *Botrytis aclada* (fungus) respectively, which cause the two of the most common postharvest diseases (sour skin and neck rot) in the U.S. onion industry, respectively. Both *B. cepacia* and *B. aclada* used in the test were isolated from naturally diseased plants in the state of Georgia and cultured on potato dextrose agar medium under controlled conditions. To inoculate onions with the sour skin pathogen, a lightly turbid suspension of *B. cepacia* was prepared in

sterile tap water and injected into onions (1.5 ml per onion) under the second flesh scale at the root cap. To prepare the onion samples with neck rot, onions were emerged in a turbid suspension of *Botrytis aclada* spores for 10 minutes and then 1.5 ml of the suspension were infiltrated into the second fleshy scale of each onion. Inoculated sour skin samples were incubated at 30±1°C for 4-6 days before testing, and the inoculated neck rot samples were incubated in a humidity chamber (20±1°C, relative humidity>80%) for 9-15 days until disease symptoms were visible on the onion surface.

4.3.2 Instrumentation setup

Figure 4.1 (A) shows the configuration of the spectroscopic system used for collecting the spectra of onion tissues. The light source was provided by a DC-regulated fiber optic illuminator (model DC-950, Dolan-Jenner Industries, Boxborough, MA, USA) with a goose neck light guide. The illuminator used a 21V 150 Watt quartz halogen lamp and the color temperature of the lamp was 3250° Kelvin. A kinematic V-clamp mount (model C1503, Thorlabs, Newton, NJ, USA) and another customized holder were used to hold the light guide in a fixed position. An integrating sphere (model 4P-GPS-060-SF, Labsphere, North Sutton, NH, USA) was used as the light trapper and diffuser. The sphere had an internal diameter of 152 mm and four 25.4 mm diameter ports at 0^o, 90^o, 180^o, and the north pole. The sphere was coated with a highly reflective material (Spectraflect®, Labsphere, North Sutton, NH, USA) that the reflectivity was greater than 98% in the test spectral range. As a result, when light entered into the sphere, it was uniformly reflected and scattered around the sphere's interior wall, which produced a spatially standardized field of radiation.

Since the measuring approach used in this study required a collimated narrow light beam as the incident ray, collimators were used to collimate the divergent light of the fiber optic

illuminator to a 1.5 mm diameter light beam. However, due to the limitation of the spectral working range of the off-the-shelf collimators, two collimators (model F240SMA-B and F240SMA-C, Thorlabs, Newton, NJ, USA) were used to cover the whole expected spectral region: one (F240SMA-B) was used for the spectral region of 500-1000 nm and the other one (F240SMA-C) was used for the spectral range of 900-1700 nm. Both collimators had the same focus length (7.93 mm) and numeric aperture (0.5). The collimator was mounted in the front of the ferrule of the light guide using a custom aluminum adapter. A needle-shaped aluminum spacer was constructed to accurately control the distance (8 mm) between the collimator and the sample so that the power and the size of the collimated light beam were consistent in all measurements.

Two collimators, two spectrometers (the visible-near infrared (Vis-NIR) spectrometer (model USB4000, Ocean Optics, Dunedin, FL, USA)) and the NIR spectrometer (model CD024252, Control Development, Inc. South Bend, IN, USA) were used in conjunction with one another to cover wavelengths both shorter and longer than 950 nm. An optical fiber (400 μm diameter and 0.37 numerical aperture) (model M32L02, Thorlabs, Newton, NJ, USA) was used to deliver the light to the spectrometer from the integrating sphere. The sample holder and the integrating sphere were mounted on an optical rail using adjustable posts. The optical rail and other optical components were mounted on an optical bench and enclosed in a custom 600×400×500 mm (W×L× H) dark chamber. Considering the sensitivity difference between the two spectrometers, the power of the illuminator and the integration times of the spectrometers were adjusted to different levels in different setups to avoid the saturation of the detector. The detailed configurations of the instrumental setups used in the Vis-NIR and NIR spectral regions are listed in Table 4.1.

According to our calibration tests, the collected spectra in the Vis-NIR had low signal-to-noise ratios (S/N) in the wavelength ranges lower than 550 nm and higher than 880 nm. The noise could be mainly caused by two factors: (1) the Vis-NIR spectrometer had low quantum efficiency in the short and long wavelength region, and (2) the anti-reflective coating of the collimator affected the light transmittance in the short and long wavelength regions. In this study, only the spectra in the wavelength range of 550-880 nm were used where the S/N of the spectra was higher than 100. Similarly, the data at the wavelengths shorter than 950 nm and longer than 1650 nm were removed from the NIR spectra due to the low S/N of the signal. In summary, the optical properties of onion tissues were evaluated between 550-880 nm (Vis-NIR) and between 950-1650 nm (NIR).

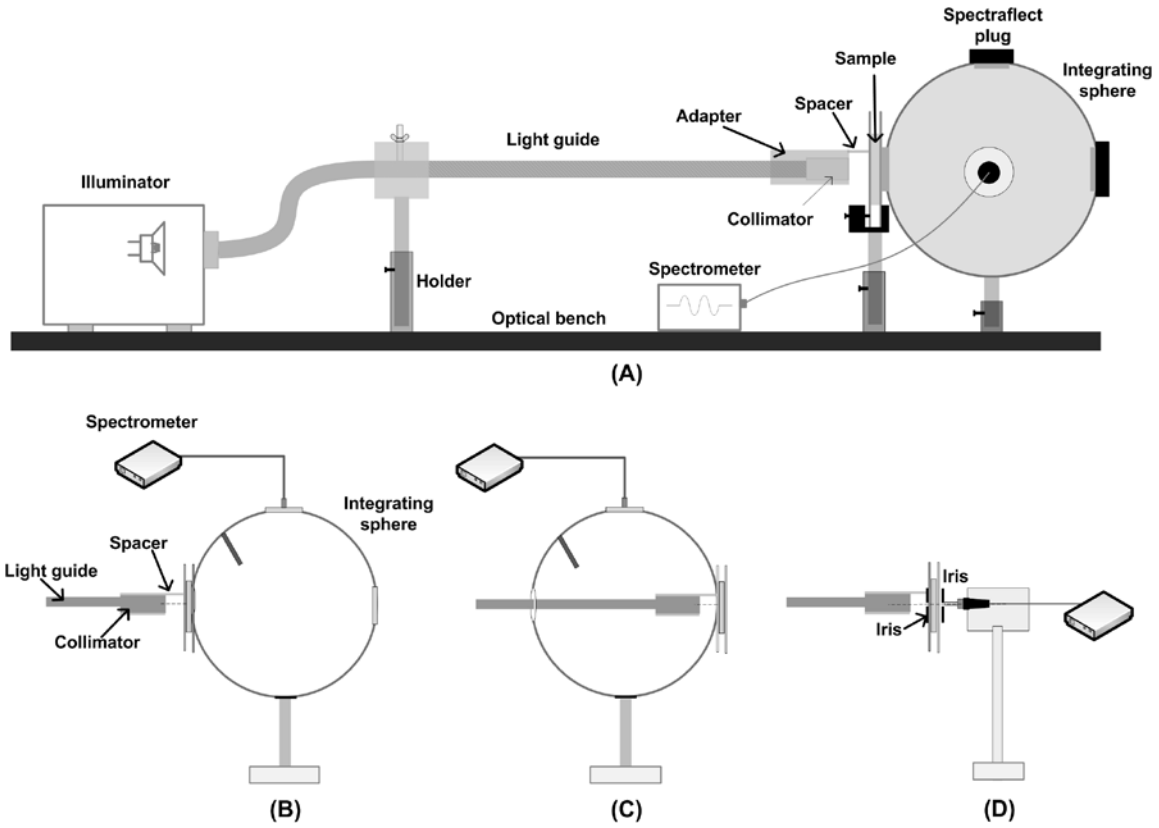

Figure 4.1. The hardware components of the integrating sphere-based spectroscopic systems (A), and the schematics for measuring the three types of the spectra: the total transmittance *T* (B), the total reflectance *R* (C), and the collimated transmittance *Tc* (D).

Table 4.1. Key devices and parameters used for collecting the reflectance and transmittance spectra of onion dry skins and flesh.

Devices	**Vis-NIR**	**NIR**
Integrating sphere	4P-GPS-060-SF, Labsphere, North Sutton, NH, USA	
Illuminator	DC-950, Dolan-Jenner Industries, Boxborough, MA, USA	
Optical fiber	M32L02, Thorlabs, Newton, NJ, USA	
Spectrometer	USB4000, Ocean Optics, Dunedin, FL, USA	CD024252, Control Development, Inc. South Bend, IN, USA
Collimator	F240SMA-B, Thorlabs, Newton, NJ, USA	F240SMA-C, Thorlabs, Newton, NJ, USA
Data collection software	Spectra Suite, Ocean Optics, Dunedin, FL, USA	Spec32, Control Development, Inc. South Bend, IN, USA
Power of the illumination	~ 50 W	120 W
Integration time	50 ms for *R* and *T*, 5 ms for *Tc*	1 s for *R* and *T*, 10 ms for *Tc*
Spectral resolution	0.2 - 0.3 nm	1 nm
Boxcar width/Average	20 nm/every 20 scans	20 nm/every 3 scans
Effective spectral range	550 – 880 nm	950 – 1650 nm

4.3.3 Experimental procedure

Onions were cut into four parts longitudinally along the neck-root axis. In each quarter of the onion, tissue samples (about 35×35 mm) were selected on the equatorial area of one flesh scale and one outermost dry skin. For the healthy onions, the second flesh scale was used. For the pathogen-infected onions, the second or third flesh scale that had apparent disease symptoms was selected. All onion skin and flesh samples were trimmed to ~ 30×30 mm squares. The flesh scales were slightly shaved to be slabs using a blade. In total, 240 pieces of onion dry skins and 240 pieces of onion flesh samples were tested. The thickness of each tissue sample was measured by using an electronic micrometer (model 35-025, iGaging, San Clemente, CA, USA) with a precision of 0.001 mm. Each onion tissue sample was measured three times and the average value was used. Then, onion tissue samples were stored in Petri dishes to minimize desiccation. In the test, the onion tissue sample was sandwiched between two pieces of 70×105×2 mm Borofloat glass slides (transmittance >90%). A U-shaped clamp was used to hold the sample

with moderate pressure on the glass slides so that the onion tissue was in a slab shape. The position of the sandwiched onion tissue was adjusted to cover the whole entrance/exit port.

As illustrated by Figure 4.1 (B), the total transmittance *T* was measured when the sample was placed in front of the entrance port of the sphere and the opposite exit port was covered by a Spectraflect plug. The total reflectance *R* was measured when the sample was placed behind the exit port (Figure 4.1 (C)). One challenge of measuring R was if the distance between the collimator and sample was too large, the collimated light beam would greatly diverge. Thus, in this test, the light guide was placed into the integrating sphere so that the collimated light beam was at the same size as the one in *T* measurements. The part of the light guide inside the sphere was wrapped by aluminum foil to minimize the light loss caused by the light guide. Figure 4.1 (D) shows the hardware configuration for the collimated transmittance T_c, which measured the light directly transmitted through the sample. The setup was similar to the approach recommended by Prahl (2011): a 1 mm diameter iris was placed between the collimator and the sample to constrain the position and the size of the incident beam, and the other iris in front of the detector blocked the ambient scattered light from entering the spectrometer.

4.3.4 System calibration and data preprocessing

A number of calibration tests were conducted to correct the responses of the systems. A serial of data preprocessing operations were applied to mitigate the system noise and prepare the data in a format to be processed easier in later steps. The whole data calibration and preprocessing process is illustrated in Figure 4.2.

At first, the wavelength accuracies of the Vis-NIR and NIR spectrometers were calibrated by using a Krypton spectral calibration lamp (Model 6031, Oriel Instruments, Stratford, CT, USA). The Krypton lamp was held by a U-shaped clamp and the bulb (about 40 mm long) was

placed inside the integrating sphere, with all other ports covered by Spectraflect plugs. The lamp was turned on and warmed up for 30 minutes before the test. For each hardware configuration, 20 spectra of the Krypton lamp were collected and the average spectrum was calculated. The wavelength shifts were evaluated by comparing the wavelength positions of the apparent peaks to their known positions, and the correction model was developed using quadratic curve fitting. According to the result of the wavelength accuracy test, the spectroscopic systems using the NIR spectrometer had very slight wavelength shifts (<1 nm) in the wavelength range of 950-1650 nm. Thus, no correction was conducted for the collected NIR spectra. The Vis-NIR configuration, however, showed substantial (>1 nm) wavelength shifts. Thus, all Vis-NIR spectra were processed using the developed wavelength correction model: n_{cal}=1.588e-5 n^2 + 1.068 n – 53.94, in which n is the original wavelength number (in nm) and n_{cal} refers to the corrected wavelength number.

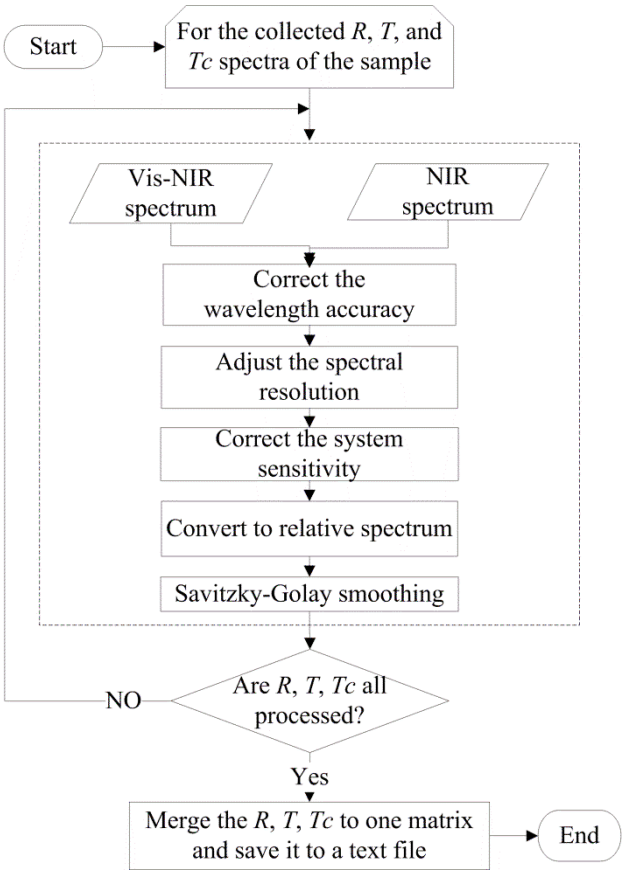

Figure 4.2. Flow chart of the system calibration and data preprocessing procedure for the collected spectra of onion tissues.

Next, the spectral sensitivities of two hardware setups were investigated and calibrated. Ideally, the response of a spectroscopic system should be linear to the intensity of the input spectral radiance. However, the spectral sensitivity of the systems used in this study could be affected by the non-linearity of spectrometer, coating of the collimators, stray light, system noises, etc. Thus, a calibration test was needed. Figure 4.3 shows the instrumental setup for the sensitivity correction test, which mainly used a multi-step contrast gradient target (Model SRT-MS-050, Labsphere, North Sutton, NH, USA). The gradient panel has four sub-panels with known reflectance rates of 99%, 50%, 25%, and 12%, respectively. The panel was placed on a

holder mounted on a rail guide so that the panel could be moved along the rail guide, while the collimator and the detector stayed in fixed positions. The collimator was a distance of 8±1 mm from the center of the illuminated area. The distance between the front end of the detector and the measuring point was 3±0.5 mm. Both the incident light beam and the detector were placed in 60^{o} angles to the horizontal surface of the reflectance target.

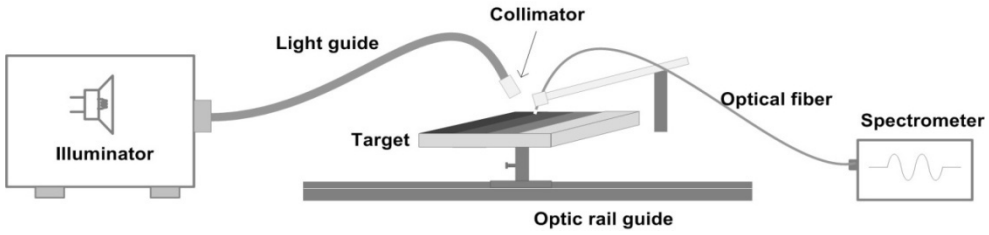

Figure 4.3. The instrumental configuration for the spectral sensitivity corrections of the Vis-NIR and NIR spectroscopic measurements.

For each sub-panel, 20 measurements were conducted and the average spectrum was collected. The baseline signals of the spectrometers, measured by covering the front of the optic fiber with a black plastic cap, were removed from all the corresponding spectra. The raw reflectance spectra of 50%, 25%, and 12% panels were converted to relative spectra, by calculating their ratios to the spectrum of the 99% reflectance panel. Then, the relative reflectance spectra of the three panels were compared to their real reflectance values (provided by the manufacture) across the whole wavelength region. The correction models were developed using linear regression between the measured and the real reflectance values. Based on the results of the spectral sensitivity calibration tests, three correction models were developed and applied to the spectra across the whole wavelength range:

$$y = \begin{cases} 0.991x + 0.633 & (550\text{ nm} < n < 700\text{ nm}) \\ 0.995\,x + 0.699 & (700\text{ nm} \le n \le 880\text{ nm}) \\ 1.006\,x - 1.524 & (950\text{ nm} < n < 1650\text{ nm}) \end{cases}$$

where x and y denotes the reflectance values before and after the sensitivity correction, respectively, and n indicates the wavelength number.

After the corrections of wavelength accuracy and spectral sensitivity, the spectral resolutions of the Vis-NIR and NIR spectra were re-sampled to the same scale (2 nm). Then, all T, R, and T_c spectra were converted to relative measurements by:

$$R = \frac{R_s - D}{R_r - D},\ T = \frac{T_s - D}{T_r - D},\ \text{and}\ T_c = \frac{TC_s - d}{TC_r - d}$$

where R_s and T_s indicate the acquired raw reflectance and transmittance spectra of the sample, respectively; R_r refers to the white reference spectrum for the total reference (Figure 4.3 (C)) and T_r refers to the total transmittance (Figure 4.3 (B)), measured when the exit port of sphere was covered by the Spectraflect plug; D refers to the dark signals of the spectrometers measured by covering the entrance port of the integrating sphere. TC_r is the original collimated transmittance spectrum of the sample (Figure 4.3 (D)); TC_s indicates the white reference spectrum for T_r, collected when no sample was presented between the collimator and the detector; d refers to the dark signal of the spectrometer, measured by covering the detecting ferrule of the optical fiber by a black plastic cap.

After the relative conversion, Savitzky-Golay filter (Williams and Norris, 2001) was applied to remove the multiplicative scattering effect in the spectra. Then, for each onion tissue sample, its R, T, and T_c spectra in the NIR region were merged to their counterparts in the Vis-NIR region. At the last step, the merged relative spectra (R, T, T_c) of each sample were saved into a single text file for the later use.

4.3.5 Estimation of optical properties

The absorption coefficient μ_a, the reduced scattering coefficient μ_s', and the scattering anisotropy coefficient g of onion tissues were estimated by the open source inverse adding doubling (IAD) program provided by Prahl (2011). Based on the measured R, T, and T_c spectra of the onion tissue, the IAD method estimated the optical properties (μ_a, μ_s', and g) of the onion sample by repeatedly solving the radiative transport equation until the solution matched the input spectral measurements. The detailed algorithm of the IAD method can be found in Pickering et al. (1993) and Prahl et al. (1993b).

The accuracy of estimating the μ_a, μ_s', and g using the proposed system and the IAD method was validated by liquid phantoms. The phantoms were made from the standard scattering material (Intralipid 20%, Sigma-Aldrich, St. Louis, MO, USA), absorption dyes (Nigrosin and Naphthol Green B, Sigma-Aldrich), and distilled water. Pure absorption solutions were first made by mixing small amounts of Nigrosin and Naphthol Green B with distilled water. The μ_a of absorption solutions were calculated by its collimated transmittance of the solutions using the Lambert-Beer law. Then, Intralipid 20% was pipetted into the pure absorption solutions to make emulsions diluted to final concentrations of Intralipid 20% at 0.5% and 1%. The reference μ_s' values of the phantoms were referred from the values reported by Ninni et al. (2011) at three wavelength bands: 632.8, 751, and 833 nm (Ninni et al., 2011). The reference values of g were calculated using the equation of van Staveren et al. (1991): $g(\lambda) = 1.1 - 0.58\lambda$. It has to be noted that low concentration scattering emulsions were used because the light path of the cuvette was relatively large and a low concentration scattering emulsion allows a detectable light transmittance signal.

A 14 ml glass cuvette with the 10 mm light path was used to hold the liquid emulsions in the course of the spectroscopic measurements. The side wall of the cuvette was 40×40 mm, which was larger than the entrance port of the integrating sphere. Three replicates were conducted for each phantom and the cuvette was cleaned by rinsing with distilled water before and after each measurement. The μ_a, μ_s', and g values of the phantoms were estimated by the IAD method based the measured spectra. The estimated μ_a, μ_s', and g values of the phantoms were compared to their reference values at the three wavelength bands: 632.8, 751, and 833 nm. The results showed that the estimations of μ_a showed 0.02%-7.64% difference to the reference value at the three verified bands, with an average error of 6.5%. The average estimation errors of the μ_s' and g were 5.0% and 0.9%, respectively. As stated by Prahl et al. (1993b), the error of estimating the μ_a and μ_s' should be caused by the experimental uncertainties such as the light loss at the edge of the sample and the scattered light included in measuring the collimated transmittance.

In all IAD calculations for onion tissues, the refractive indices of onion dry skin and flesh were set to be 1.334 and 1.352 respectively based on our experimental measurements using the Abbe refractometer (Abbe Mark II, Reichert, Inc., NY, USA). The reflectivity of the integrating sphere was set as 98% based on the data sheet provided by the manufacturer. A Python program (Figure 4.4) was developed to process the spectra of the onion tissues and execute the IAD estimations in batch. The program preprocessed the collected spectra using the algorithms stated in the previous section and created the input files for the IAD program. It generated a script file to batch execute the IAD calculations. After all IAD estimations were complete, the program extracted the results from the IAD output files and saved the results to a text file. The program also provides functions for visualizing the spectra of estimated μ_a, μ_s', and g.

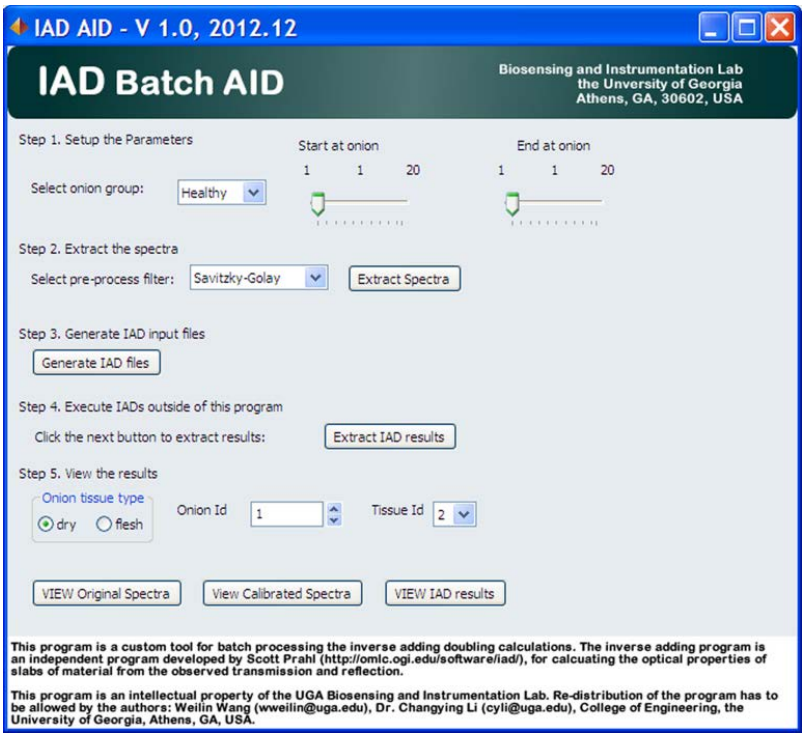

Figure 4.4 Program for preprocessing the spectra of onion tissues and batch processing the inverse adding doubling calculations.

For each onion tissue sample, the un-converged IAD estimations were removed from its μ_a, μ_s', and g spectra. To evaluate the difference between the optical properties of onion tissues in different groups, statistical tests were performed at the wavelengths divisible by 50 nm, respectively. The normality of the data at each wavelength was examined using Jarque-Bera test. If the distributions of the both groups under comparison were normal, student t-test was conducted to compare the mean values of two groups using the significance level of 0.05. Otherwise, non-parametric statistic Wilcoxon rank sum test was used to compare the medians of the two groups. All statistical tests were conducted using the functions provided by the statistic toolbox of MATLAB (v2012b, MathWorks, MA, USA).

4.4 Results and Discussion

4.4.1 Optical properties of healthy onion tissues

Figure 4.5 (A) shows the average spectra of the absorption coefficient μ_a of onion dry skins and flesh. In the visible spectral range of 550-750 nm, the μ_a of onion dry skins (the solid curve in Figure 4.5 (A)) showed a consistent trend of decreasing as the wavelength increased. The μ_a of the dry skin at 550 nm was 12 times higher than that of 750 nm. It is known that the onion dry skin has a high content of pigments such as flavonols and anthocyanin (Griffiths et al., 2002), which strongly absorb light in the blue (450-495 nm) and green (495-570 nm) spectral regions, respectively. Thus, the decreasing absorption curve in 550-750 nm on the right side of the light absorption crests was caused by pigments in the onion dry skin. In the spectral regions in 750-1350 nm, the mean spectrum of the μ_a of the onion dry skin was relatively flat, without any apparent absorption peak. From 1350 nm to 1650 nm, a strong absorption crest occurred, in which the greatest μ_a was about three times higher than those at 750-1350 nm. This strong light absorption peak was most likely caused by residual moisture retained in the onion dry skin.

The μ_a of onion flesh (the dashed curve in Figure 4.5 (A)) were 10-180 times lower than those of dry skins in the visible spectral region. The results fit the expectation since the pigment content of the onion flesh is much smaller than that of the dry skin. In the wavelengths shorter than 880 nm, no obvious absorption peak was observed in the μ_a spectrum of onion flesh. In the NIR region, three absorption peaks were observed around at 970, 1190, and 1450 nm, which should be caused by the light absorption of water. The μ_a values of onion flesh in 930-1300 nm were significantly lower than those of onion dry skins whereas the μ_a of the flesh in 1400-1550 nm were much higher than those of dry skins. This is reasonable since the moisture content of

onion flesh is much higher than that of the dry skin, which significantly increases the light absorption in the spectral region around 1450 nm.

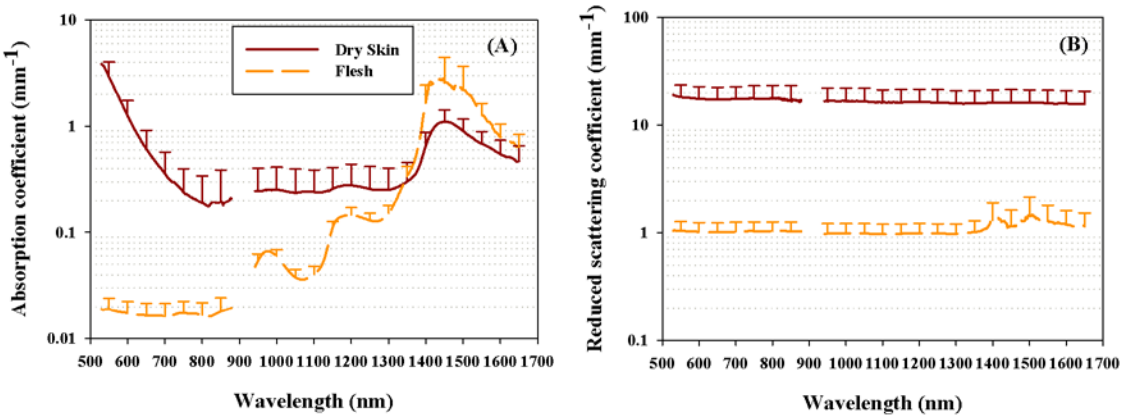

Figure 4.5. Average absorption coefficient (A) and reduced scattering coefficient (B) spectra of 80 onion flesh samples and 80 onion dry skins. The vertical lines denote one-standard deviations at the wavelengths divisible by 50 nm.

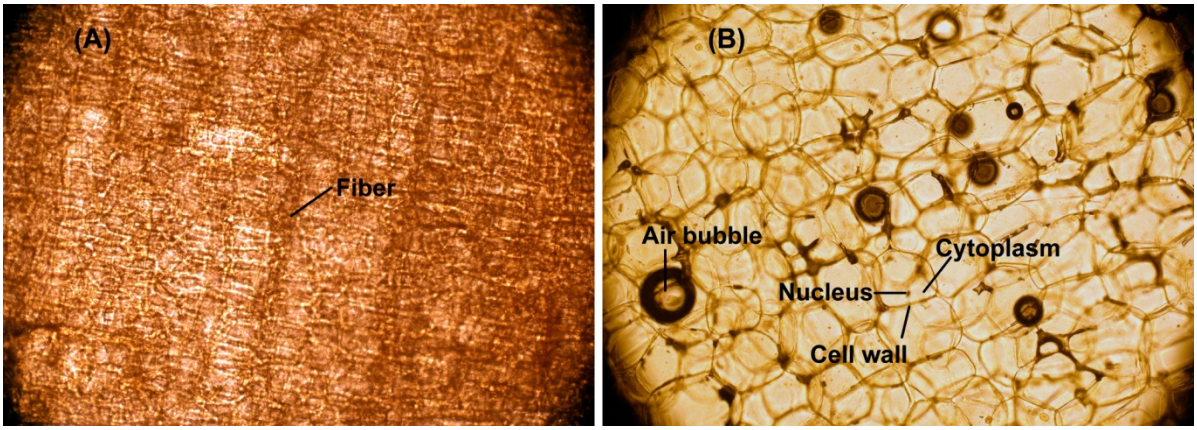

Figure 4.6. Microscope images of an onion dry skin (A) and onion flesh (B). Images were taken by Olympus IX71 microscope system using a 10X objective lens.

The mean μ_s' of dry skin (the solid curve in Figure 4.5 (B)) was about 10 times higher than those of flesh (the dashed curve in Figure 4.5 (B)) across the whole spectral region. It is known that the μ_s' of a biological tissue often reflects micro structural characteristics such as firmness (Lu, 2008). The greater μ_s' of the onion dry skin indicates that it has a denser cellular structure than that of the onion flesh, which was illustrated by the microscope images of onion dry skin and flesh shown in Figure 4.6. For either dry skin or flesh, the average μ_s' spectrum was a relatively flat curve across the whole spectral region. There were two small peaks at 1450 nm and 1500 nm in the μ_s' spectrum of onion flesh. But considering the large standard deviations, the μ_s' in this range were not significantly greater than those of other wavelengths.

The average μ_a (0.2-4 mm^{-1}) and μ_s' (15-18 mm^{-1}) of onion dry skins were in the same order of magnitude as those of apple skin (μ_a<6 mm^{-1} and $\mu_s'\approx$10-15 mm^{-1}) (Saeys et al., 2008) in the spectral range of 550-1650 nm. The estimated mean μ_a and μ_s' of onion flesh were similar to the reported optical properties of apples, kiwifruits, and pears (Qin and Lu, 2008; Saeys et al., 2008) in terms of the overall trend of the spectra and the magnitude of the values. In this work, the spectral data between 880 nm and 950 nm of the onion tissues were not included due to the limitation of the sensing capability of the employed spectroscopic systems. Based on the overall trend of the μ_a and μ_s' spectra shown in Figure 4.5, it could be expected that the μ_a and μ_s' values of the onion dry skin and flesh between 880 nm and 950 nm are in-between their counterparts at 880 nm and 950 nm. This hypothesis, however, needs to be validated in the future.

Figure 4.7 shows the mean spectra of the estimated scattering anisotropies of onion dry skins and flesh. The mean *g* values of dry skins were between 0.37 and 0.44 in the measured spectral range, indicating a moderate forward light scattering in the onion dry skin. Light in the onion flesh had relatively strong forward scattering in the wavelengths shorter than 1300 nm, and

tended to be more isotropic in the spectral region around the water absorption peak at 1450 nm. Compared to the dry skin, the onion flesh had greater forward scattering in the spectral region of 550-850 nm while showing smaller forward scattering in the wavelengths longer than 1350 nm. The large degree of variation observed in the estimated values was likely caused by biological variations within onion tissue samples. It should be noted that estimating the g by the IAD method is often prone to error since it's difficult to accurately measure the collimated transmittance T_c, particularly for the T_c through a thick biological sample (Prahl, 2011). A more accurate measurement of the g of onion tissues could be conducted by an independent study using more specific experimental devices in the future.

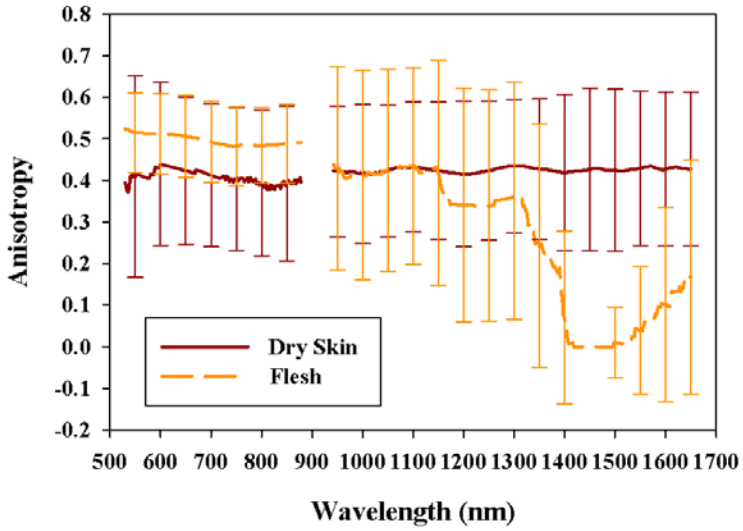

Figure 4.7. Means and standard deviations of the estimated anisotropies of 80 onion flesh samples and 80 onion dry skins.

As shown in Figure 4.8 (A), the total light attenuation coefficient ($\mu_t = \mu_a + \mu_s$) of onion dry skin (about 12 mm^{-1}) was about 10 times greater than that in flesh. For onion flesh, the relatively

strong light attenuation in the spectral region of 1400-1550 nm probably caused by water. Figure 4.8 (B) illustrates the albedo (albedo = μ_s/μ_t) spectra of the onion dry skin and flesh. It is shown that the onion dry skin is a scattering-dominated (high albedo) material in the test wavelength regions. In the wavelength region below 1300 nm, onion flesh is also a scattering dominant (albedo>0.8) material. In the wavelengths longer than 1300 nm, due to the strong light absorption at 1450 nm caused by water, the μ_a has greater impact to the overall light attenuation in the onion flesh.

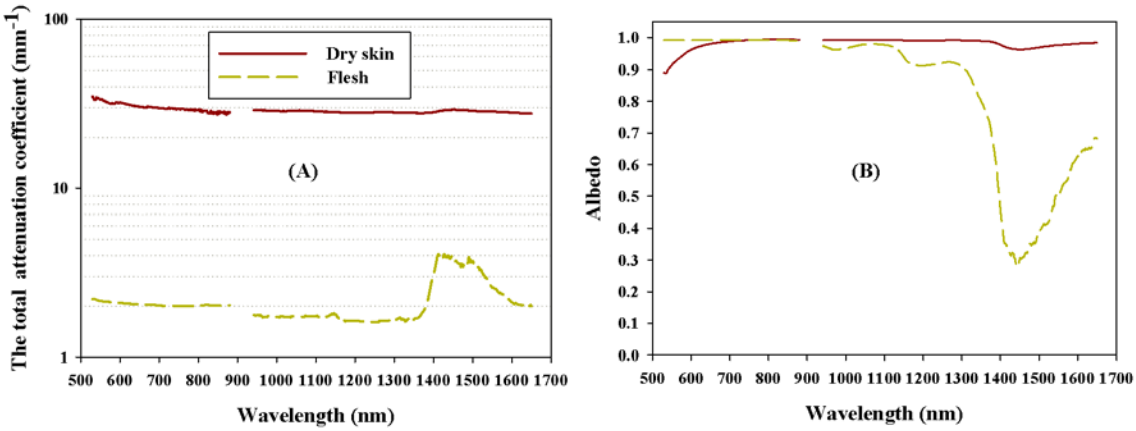

Figure 4.8. Average total attenuation coefficient (A) and albedo (B) of the measured onion flesh and onion dry skins.

4.4.2 Optical properties of the dry skins of pathogen-infected onions

In the visible spectral region of 550-600 nm, the results of the t-tests showed that the mean μ_a of the dry skins of the onions with sour skin (SS dry skins) are significantly greater than those of the dry skins of the healthy onions (HL dry skins) (Figure 4.9 (A)). This difference should be related to the color change of the SS dry skins: sour skin infection in onions usually could change the skin color of onions to be more pale yellow, which increased the light absorption in

visible spectral region. In the NIR spectral region longer than 1000 nm, the μ_a values of the SS dry skins were significantly higher than those of healthy onions, which can be explained by the change of the moisture content of the SS dry skins. When onions were infected by *B. cepacia*, they became water-soaked along with the break-down of the inner scale (Gitaitis and Nischwitz, 2006; Schwartz and Mohan, 2008b). The onion juice discharged from the rotten flesh was often absorbed to some extent by the dry skin. As a result, SS dry skins absorbed more NIR light at 1450 nm than HL dry skins due to the strong NIR light absorption band (O-H) of water.

As shown in Figure 4.9 (B), the mean μ_s' of the dry skins of the onions with sour skin were slightly (1-2 mm^{-1}) greater than those of the dry skins of healthy onions throughout the whole spectral region, while the μ_s' of the SS dry skins showed fairly large (about 6 mm^{-1}) standard deviations. T-tests confirmed that no significant difference occurred between the mean μ_s' of the SS dry skins and HL dry skins. This is reasonable since *B. cepacia* mostly resides in the onion flesh instead of the dry skin. The main impact of a sour skin infection to the onion dry skin could be from fluid discharged from the decomposing flesh scales which increases the moisture content of onion dry skins without significantly altering the cellular structure.

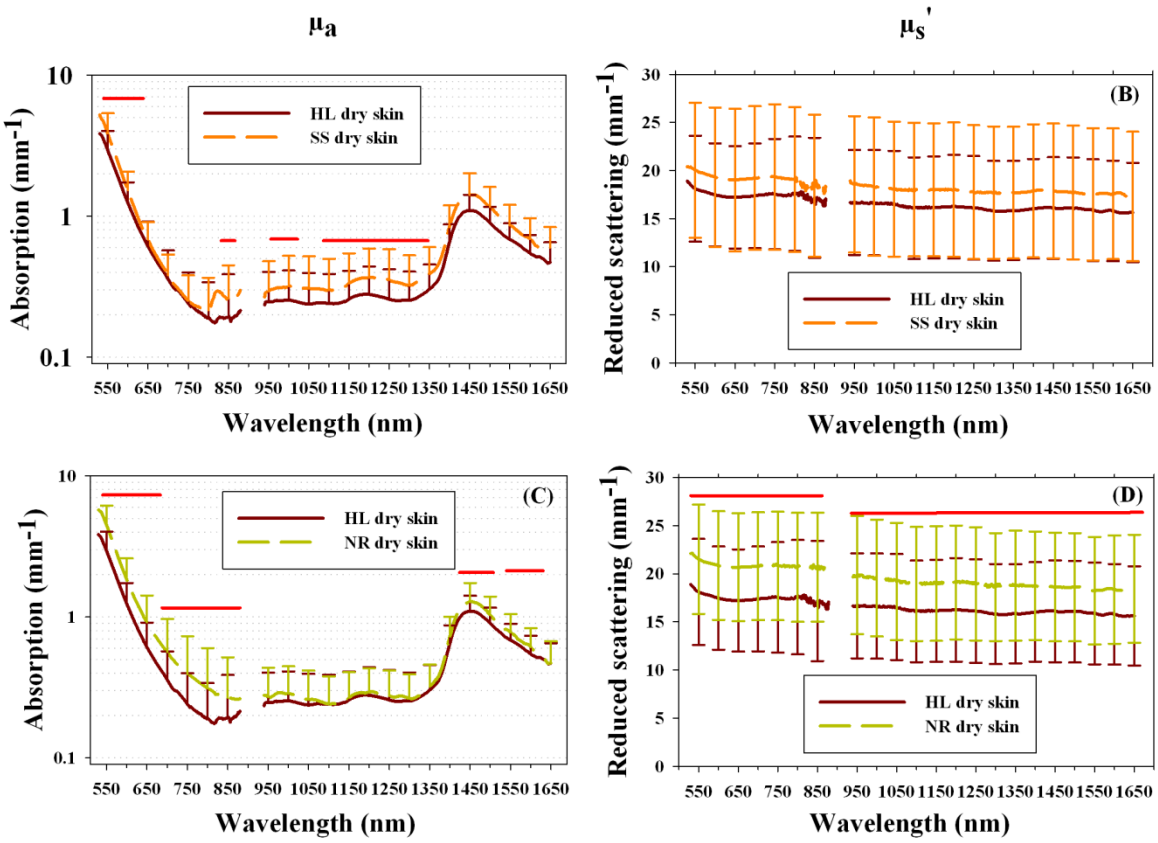

Figure 4.9. (A) average μ_a of the dry skins of the onions with sour skin (SS dry skins), and one standard deviations (upper bars) of the SS dry skins at the wavelengths divisible by 50 nm; (B) average and standard deviations of the μ_s' of the SS dry skins; (C) average and standard deviations of the μ_a of the dry skins of onions with neck rot (NR dry skins); (D) average and standard deviations of the μ_s'of the NR dry skins. The red lines indicate the spectral regions where the μ_a or μ_s'of the dry skins of the diseased onions were significantly different from those of HL dry skins (using the significance level of 0.05).

The mean μ_a spectrum of the dry skins of the onions with neck rot (Figure 4.9 (C)) showed similar patterns with the μ_a spectrum of healthy onions in terms of the overall trend. In the

visible spectral range, the mean μ_a values of the dry skins of the onions with neck rot (NR dry skins) were significantly greater than those of HL dry skins. This was probably caused by the absorption of more visible light due to the black color of the fungus growing and sporulating on the onion dry skins. In the NIR spectral range, the μ_a of the NR dry skins was not significantly different from those of healthy onions except for the region with the strong water absorption (1400-1600 nm). These results matched observations in the experiment as onions with neck rot developed significant decay later, and they had less water-soaked symptoms than the onions with sour skin during the testing period of this study. Therefore, the light absorption effect in the NIR region was less intense in the NR dry skins than in the SS dry skins.

As shown in Figure 4.9 (D), the mean μ_s' of the NR dry skins were significantly (about 3 mm^{-1}) greater than those of the HL dry skins throughout the whole spectral region. Since sour skin infections from *B. cepacia* mainly developed in the onion flesh scales and the neck rot fungus grew on both the outer dry skin and the inner flesh of onions, the light was more scattered in NR dry skins than in HL dry skins. The fungal cells on dry skins could have significantly increased the elastic light interactions which resulted in higher light scattering.

The above results showed that the sour skin (bacterial) and neck rot (fungal) infections on the onions could significantly change the light absorption and scattering characteristics of the dry skin at certain spectral regions. To distinguish the dry skin of onions with sour skin infection from that of healthy onions, the light absorption characteristics in the NIR region could be potentially useful. To detect the dry skin of onions with neck rot infections, both the μ_a and μ_s' of the onion dry skin could be indicative.

4.4.3 Optical properties of the flesh of pathogen-infected onions

Figure 4.10 (A) illustrates the mean and standard deviations of the μ_a of the onion flesh with sour skin infection (SS flesh). In the visible wavelengths, the mean μ_a values of the SS flesh were significantly greater (about 5 times) than those of the flesh of healthy onions (HL flesh). It is known that onion scales infected with *B. cepacia* would have pale yellow to light brown symptoms (Schwartz and Mohan, 2008b). This color change of the SS flesh should be the reason for the greater μ_a in the visible region. In the NIR wavelength region of 950 to 1300 nm, the mean μ_a of sour skin-infected and healthy onion flesh were not significantly different. In the spectral region where water has strong light absorption (1350-1650 nm), the average μ_a of the SS flesh was close to that of healthy onions. It should be noted that both HL flesh and SS flesh have high water content. The decayed tissue and water-soaked symptoms of the SS flesh might change the moisture content of the SS flesh, which would be the reason that the μ_a of the SS flesh showed significant differences from that of the HL flesh at certain regions in 1350-1650 nm. The difference, however, was much less profound compared to the difference shown in the visible spectral region.

As illustrated in Figure 4.10 (B), the mean μ_s' of SS flesh were significantly smaller than those of HL flesh across the whole wavelength region. It is known that onion scales with sour skin turn soft and watery since the bacterium breaks down key structural components of plant cells and their walls (Schwartz and Mohan, 2008b), as illustrated in Figure 4.11 (A). Infected onion scales even could be detached from the adjacent scales at the later stage of the infection. The changed physical properties of the SS flesh were reflected by the smaller μ_s' shown in Figure 4.10 (B). The results of t-tests confirmed that the differences between the mean μ_s' of SS flesh and the HL flesh were statistically significant.

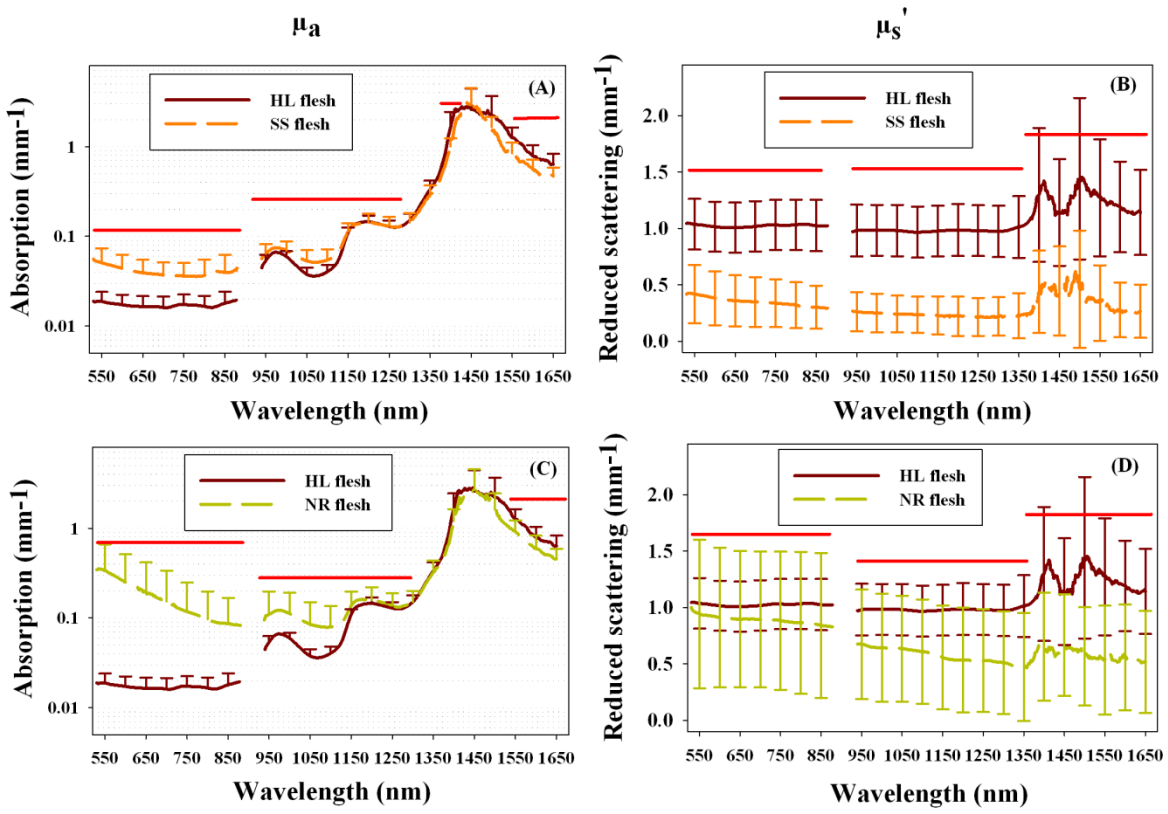

Figure 4.10. (A) average and standard deviations of the μ_a of the flesh of the onions with sour skin (SS flesh); (B) average and standard deviations of the μ_s' of the SS flesh; (C) average and standard deviations of the μ_s' of the flesh of onions with neck rot (NR flesh); (D) average and standard deviations of the μ_s' of the NR flesh. The red lines indicate the spectral regions where the μ_a or μ_s' of diseased flesh were significantly different from those of the healthy ones (using the significance level of 0.05).

The spectrum of the mean μ_a of the NR flesh (Figure 4.10 (C)) showed a similar pattern to that of the SS flesh. In the visible spectral region, the mean μ_a values of the NR flesh were about 10 times greater than those of healthy onion flesh. The greatly increased light absorption in the visible region was probably caused by sporulation and production of sclerotia by the fungus

Botrytis aclada (Schwartz and Mohan, 2008b), which would have turned the color of the NR flesh much darker (Figure 4.11 (B)). In the NIR wavelengths shorter than 1200 nm, the mean μ_a of the NR flesh was still significantly greater than those of healthy ones, which might be caused by the chemical constituents in or produced by *Botrytis aclada*. In the NIR range longer than 1200 nm, the μ_a of the NR flesh was much greater due to the strong light absorption around 1450 nm caused by water, whereas the mean μ_a of the NR flesh was mostly not significantly different from those of HL flesh in this spectral region.

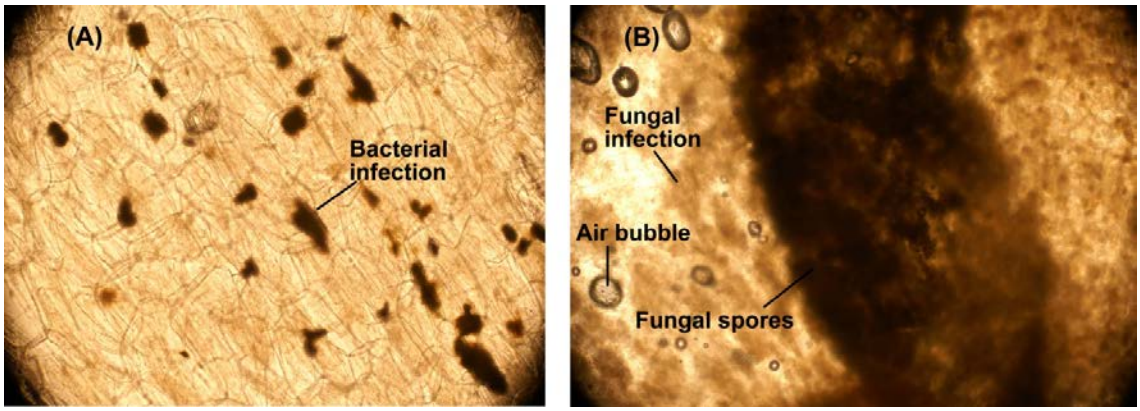

Figure 4.11. Microscope images of the onion flesh with sour skin (A) and with neck rot (B). Images were taken by Olympus IX71 microscope system using a 10X objective lens.

The mean μ_s' of the NR flesh (Figure 4.10 (D)) were generally smaller than those of the HL flesh, indicating a lower light scattering in the NR flesh than in the HL flesh. The results of the t-tests showed that the mean μ_s' of the NR flesh were significantly (about one fold) smaller than those of the healthy onions in the NIR region longer than 700 nm. As shown in the Figure 4.10 (C) and (D), the μ_a and μ_s' of the NR flesh showed relatively large standard deviations, which were caused by biological differences among the onion samples and the variations of the disease levels of the NR flesh samples.

It is observed that the differences of the mean μ_s' between the NR flesh and HL flesh were less distinctive compared to the differences of the μ_s' between the SS and HL flesh. This could be explained by the following reasons. First, the breaking down of cell walls and colonization of onion tissues by *B. aclada* would reduce the light scattering effect, while spores and sclerotia on decaying tissues would increase the light scattering as compensation. On the other hand, although in this study the mean μ_s' decreased more in the SS flesh than in the NR flesh, the changes of the optical properties of the diseased onion flesh could be related to the actual level of the infection.

In summary, both sour skin (bacterial) and neck rot (fungal) infections significantly affected the light absorption and scattering properties of onion flesh. The differences between the μ_a and μ_s' of healthy and pathogen-infected onion flesh were more profound than the differences between those of healthy and pathogen-infected onion dry skin. It is promising to distinguish the pathogen-infected onion flesh from the healthy onion flesh by investigating their μ_a in the visible wavelengths and their μ_s' in the Vis-NIR spectral range.

4.5 CONCLUSIONS

The optical properties of onion dry skins and flesh were measured in the spectral region of 550-1650 nm. The results showed that onion tissues are a scattering dominated (high-albedo) medium in the spectral region of 550-1300 nm. The μ_a of onion tissues is mainly associated with the pigment content in the visible spectral region and is affected by the moisture content in the NIR spectral region of 1400-1650 nm. The μ_s' values of onion dry skins are more than 10 times higher than those of onion flesh. Overall, the estimated μ_a and μ_s' of onion tissues were comparable to the reported optical properties of other fruits and vegetables. The measured optical

properties of onion tissues can be used to simulate light propagation in onion tissues using theoretical models and simulation tools.

This study illustrated that there are several potentially useful optical parameters for detecting pathogen-infected onions: (1) the μ_a of the onion dry skin/flesh in the visible spectral range, which reflects the color change of the dry skin/flesh caused by the pathogen; (2) the μ_a of the onion dry skin in the NIR spectral range, which indicates the moisture content of the dry skin; and (4) the μ_s' of the onion flesh in the Vis-NIR region, which could be a good indicator of level of decomposition in the onion flesh. These results can be applied to develop appropriate optical techniques and systems for the safety and quality inspection of onions.

4.6 ACKNOWLEDGEMENTS

This work was funded by the USDA NIFA Specialty Crop Research Initiative (Award No. 2009-51181-06010). The authors also gratefully acknowledge Mr. Anthony M. Dean for his assistance in data collection.

CHAPTER 5

PHENOTYPING OF SWEET ONIONS USING CONSUMER-GRADE RGB-DEPTH SENSOR[3]

[3] Weilin Wang and Changying Li. To be submitted to Transactions of the ASABE.

5.1 ABSTRACT

Size estimation is an important step in the postharvest sorting and grading of onions. This work applied the RGB-depth (RGB-D) sensor to measure the size (maximum diameter and volume) of sweet onions and to estimate their density nondestructively. In the study, RGB-D images of Vidalia sweet onions and Mexican sweet onions were acquired when placed at six different orientations. The maximum diameter of onions was calculated in 2-D and 3-D Euclidean space using their color and depth images, respectively. The depth images of onions were converted to voxel images. Based on the volume of the voxel images, mathematical and linear regression models were developed to predict the volume of the onions. Results showed that using single color image or depth image captured at random orientation, the onion diameter estimated by the depth image achieved a higher accuracy and robustness (root mean squared error (RMSE) was 2 mm) than the method using the color image (RMSE=3.4 mm). Using single depth image, the volume of onions predicted using linear regression model showed a RMSE of 18.5 cm^3 and an accuracy of 96.3%. The accuracy of estimating the maximum diameter and volume of onions can be further improved by using the average of multiple measurements. Statistical tests illustrated that the density estimation method based on the depth imaging was statistically comparable to the conventional experimental approach. The results of this study could be applied to improve the efficacy and efficiency of the size estimation of onions in postharvest sorting and classification. The proposed methods can also be adapted for the size estimation of other fruits and vegetables.

5.2 INTRODUCTION

Sweet onion is an important specialty crop widely grown in North America and Europe for the past two centuries (Brewster, 2008). Compared to pungent onion varieties, sweet onions have low sulfur content, higher sugar content, and higher water content, resulting in s sweeter and milder taste. Due to the lower content of natural disease inhibitors (such as sulphur-containing compounds), sweet onions often have shorter shelf life and are more prone to mechanical injury and postharvest diseases than other onion varieties. To guarantee clean and safe products for customers, sweet onions have to be handled and graded with stringent quality inspection in harvest and postharvest operations.

Size is one of the most important metrics for grading sweet onions. Grading sweet onions into size groups is highly necessary for packing and assigning price differentials since large sweet onions are generally more preferred by customers. Moreover, it is reported that the total onion yield has a direct relationship with the plant density: greater plant density can increase the amount of small and nonmarketable onion bulbs (de Visser and van den Berg, 1998). If the size information of mature onion bulbs can be accurately estimated, growers can adjust the plant density accordingly to achieve higher marketable bulb yield the following year. In addition, the size and the size uniformity of mature onion bulbs are important traits for evaluating the cultivars in breeding and phenotypic selection of sweet onions (Mallor et al., 2011). In summary, monitoring the size of mature onion bulbs in postharvest is essential for sweet onion production.

The size of fresh fruits and vegetables can be described by different parameters such as volume, weight, length, and diameter (Moreda et al., 2009). For sweet onions, volume might be the most accurate description of the size of onion bulbs. However, it is quite difficult to measure the volume of the bulb in traditional onion postharvest handling. In practice, weight is

commonly used for bulk estimation since it is directly related to packing. Because most onions are approximately spheroid or ellipsoid shaped, the maximum diameter of the equatorial section of onion is defined as the main sizing metric in onion sorting and marketing standards. According to the onion grading standard of United States Department of Agriculture (USDA, 1995), the diameter of the U.S. No. 1 grade onions must be larger than 38 mm and 40% should have a diameter larger than 50.8 mm.

Currently, several types of automated sizing devices are predominantly employed in the U.S. onion packinghouses: mechanical, machine vision-based, and electronic weight sizers. Mechanical onion sizers use mechanical conveying devices and shakers to move onions over a set of holes/spaces of stipulated sizes where small-sized onions fall through the smaller holes first and larger-sized onion bulbs fall successively in the following bigger holes. This is a relatively efficient method since sizers evaluate onion size and separate onions into different size groups during one operation. Nevertheless, this method physically impacts the onion bulbs and results in invasive injuries. Electronic weight sizer is a low-cost alternative of mechanical onion sizers for sorting onions into different sizes. However, estimating the maximum diameter of onion from its weight is not very accurate since the length ratio and the density of onions vary in different bulbs (Brewster, 2008). Consequently, contemporary commercial onion sorting systems often use machine vision-based methods to measure the maximum diameter of onion nondestructively. The main technical limitation of current machine vision-based methods is that they are based on monocular grayscale or color imaging methods and lack the information of the test object in the third dimension (the camera-to-onion axis). To improve the accuracy, onions have to be rotated by mechanical or electronic rollers to take multiple images and make several estimations, which can cause more physical injury in onions and reduce the throughput of the

online sorting. Moreover, these 2-D monocular imaging systems are not capable of estimating the volume of sweet onions.

Recently, three-dimensional (3-D) machine vision systems have been increasingly researched and applied to measure the size of agricultural products. Based on the method of generating 3-D graphs, Moreda et al. (2009) classified the 3-D machine vision methods into *passive* and *active*. *Passive* 3-D imaging methods extend the conventional 2-D imaging methods to multiple views and then combine the multiple 2-D images into a 3-D image cue (known as *shape from X*). Among various *passive* techniques, the volume intersection (VI) method has been considered to be a promising approach for estimating the volume of fresh fruits and vegetables (Imou et al., 2006; Lee et al., 2006). The VI method takes 2-D images (silhouettes) of the object with prior knowledge of its shape, and applies a relatively comprehensive image processing algorithm to extract its size feature (Laurentini, 1994; Mulayim et al., 2003). *Active* 3-D machine vision methods refer to the triangulation 3-D systems which use patterned lighting such as laser point scanners and encoded light-stripe to measure the shape and depth features of the object. A classic device used by *active* 3-D machine vision systems is the laser-based range camera, which measures the distance information from the surface of the object to the camera using the time of flight (TOF) technique. Partly due to the high cost and complexity of building the system, *active* 3-D machine vision methods like TOF techniques have not been well adapted in fruit and vegetables industry for estimating the size of products.

RGB-depth (RGB-D) sensor provides a new prospect of *active* 3-D machine vision techniques. As a range camera, a RGB-D sensor can simultaneously capture depth and color images of the scene and automatically map the depth and color data, resulting in a colored point cloud in a 3-D spatial domain. An innovative product of the RGB-D sensor is the consumer-

grade Microsoft Kinect sensor released in November 2010 (Microsoft, 2010), which was developed for natural interaction in computer games (Freedman et al., 2010). As a low-cost (approximately 150 U.S. dollars) alternative for conventional laser scanners (5-10 thousands U.S. dollars or higher), the RGB-D sensor has been quickly adapted in various application areas such as robotics, indoor mapping, 3-D modeling, and forensics in the past several years (Canessa et al., 2013; Henry et al., 2010). The possibility of using the consumer-grade RGB-D sensor for the phenotyping of plant trees has been demonstrated recently by Chéné et al. (2012) and Wang and Zhang (2013). The feasibility of using a RGB-D sensor to measure the size of fruits and vegetables, however, is rarely reported in the literature.

This work aimed to measure the size of sweet onions using nondestructive imaging methods based on the RGB-D sensor. Specific objectives of this work were to:

(1) integrate a machine vision system to collect RGB-D images of onions,

(2) measure the maximum equatorial diameter of onion bulbs from their color and depth images,

(3) estimate the volume of onions using depth image, and

(4) evaluate the possibility of monitoring the density of onions nondestructively using a depth image-based approach.

5.3 Materials and Methods

5.3.1 Onion samples

Two common types of sweet onions were tested in the study: sweet onions produced in the state of Tamaulipas in Mexico, which were purchased from a local supermarket in Athens, Georgia, USA in the first week of April, 2013, and Vidalia sweet onions, which were harvested in Toombs County, Georgia, USA in the last week of April, 2013. Both Granex types of onions

had relatively flat shape. Onion bulbs of various sizes were selected from two groups of onions, with 40 for each group and 80 onions in total. In the experiment, onion samples were stored individually in zipper storage bags labeled with consecutive integer numbers and were stored at room temperature (20±1 $^{\circ}$C) for 1-2 weeks before testing.

The major equatorial axis of each onion bulb was manually recognized by searching along the equatorial area using a digital caliper with an accuracy of ±0.01 mm. The length of the major equatorial diameter was measured three times and the average value was calculated. The weight of onions was measured using a digital precision balance (Veritas L1502, H & C Weighing Systems, Columbia, MD), with an accuracy of ±0.01 gram.

5.3.2 Measuring onion volume by water displacement method

The volume of each onion was measured using the water displacement (WD) method. To avoid the water entering into the internal spaces between onion blades or being absorbed by onion dry skins, the onion was enclosed in a zipper vacuum bag (1 gallon) and then the air in the bag was vacuumed out with a handheld air pump. A square-shaped plastic bin (150×150×178 mm) was used as the measuring container. The total volume of the bin was measured by using a 500 ml and a 100 ml graduated cylinder. To minimize the error caused by water surface tension, a flat steel bar (200×15×5 mm) was placed on the top of bin as the stopper for the water filling operation.

In the test, an onion encased in the vacuumed zipper bag was placed into the plastic bin. An 8 mm diameter steel rod mounted on a stainless steel tube was placed on the top of the bin, and the height of the rod was adjusted so that the end of about 40 mm inside the bin (Figure 5.1). By this means, the onion would stay inside the bin instead of floating on the surface of the water. Water was added into the container gradually using the 500 ml and 100 ml graduated cylinders

until the top surface of the water touches the bottom edge of the stopper (the steel bar). The volume of the onion was calculated using the following equation: $V_{onion} = V_{container} - V_{zipper\ bag} - V_{rod\ in\ water}$. The volume of the empty zipper vacuum bag ($V_{zipper\ bag}$) and the portion of the steel rod immersed in the water ($V_{rod\ in\ water}$) were measured using the 100 ml graduated cylinder using WD method for three times and the average values were used. All aforementioned measurements were conducted at room temperature (20±1 $^{\circ}$C).

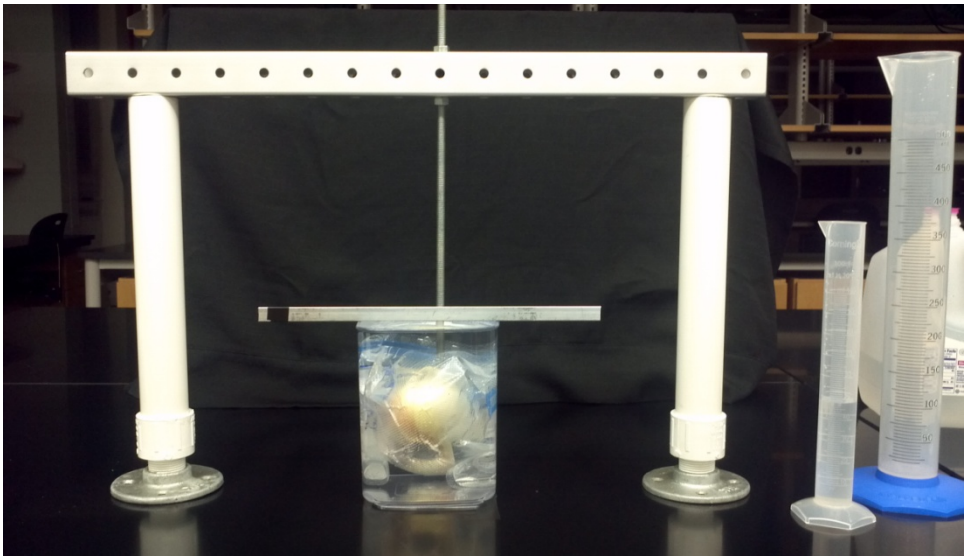

Figure 5.1. The setup of the water displacement test for measuring the onion volume

To estimate the accuracy of the proposed WD method in measuring the volume, a hard plastic ball was purchased from the local supermarket. The diameter of the ball was calculated using the digital caliper (measuring multiple times at different positions and the average diameter was used). The volume of the ball was calculated using the equation: $V = \frac{4}{3}\pi r^3$, in which r (60.4 mm) is the half of the mean diameter of the plastic ball. Then, the volume of the ball was

measured five times using the WD method and compared with the reference (calculated) value (519 cm^3). The results showed the measuring error of this WD method was 1%.

5.3.3 Imaging system

A machine vision system (Figure 5.2) was assembled to acquire RGB-D images of onion samples. A lighting chamber (1100×600×1000 mm) was built using wood and aluminum bars. The system used two 18 inch long cool-white fluorescent lamps (15 Watt, 4200 K) mounted at the upper left and upper right part of the chamber, respectively. An adjustable scanning stage was made from a compact laboratory scissors jack and wood panels. A 160×160×1 mm piece of black cardboard was glued on the top wood panel of the scanning stage to provide black background for onion images. To hold the onion in place, a small hole (30 mm diameter and 7 mm deep) was drilled at the center of the top panel of the scanning stage, which mimicked the cup holder and the roller in commercial onion processing lines. The scanning stage was placed at the center of the lighting chamber.

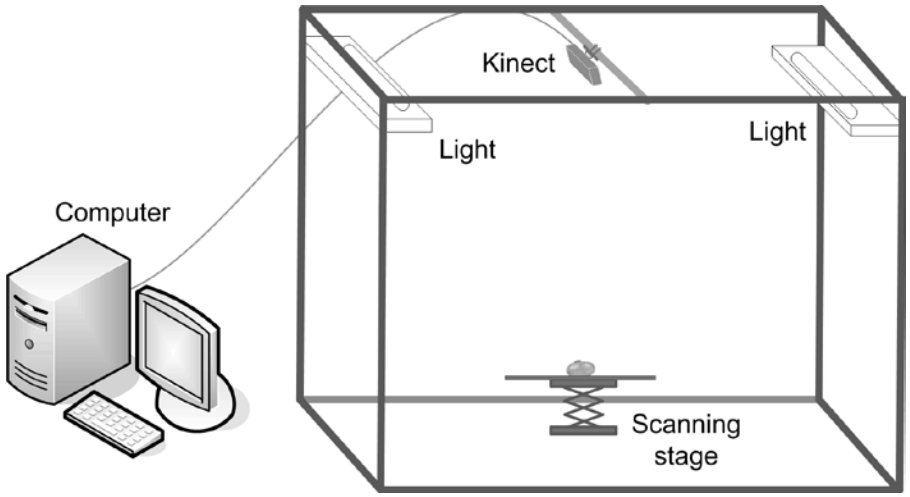

Figure 5.2. Schematic of the RGB-depth sensor-based machine vision system for measuring the size of sweet onions.

The RGB-D sensor (Model Kinect, Microsoft, Seattle, WA, USA) was mounted at the top of the scanning stage. The Kinect sensor consists of an infrared laser emitter, an RGB (color) camera, a monochrome infrared camera, and stereo microphones (Microsoft, 2010). The laser emitter projects the structured infrared lighting pattern to the space and the infrared camera captures the imposed pattern shined on the scene. The spatial information of the scene is calculated based on the correlation and triangulation between the captured pattern and the reference pattern stored in the sensor. In this system, the sensor was connected to a computer via a USB cable. A C++ software program was developed based on an open source driver (OpenNI, http://www.openni.org/) and the PrimeSensor module for OpenNI. The High GUI module of the OpenCV library (Open Source Computer Vision, http://opencv.willowgarage.com) was used to acquire the color image (640×480 pixels) and the depth map (640×480 pixels), which were spatially registered to each other. The program can acquire the RGB-depth images at a speed of 30 frames per second, and save 24-bit RGB image and 11-bit depth map of the scene into the predefined folder in Tiff (tagged image file format) and XML (extensible markup language) format, respectively.

Calibration tests were conducted to evaluate the accuracy and the spatial resolution of the system. The general performance and accuracy of the Kinect sensor has been evaluated previously (Canessa et al., 2013; Khoshelham and Elberink, 2012), which showed that error in the depth image increased with a quadratic relationship to the object-to-sensor distance, from a few millimeters (at 0.5-1 meters distance) to several centimeters (at 4-5 meters distance). Thus, our calibration tests mainly focused on evaluating the depth accuracy and the spatial resolution of the system at the distance range (70-80 cm) that onions were scanned. Figure 5.3 shows the system configuration used for measuring object-to-sensor distance in the calibration test. A big

T-shaped ruler was mounted on the frame of the light chamber to provide a reference for measuring the distance. Gradienter was used to ensure the top surface of the scanning stage was flat and the ruler was perpendicular to the top of the scanning stage.

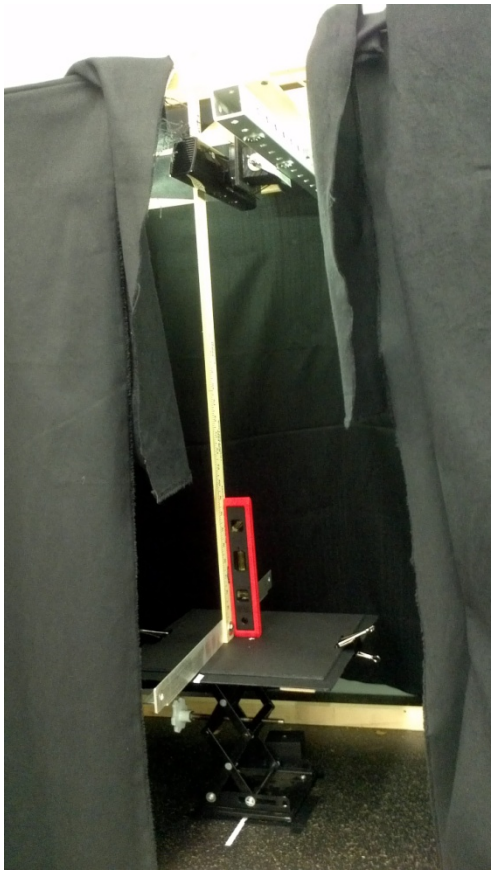

Figure 5.3. Configuration for measuring the object-to-sensor distance in calibration tests.

After the system was aligned and object-to-sensor distance was adjusted, a metal ruler was placed on the scanning stage and the center 20 cm portion of the ruler was marked by black tapes. The position of the ruler was manually adjusted so that the marked portion of the ruler was at the center of the image and its edge was horizontally flat in the image. The ruler was imaged at 5 different object-to-sensor distances (from 70 cm to 80 cm, with 2.5 cm intervals) and RGB-D

images were saved. At each distance, three measurements were conducted. For the RGB-D images taken at each height, the total pixel number of the 20-cm long ruler was counted on each color image and the mean depth value of the ruler was extracted from the depth image by a MATLAB program. By comparing the value extracted from the depth image with the value read from the reference ruler, the accuracy of the depth value was evaluated, which showed a mean error of ±1.3 mm when the object-to-camera distance was between 70 and 80 cm. The pixel resolution (mm/pixel) at each measured distance was calculated by dividing 200 mm by the total pixel number counted on the image. A linear regression model was developed between the object-to-camera distances and the measured image resolutions. By this means, the pixel resolution of the system can be calculated based on its depth value.

5.3.4 Onion image acquisition

Onions were scanned individually by the system. The center of the color camera of the Kinect sensor was aligned to the center of the scanning stage by using a plumb bob attached to a string. The angle of the sensor was tuned until the center of the stage was shown at the center of its color image horizontally and vertically. During scanning, the chamber was enclosed by black commando cloth to avoid the interference by outside ambient light. The RGB-D images of the background scene were first acquired when the middle hole of the stage was covered by a piece of 50×50 mm thin black paper. Onion was first placed on the center area of the scanning stage, with the neck area facing to the sensor. Before each image acquisition, the onion was manually rotated at random degrees around both the longitudinal and horizontally axes to a different orientation. After three images acquisition operations, the onion was flipped along the longitudinal axis so that the root area was faced to the sensor. Then, another three image acquisitions were conducted at different onion positions. Therefore, for each onion bulb, six

color images and six depth images at the six different orientations were collected. In total, 480 color images and 480 depth images of 80 onions were acquired.

5.3.5 Onion diameter estimation using the color image

The maximum diameter of an onion was estimated by color image using the imaging processing method outlined in Figure 5.4. At first, sub-images (160×160 pixels) were extracted from the center of color images (the area of the scanning stage) and were converted into grayscale images. The background image of the stage was subtracted from the images of onions to extract onions from background scene. Then, onion images were converted to binary images using the Otsu's method. Morphological close operation was then applied to remove the internal spots within the regions. The region with the largest area in the binary image was recognized as the region of onion. A peripheral ellipse that has the same normalized second central moments as the region was calculated, and the major axis of the ellipse was identified as the major axis of the onion. At last, the maximum diameter of the onion bulb was computed by multiplying the pixel length of the major axis by the pixel resolution.

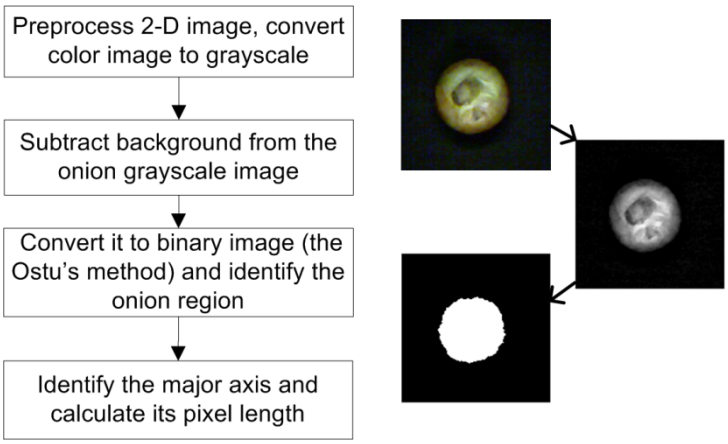

Figure 5.4. Flow chart for calculating the length of the maximum diameter of the onion using color image

5.3.6 Onion diameter estimation using the depth image

The depth image collected by the RGB-D sensor is essentially a range image, which contains a cloud of points and each pixel refers to the distance between the sensor and a point on the scene. If the points in a range image are fitted into a coordinate system, the range image can be called a point cloud image. In this application, a simple 3-D coordinate system (X, Y, Z) was constructed, in which X, Y refer to the row and column number in the image, and Z refers to the height of the imaged point, the distance from the surface point of the onion to the top plane of the scanning stage.

Figure 5.5 shows the flow chart employed to calculate the maximum onion diameter from its depth image. In the preprocessing step, the center area of 160×160 pixels of each depth image was extracted. The pixels in dark holes in the depth image were replaced by the mean value of the four valid pixels of its nearest neighborhood points. The mean depth of the scanning stage was calculated using the background depth image. The depth image of the onion was then

converted into a point cloud image by subtracting the depth value by the mean depth of the scanning stage at each pixel. The mask for segmenting onion from background was calculated by differentiating the depth images of the background and the scene with onion. The difference image was converted into a binary image after applying a threshold of 8 mm, which was used to remove the false foreground objects on the scanning stage such as small debris of onion dry skins. The binary region with the largest area was recognized as the initial onion mask. The background in the point cloud image of the onion was then removed by applying the mask.

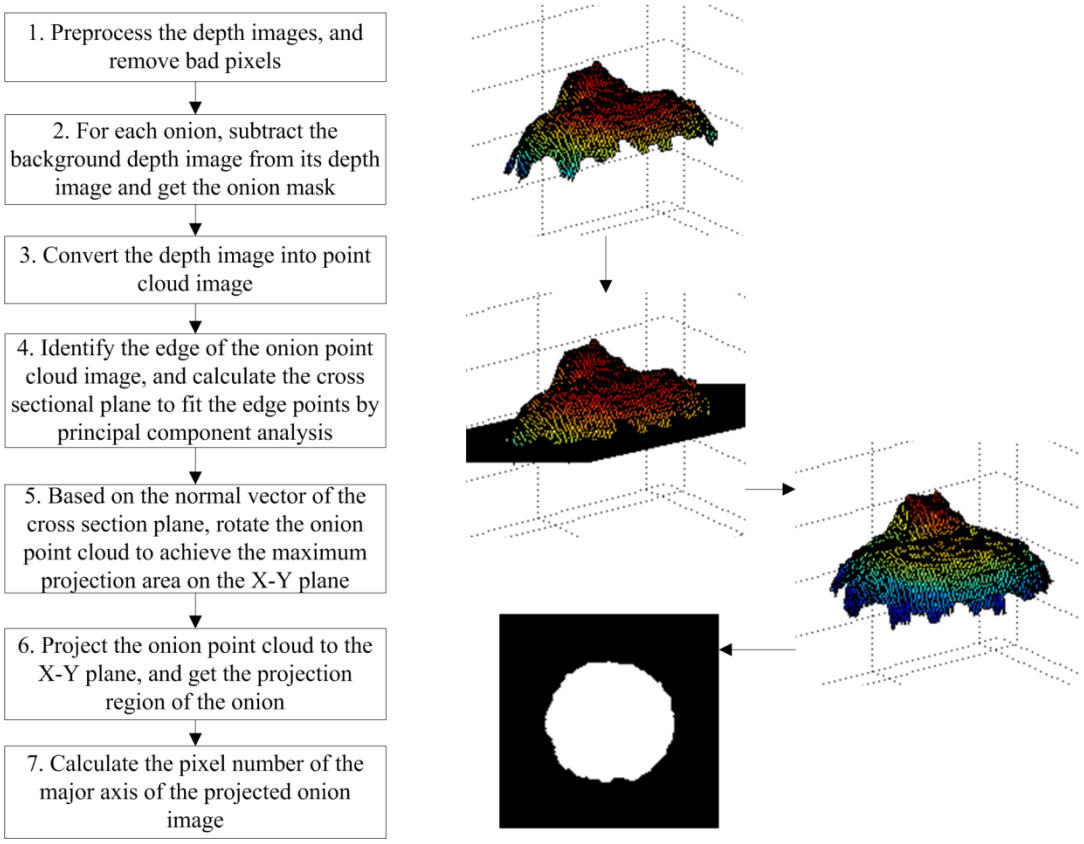

Figure 5.5. Flow chart for calculating the maximum diameter of the onion using its point cloud image.

As shown in Figure 5.5, the point cloud image of the onion describes the height of the half onion of the image. Using the point cloud image, the orientation of the onion bulb in the 3-D space can be well identified. To estimate the orientation of the onion bulb, principle component analysis (PCA) was applied to identify a cross section that has the maximum projection area. Since the sweet onions tested in this work were oblate ellipsoid shape, the maximum cross section area is close to the equatorial area. Thus, the plane fitted by PCA was approximately the section plane crossing the equator of the onion. The normal vector of the fitted plane provided a good estimation of the overall orientation of the onion bulb. Using the normal vector, the angles between the plane and the X, Y axes were calculated, respectively. According to the calculated angles, 3-D geometrical transformation matrixes were calculated and applied to rotate the point cloud image along X and Y axis, so that the maximum projection area is parallel to the X-Y plane. Then, the transformed point cloud was then projected into the X-Y plane to generate the binary map for the onion. Using the projected binary map, the longest axis of the onion region was identified and the maximum diameter of the onion bulb was calculated using the same method presented in the approach of using color images.

5.3.7 Onion volume estimation based on the point cloud image

To calculate the volume of the onion, the transformed point cloud image of the onion was converted into a voxel image. In the voxel image, each pixel is treated as a box rather than a point. By this way, the point cloud image of the onion was converted into a 3-D block (Figure 5.6). The total volume of the onion block could be calculated by summing up the volume of all boxes in the voxel image. The volume of each box was calculated by the equation V = height (mm) × pixel resolution (mm/pixel) × pixel resolution (mm/pixel).

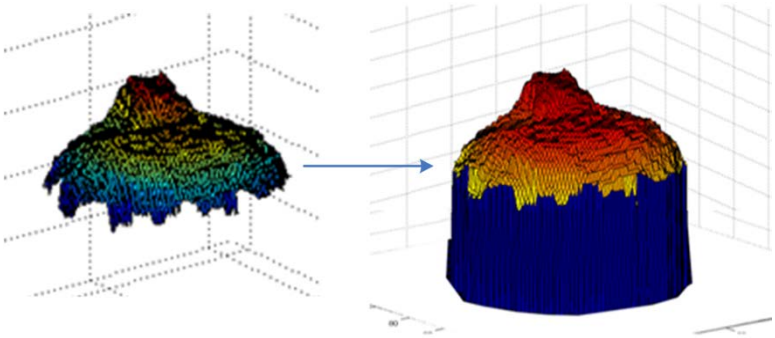

Figure 5.6. Demonstration of the onion voxel image based on the transformed point cloud.

The total volume of the onion voxel image included both the volume of the onion and the volume of the space between the bottom surface of the onion and the scanning stage. To accurately estimate the volume of the onion bulb, the volume of the gap should be subtracted from the total volume. As demonstrated in Figure 5.7, if the onion bulb is an ellipsoid shape, the volume of the onion block is the sum of the top half of the ellipsoid and the bottom bar, in which a, b, c are the radius of the three principal axes of the ellipsoid. The volume of the bottom space is about 20% of the total volume of the onion block. In this regard, the volume of the onion (V_{onion}) should be 80% of the total volume of its voxel image (V_{voxel}).

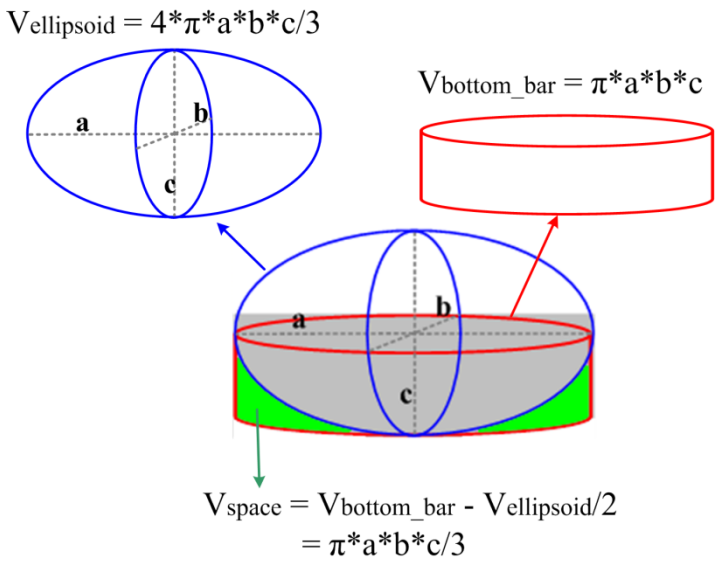

Figure 5.7. Mathematical description of the volume of the voxel image of the onion

However, sweet onions were not an exact ellipsoidal shape. Thus, linear regression analysis was also applied to model the linear relationship between the volume of onion and the total volume of the voxel image of onion. The linear regression analysis was conducted using the statistical toolbox of MATLAB (ve2013a, MathWorks, MA, USA) using 2-fold data partition method, in which 50% data were used for training and the other 50% data were used as the testing dataset. The accuracy of the volume estimation was calculated by comparing the predicted volume using the RGB-D imaging method ($V_{Imaging}$) with the volume measured by water displacement test (V_{WD}): accuracy = $1 - |V_{Imaging} - V_{WD}|/V_{WD.}$

5.3.8 Onion density estimation

Density of onion bulbs is useful information for the quality assessment of onions, particularly for onion powder manufacturers who favor onion bulbs of higher density. In the current postharvest onion sorting, estimating the density of onion bulbs individually is a very challenging task due to the complexity of measuring the onion volume. Measuring the onion

volume using RGB-D sensor and depth image leads to a potential solution to monitor onion density online and nondestructively. In this study, the density of each onion was calculated by dividing its weight by volume calculated using individual depth image of the onion. The density value calculated by dividing its weight by the volume measured by the WD method was used as the reference. It's known that onions of different cultivars can have different density distributions. Thus, the mean values of the reference densities of onions were compared between two onion cultivars using two-tailed t-tests with a significance level of 0.05 to examine whether they have significant difference. The means of the density estimations made based on depth image were compared between two onion cultivars using t-tests. For each type of onion, its density distribution of densities measured by depth image was compared with its counterpart of the reference density values. All image processing operations and t-tests were conducted using the image processing toolbox and the statistic toolbox of MATLAB (v2013a, MathWorks, MA, USA).

5.4 Results and Discussion

5.4.1 Onion maximum diameter

Figure 5.8 shows the maximum diameters of onions calculated from their color images. For each onion, there were six data points shown in Figure 5.8 since the onion was scanned at six different orientations in the test. These six data points are vertically aligned in the figure since they share the same ground truth. The R-squared value (0.89) indicated a relatively strong correlation between the estimated maximum diameter of onions by the color imaging and the reference value. Compared to the maximum diameters measured by the caliper, the maximum diameters of onions estimated by using color imaging showed a root mean square error (RMSE)

of 3.4 mm, which was about 3.37% of the mean maximum diameter (101 mm) of the tested onions.

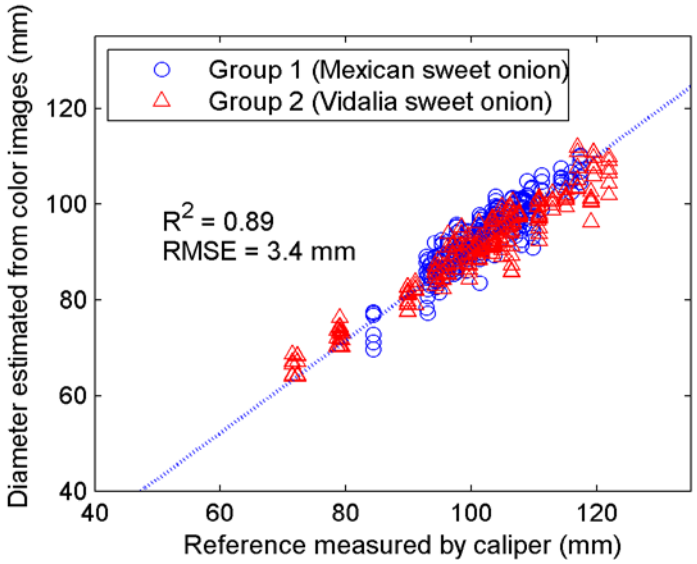

Figure 5.8. Comparisons between the onion maximum diameters estimated using color images and the maximum onion diameter measured by digital caliper.

Overall, the maximum diameters measured using color images underestimated the size of the onions, as most data points shown in Figure 5.8 were below the diagonal line. This could be caused by several factors. First, onion bulbs are ellipsoidal and their peripheral area tended to be darker since less light on the equatorial area of onions can be reflected to the camera. Some of those dark areas could be easily segmented as the background. Second, the projected length of the maximum axis (the maximum diameter) could be significantly reduced if the onion was tilted vertically along its maximum axis. Moreover, the intensity of the color image varies with the lighting conditions. For instance, the edge area on the color image would be affected by the shade of its neck, which reduces the intensity of the edge points. Under any of the above

situations, the maximum diameter of the onion estimated from its color image would be smaller than the real value.

Figure 5.9 shows the results of the onion maximum diameters calculated based on their depth images. The result showed that the method using depth images performed better than the method using color image. The R^2 (0.96) and the RMSE (2 mm) were 0.7 greater and about 40% smaller than those of the color image-based method, respectively. In addition, for each onion sample, the six measurements at different orientations showed more compact distribution in Figure 5.9 than in Figure 5.8. This indicated that the method of using the depth image is more invariant to the change of the onion orientation. The improved performance of estimating the onion maximum diameter by the method using depth image could be attributed to several factors: (1) RGB-D sensor uses the structured light to actively scan the object. Thus, the depth image is not (or less) affected by the illumination changes or the ambient light. (2) In the proposed method, onion at a tilted position was rotated back to the upright position in the 3-D space so that a more accurate length of the maximum equatorial axis could be projected to X-Y plane.

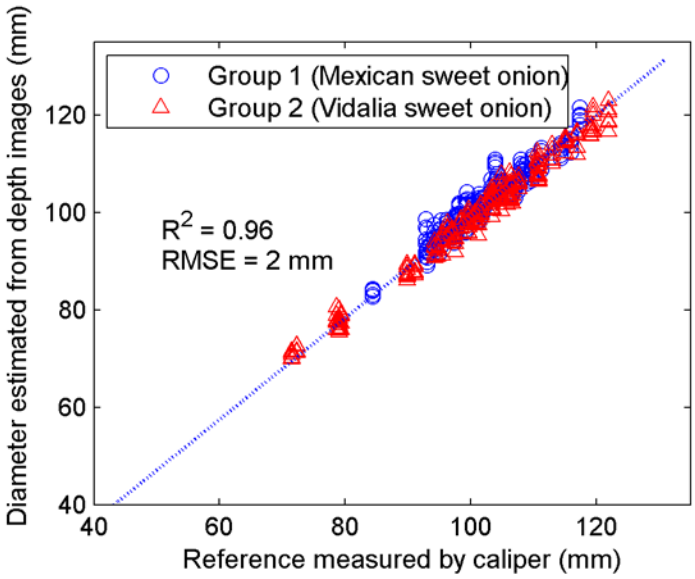

Figure 5.9. Comparisons between the maximum diameters of onions estimated by the image processing method based on depth images and the maximum onion diameters measured by the digital caliper.

To estimate the diameter of fruits and vegetables using machine vision systems, it's a common practice to average multiple scans and utilize the mean value to make the estimation. In this study, the six measurements of each onion at different orientations were averaged and compared to its reference value (Figure 5.10). For the method using color images, using the mean value of six measurements, the RMSE decreased 0.9 mm (from 3.4 mm to 2.5 mm) and R^2 increased 0.5 (from 0.89 to 0.94). For the method using depth images, the RMSE reduced 0.5 mm (to 1.5 mm) and R^2 increased 0.2 (to 0.98) by using the mean of six measurements. In general, estimation using depth image performed better than the approach of using color image. For using either color image or depth image, making multiple estimations and using the average value improved the accuracy of the estimation of the maximum diameter of the onion. It has to

be noted that scanning the onion multiple times will decrease the processing speed and reduce the throughput.

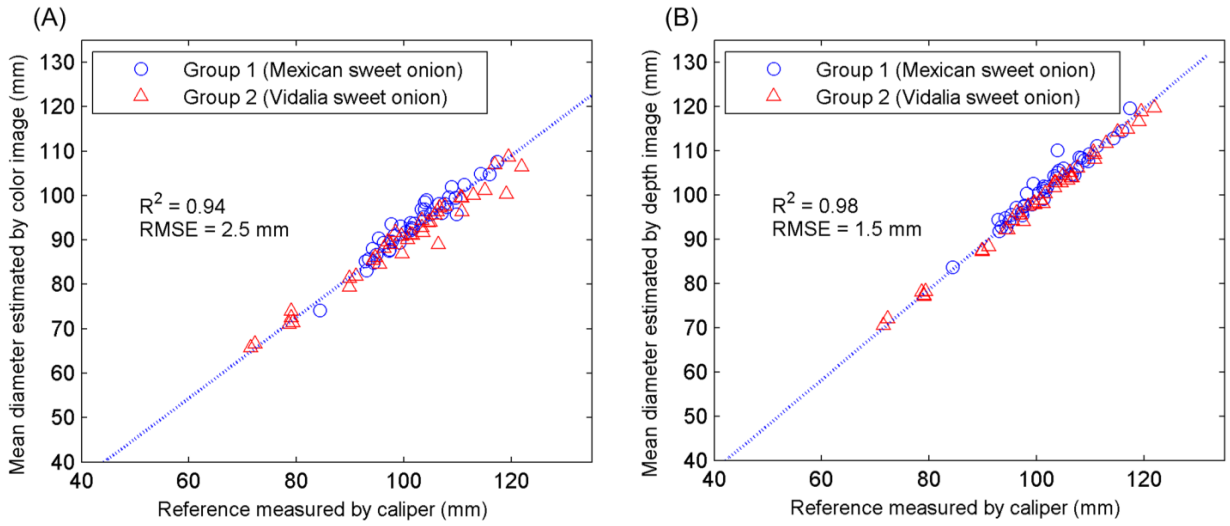

Figure 5.10. Average maximum onion diameter estimated based on six measurements using color images (A) and depth images (B).

Considering the diameter estimation method using single depth image, the ratio of the RMSE to the average diameter of onions was 1.98% (2/101 mm), which illustrated a slightly better performance than conventional 2-D machine vision systems reported in the literature such as Blasco et al. (2003) (accuracy=93%). The RMSE (2 mm) was close to those (0.5-2 mm) of the size estimation of strawberries using the volume intersection method reported by Imou et al. (2006). Since the size of onions (70-120 mm) were about 3 times the size (20-40 mm) of the strawberries used in Imou et al. (2006), the percentage RMSEs of this depth image-based method were much smaller than those of the VI method.

In the U.S. onion industry, sweet onions are classified into several size groups based on their maximum diameters. The range of the diameter for each size group is often between 12.7 mm

(1/2 inch) and 31.75 mm (1-1/4 inches), depending on the type of the onions. For instance, Vidalia sweet onions for fresh market are often classified into Colossal (101.6 mm and up), Jumbo (76.2-101.6 mm), and Medium (50.8-76.2 mm) based on the diameter. Using the method based on single depth image, the RMSE (2 mm) of the diameter estimation is 7.9% of the average size range of each grade (25.4 mm), which is two times smaller than the tolerance rate (25%) required by the standard of U.S. Onion Number 1 (USDA, 1995). This accuracy can be further improved when multiple scans are involved. In general, the proposed approach provides an promising alternative approach to the traditional diameter measurement methods of using onion gauge, mechanical sizers, or 2-D camera based machine vision systems.

5.4.2 Volume estimation

Figure 5.11 (A) shows the result of estimating the onion volume calculated from their depth images using the linear relationship based on the ellipsoidal model ($V = 0.8*V_{voxel}$). Using the volume measured by water displacement method as the reference value, the RMSE was 22.2 cm^3 and the average accuracy of measurements was 95.3%. One contributing reason for the error was that the shape of the onion bulb was not perfectly ellipsoidal, so that the volume of the onion bulb was not exactly 80% of the volume of the vortex image of the onion.

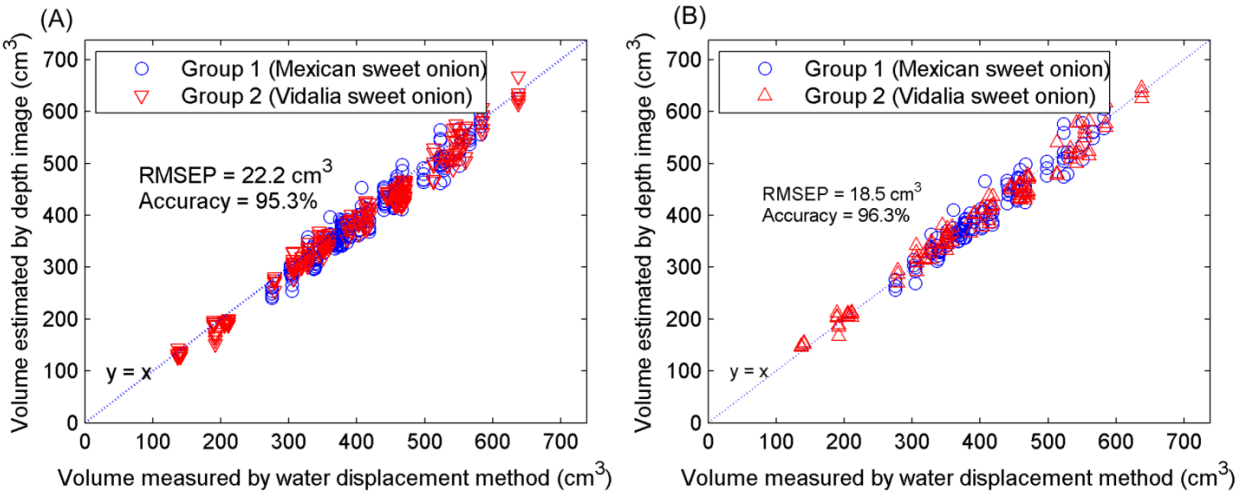

Figure 5.11. Onion volume calculated from the depth images based on the ellipsoidal model (A) and estimated by linear regression model (B).

To improve the accuracy of the volume estimation, regression analysis was conducted to develop a linear regression model to predict the onion volume from the volume of its vortex image. Trained by half of the dataset, the linear regression analysis suggested a model: $V_{onion} = 0.79 \times V_{voxel} + 17.95$ (Figure 5.11 (B)), which indicated a relationship between the volume of the onion bulb and the measured volume of its vortex image similar to the one suggested by the ellipsoidal model. The prediction model based on linear regression model achieved a root mean square error of prediction (RMSEP) of 18.5 cm^3 on the testing dataset. The average accuracy was 96.3%, which was 1% higher than that of using the ellipsoidal model. Overall, using single depth image, the onion volume estimation calculated either using the mathematic model derived from the ellipsoidal model or using the proposed linear regression model achieved an accuracy higher than 95%.

When six measurements of the same onion were averaged, the accuracy of the onion volume estimation was improved to 96.1% and 97.9% using the ellipsoidal model or the linear regression

model, respectively (Figure 5.12). Similar with the estimation of the diameter, acquiring the depth images of the onion bulb for multiple times can lead to a slightly better estimation of the volume. But acquiring the depth images of the onion bulb for multiple times at different orientations and making multiple estimations is more time consuming. Depending on the specific requirements of application, the number of depth images for each onion can be determined. For the method using either single or multiple depth image(s), the volume estimation error could be caused by several factors, such as onions with irregular shapes, error introduced by over lengthy onion neck leaves, and the error (±1%) of the WD measurement.

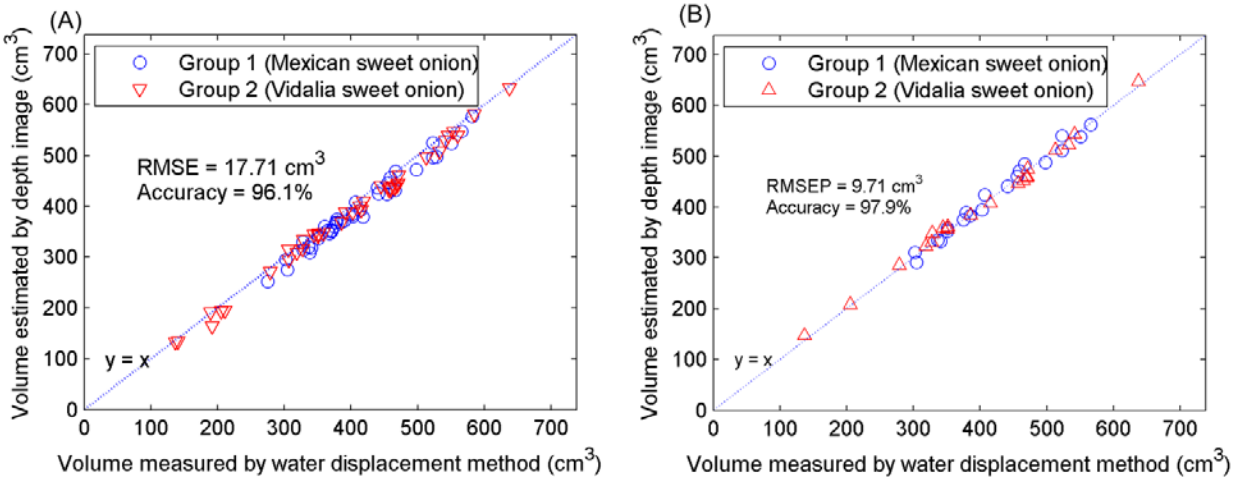

Figure 5.12. Onion volume averaged from six measurements calculated from the ellipsoidal model (A) and estimated by linear regression model (B) using depth images of onions.

In summary, the volume estimation of sweet onions using RGB-D sensor and linear regression model achieved accuracies of 96.3-97.9%, which were similar to those (94-100%) of the volume estimation of strawberries, cantaloupes, apples, and tomatoes using the VI method based on multiple silhouettes reported in Lee et al. (2006). Moreover, the proposed method

requires a less complicated system setup and can scan samples in a higher speed than the VI system reported by Lee et al. (2006). Compared with other types of non-destructive systems for measuring the volume of fruits and vegetables, such as the ring sensor (error=5.7%) developed by Gall et al. (1998) and the volume meter based on air replacement (error=3.8%) proposed by Iraguen et al. (2006), the RGB-D sensor based system showed a comparable accuracy, while the system cost is much lower. The proposed method provides a simple, economic, and accurate method to estimate the onion volume nondestructively. Since the cost of RGB-D sensor (such as Microsoft Kinect sensor) is quite low, this type of system can be easily assembled to estimate of the size of sweet onions at various circumstances of onion production, as the alternative method of the traditional troublesome water displacement method.

5.4.3 Density estimation

Successful measurement of the onion volume using depth image leads to a non-destructive solution to measure the density of onion: weighing each onion bulb by a weight sensor and then dividing its weight by the volume. Figure 5.13 (A) illustrates the distributions of the density values of onions of two cultivars, which were calculated from the weight and volume measured by digital scale and water displacement method. Densities of the tested Mexican sweet onions (mean ± SD: 0.895 ± 0.032 g/cm^3) were significantly different from those of Vidalia sweet onions (0.929 ± 0.037 g/cm^3) according to the result of the t-test ($p<0.001$).

Using the method based on RGB-D imaging, the densities of Mexican sweet onions and Vidalia sweet onions were 0.902 ± 0.047 g/cm^3 and 0.924 ± 0.034 g/cm^3, respectively (Figure 5.13 (B)). The results shown in Figure 5.13 (B) were derived from the onion volume estimated using a single depth image collected by the RGB-D sensor, which achieved an accuracy of 96.3% using the density measured by the experimental method as the reference. The accuracy of

the density estimation using the RGB-D imaging-based method was mainly determined by the accuracy of the volume estimation since the accuracy of the digital scale used for measuring the weight was quite high (±0.1 g). The same situation could be expected in real applications since high precision weight sensor is often integrated in onion classification systems. Thus, the key issue of estimating the onion density online is to accurately measure the volume of the onion using a non-destructive method.

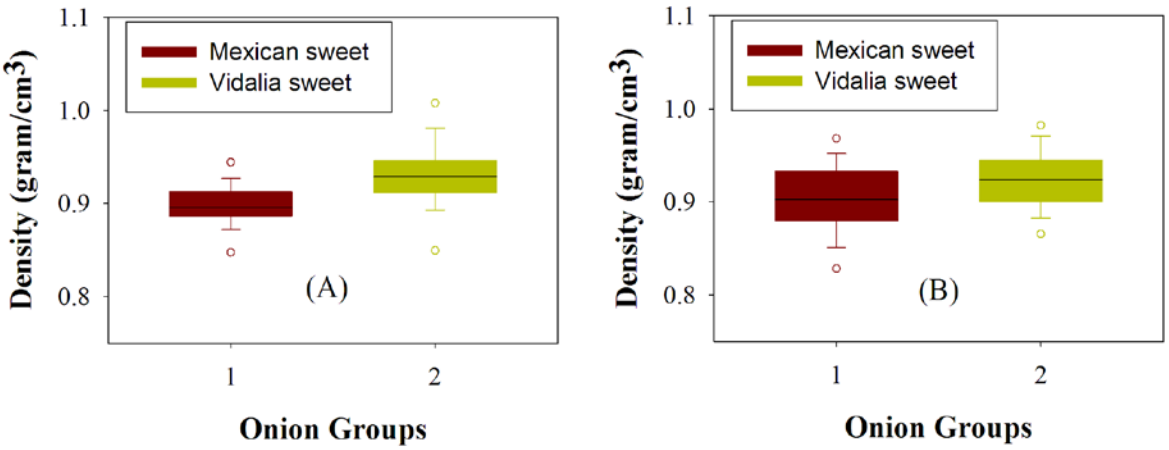

Figure 5.13. Box plots of the densities of the two cultivars of onions in which onion densities were calculated based on the manually measured weight, and the volume measured by water displacement method (A) and the volume calculated from depth images of onions (B).

Based on the results of t-tests, the densities measured using the experimental method and by the method based on the RGB-D imaging were not significantly different for either Mexican sweet onions ($p=0.333$) or Vidalia sweet onions ($p=0.396$). On the other hand, similar to the measurements using the experimental method, the difference between the mean values of the

estimated densities of the two onion cultivars was significant ($p<0.001$). In summary, the proposed method of measuring the density of onions by the imaging-based method is statistically comparable to the conventional approach of measuring onion density by experimental method.

5.5 Conclusions

A machine vision system was designed based on the RGB-depth sensor to measure the maximum diameter and volume of sweet onions. Compared to the method using the color image, the diameter estimation using the depth image was more accurate and robust to the change of the orientation of onion. Based on the onion voxel image, the volume of the onion can be estimated by using a mathematical model derived from the ellipsoidal model or by a linear regression model. Using the volume measured by water displacement method as the ground truth, the proposed volume measurement method based on single depth image achieved accuracies of 95.3% and 96.3% using the mathematical model or the linear regression model, respectively. The density of onions estimated by the depth imaging-based method was statistically comparable to the conventional experimental approach.

This work illustrated the potential of using the consumer grade RGB-depth sensor to measure the geometrical features of sweet onions nondestructively. The RGB-depth sensor demonstrated the capability of collecting depth images of the test object fast and accurately, with advantages of being invariant to the changes of lighting conditions and robust to the changes of the object orientation. As demonstrated in this study, the RGB-depth imaging technique leads to novel low-cost solutions to measure the volume and density of onions nondestructively, which can be practical if applied to online sorting of onions in packinghouses. The methods proposed in this study can also be extended to applications of other fruits and vegetables.

5.6 Acknowledgements

This work was funded by the USDA NIFA Specialty Crop Research Initiative (Award No. 2009-51181-06010). Authors also sincerely acknowledge the Vidalia Onion Research Farm for providing onion samples for this work.

CHAPTER 6

MACHINE VISION SYSTEM BASED ON MULTIPLE IMAGING SENSOR FOR QUALITY INSPECTION OF ONIONS[4]

[4] Weilin Wang and Changying Li. To be submitted to Trends in Food Science & Technology.

6.1 ABSTRACT

This chapter reports a novel multisensor machine vision system for quality inspection and classification of onions. The multisensor system integrated color, 3-D, hyperspectral, and X-ray imaging technologies in one platform to evaluate onion quality holistically and nondestructively. A LabVIEW program was developed to control and synchronize hardware devices to acquire spatial color, near-infrared spectral, depth, and X-ray images of onions, and measure the weight of onions by a custom weighing device integrated in the system. A validation test was conducted to employ this system to measure key quality factors of onions. Three treatments of sweet onions (regular onions without inoculation, inoculated with *Burkholderia cepacia*, and inoculated with *Pseudomonas viridiflava*) were scanned by the system. Algorithms based on image processing, statistical, and machine learning techniques were proposed to calculate the maximum diameter, volume, and density of onions nondestructively, and evaluate the defect situation based on the multisource information of onions collected by the system. Results showed that the system accurately measured the weight (RMSE=3.7 grams), diameter (RMSE=1.7 mm), volume (accuracy=96.9%), and density (RMSE=0.03 gram/cm^3) of onions. Using selected image features of onions X-ray and spectral images, one classifier using two SVMs cascaded at decision level successfully classified 81.58% onions (as healthy or defective). Another classifier (a classification tree) utilizing combined features at feature level successfully distinguished 84.21% onions. Classifiers based on sensor fusion achieved much higher detection rates of defective onions than those (78.95% and lower) of classifiers using single imaging sensor. The proposed multisensor system is a useful platform for quality inspection of onions and provides a prototype for further development of fully automated onion classification systems that can evaluate both external and internal quality parameters of onions effectively and efficiently. The

system and methods presented in this chapter are potentially applicable to postharvest quality inspection of other agricultural products.

6.2 INTRODUCTION

Onion (*Allium cepa* L.) is one of the top three fresh vegetables grown in the United States. The annual farm gate value of U.S. onion production exceeded one billion dollars for several years (USDA, 2013). In a typical onion packing house in the United States, onions are sorted by automated sorting lines based on the diameter, and then pass by the quality inspection station where trained human inspectors check the quality of onions on moving conveyor belts. This quality inspection method, however, is unreliable since humans are prone to making subjective and inconsistent decisions due to fatigue and distractions. Particularly, onions are a multilayered vegetable with heterogeneous outer dry skins. Their internal conditions are often hard to examine from the visible clues shown on the surface. Moreover, labor shortages in many U.S. onion production states and rising labor costs also decrease the accuracy of labor-intensive human visual inspections (HVI) since fewer inspectors are employed and thus making their inspection tasks more difficult.

Similar to other vegetables, onions are susceptible to many postharvest diseases, such as sour skin (*Burkholderia cepacia*), neck rot (*Botrytis allii*), and bacterial streak and rot *(Pseudomonas viridiflava*) (Schwartz and Mohan, 2008a). Infections can occur at both outer and internal scales and symptoms of many diseases are latent in early stages in onion bulbs (Mark et al., 2002). Many diseased onions can easily pass HVI in postharvest sorting and further affect other clean onions in the same container, causing secondary yield losses in packing, transportation, and storage. Particularly, U.S. onion growers store a large portion of their produces in cold rooms and controlled atmosphere rooms for a fairly long period (1-6 months).

Pathogens brought into the storage room by defective onions could cause very significant postharvest production losses. Diseased onions not only cause significant economic losses and reduce the profits of growers and shippers, but also could affect the health of consumers and damage the reputation of onion brand owners. Thus, in postharvest sorting of onions, there is a need to detect diseased onions effectively using automated nondestructive methods so that they can be redirected for alternative processing.

A considerable amount of nondestructive computer vision and sensing techniques have been reported for the quality inspection of agricultural and food products, such as color and grayscale imaging methods (Blasco et al., 2009), VIS/NIR spectroscopy (Nicolaï et al., 2007), X-ray imaging (Shahin et al., 2002; Tollner et al., 2005), multispectral imaging (Ariana et al., 2006; Yang et al., 2005), hyperspectral imaging (Gowen et al., 2008), magnetic resonance imaging (Marcone et al., 2013), and electronic nose (Li and Heinemann, 2007). Using these nondestructive technologies, computer vision-based systems have been intensively studied for automated classification of fruits and vegetables (Blasco et al., 2003; Cubero et al., 2011; Zude, 2008). A number of techniques have also been studied for nondestructive quality inspection of onions. Tollner et al. (2005) pointed out that X-ray imaging is a promising method for detecting internal defects of sweet onions including voids and foreign inclusions. Li et al. (2009) used the gas sensor array to detect sour skin in onion storage rooms. Wang et al. (2012a) developed a spectral imaging system to distinguish sour skin-infected onions from healthy onions using spectral images acquired at two NIR wavelength bands. Wang et al. (2013) applied Vis-NIR to determine the internal quality factors of onions such as soluble solids content and dry matter content. These studies focused on evaluating certain specific quality aspects of onions. The quality of an onion bulb, however, is determined by a combination of many important quality

factors such as size, maturity, shape, and defect level. Thus, it is very necessary to develop an onion sorting facility capable of evaluating key quality factors of onions accurately and holistically.

As an emerging technique, multisensor data fusion exploits the synergy in information acquired from multiple sources to make a better decision than using any of the information sources individually (Hall and Llinas, 1997). This technique has gained increasing attention in various areas including nondestructive quality evaluation for fruits and vegetable. Steinmetz et al. (1999) discussed the general strategies for applying multiple sensors to assess the quality of fruits using different levels of data fusion process models. In many reported applications (Li et al., 2007; Mendoza et al., 2012; Olafsdottir et al., 2004; Ruiz-Altisent et al., 2006), data fusion techniques were applied to integrate different manually operated measuring instruments together or with nondestructive, automated measuring instruments. In recent years, a number of applications combining multiple automated sensor techniques have also been reported in the food and agricultural area. Henningsson et al. (2006) proposed a multiple sensor system to monitor milk quality, which integrated a conductivity meter, a density meter, and an optical instrument for measuring the turbidity of milk. Bulanon et al. (2009) used an image registration technique to combine color and thermal images of the canopy of orange trees to detect oranges in the orchard. Fricke and Wachendorf (2013) combined the sward height measured by ultrasonic instrument with the vegetation indices measured by spectral devices to assess the biomass of legume-grass swards.

Since automated quality inspection and grading of onions involves many quality aspects in different domains, multisensor data fusion and integration could be helpful. An example of multisensor classification system for fruits and vegetables is the eggplant grading system

developed by Kondo et al. (2007), which integrated five color and monochrome cameras to grade eggplants based on color, size, and surface defects. Although many machine vision-based grading systems have been reported for fruits and vegetables (Blasco et al., 2003; Kondo, 2010), there is no existing automated system that can be used to measure all key external and internal quality factors of onions. On the other hand, rapid advances in sensing and computer vision technologies in recent years, such as hyperspectral imaging and 3-D imaging, provide an opportunity to develop a more capable quality inspection system to address these challenges in the onion industry.

This work was aimed to design and implement a multiple sensor system that can inspect key external and internal quality factors of onions nondestructively and holistically. Specific objectives of the study were to:

(1) select appropriate nondestructive sensing technologies and design a multiple sensor computer vision system for onion quality inspection and classification;

(2) implement a hardware platform to integrate the hardware devices and develop a software program for data acquisition;

(3) develop image analysis algorithms to measure key onion quality parameters;

(4) evaluate the performance of the proposed system by a validation test under laboratory conditions.

6.3 Multi-sensor Inspection System

6.3.1 System design

The main purpose of system development was to design and implement a prototype system to collect multimodal images of onions for measuring key quality factors of onions. Thus, the design of this system emphasized the strong capability of collecting onion information useful for

evaluating both external and internal quality factors of onions. The cost and scanning speed of the imaging/sensing devices were also considered in the system design.

In the course of the system design, various nondestructive sensing techniques were considered and evaluated. Aimed at providing a line-scan sorting solution that potentially can be applied for online onion classification, imaging techniques with line or area field of view were favored so that onions can be scanned in a relatively high speed. Techniques requiring long data acquisition time such as MRI and computer tomography (CT) were not included for the same sake. The final system design (Figure 6.1) consisted of several imaging techniques with complementary sensing capabilities: color, RGB-depth (RGB-D) imaging (Henry et al., 2010), spectral imaging (Sun, 2010), and X-ray imaging (Haff and Toyofuku, 2008). The rationales for selecting these image techniques were: color imaging provides spatial color and size/shape information of onions; spectral imaging can be used to exam surface blemish and rottenness of onions; RGB-D can measure size and geometry information of onions based on the topology data it collects; X-ray imaging can be used to detect internal defects and disease infections in onions.

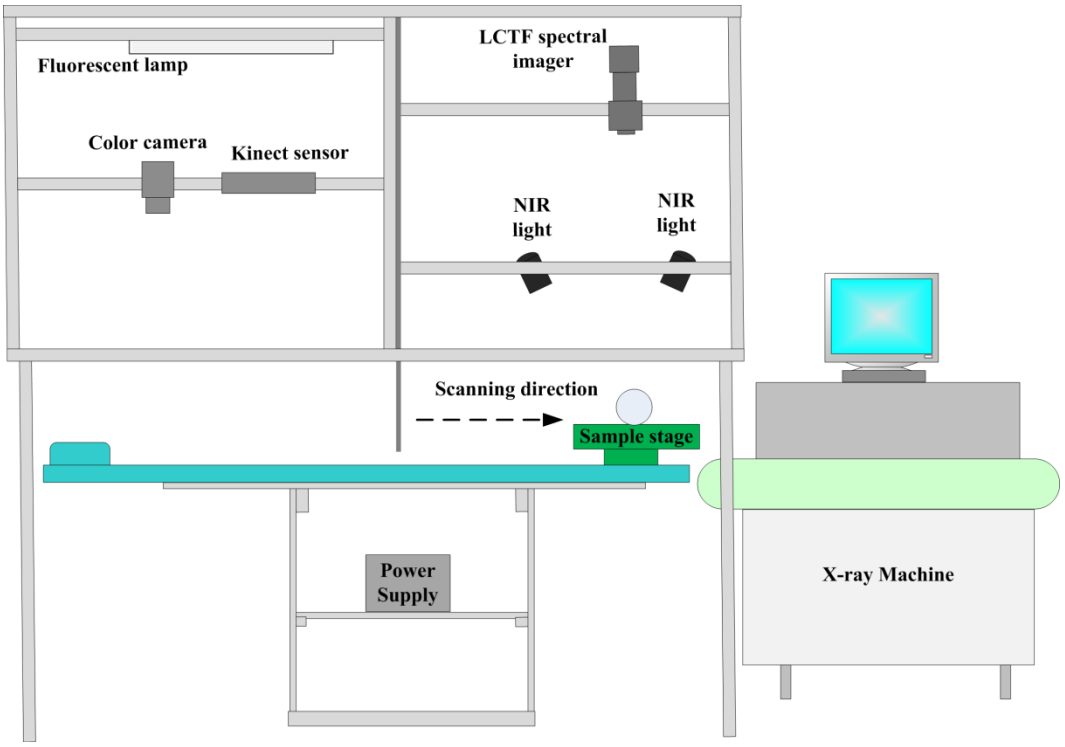

Figure 6.1. Schematic of the multiple sensor onion quality inspection system.

Using the proposed system, a test object is scanned at three sequential imaging stages. In the first stage, a GigE Vision camera (Manta 504c, Allied Vision Technologies, Stadtroda, Germany) acquires color images (1400×1200 pixels) at a speed of 12 frames per second (fps). The camera was connected with computer by a 2 meter long CAT 6 Ethernet cable. After that, a RGB-depth (RGB-D) sensor (Kinect Sensor, Microsoft, Seattle, WA, USA) was used to acquire depth images, which can acquire depth images of 640×480 pixels at the speed of 30 fps. The RGB-D sensor was connected to a desktop computer by a USB 2.0 cable.

In the second stage, a liquid crystal tunable filter (LCTF) based near-infrared (NIR) spectral imager was employed to acquire hyperspectral images of the test object. The imager consisted of three key hardware components: a 320×256 pixels InGaAs camera (SU320KTS-1.7RT, Sensors

Unlimited, Inc, Princeton, NJ, USA), a NIR lens of 50 mm focal length (SOLO 50, Sensors Unlimited, Inc., Princeton, NJ, USA), and an LCTF (Varispec LNIR-20-HC-20, Cambridge Research & Instrumentation, Cambridge, MA, USA) with a wavelength selection range from 900 nm to 1700 nm.

The third imaging stage used a commercial X-ray line-scanner (Model 4262, Autoclear, Fairfield, NJ, USA), which has a bottom-up generator design. The X-ray scanner has a single X-ray generator operating at 140 KV. The scanner has a 46×57×27 cm (W×L×H) scanning tunnel and its conveyor belt (33 cm wide) moves 24 cm per second at scanning. The X-ray line-scanner is powered by 120 KV, 60 HZ AC and controlled by a separate operation panel. The collected X-ray images are automatically saved into the hard disk of a desktop computer.

In addition to imaging sensors, a custom weighing device was installed to measure the weight of onions. The weighing device was made based on a micro shear load cell (Model 3133, Phidgets Inc., Alberta, Canada) and a data acquisition PCB assembly (Model PhidgetBridge 1046, Phidgets Inc., Alberta, Canada). The load cell can measure weights up to 5 kilograms with an accuracy of ±2.5 g.

6.3.2 System integration

Figure 6.2 shows the layout of the hardware devices used in this system. The whole system is enclosed in a chamber in which the main frame was made from perforated square aluminum tubing (1.5 inches square, 0.125 inch thick wall) and connectors. The chamber is covered by coated wooden panels and black curtains. For each type of camera, a custom mounting bracket was made to install the camera on the frame through the bolt holes of the aluminum tubing.

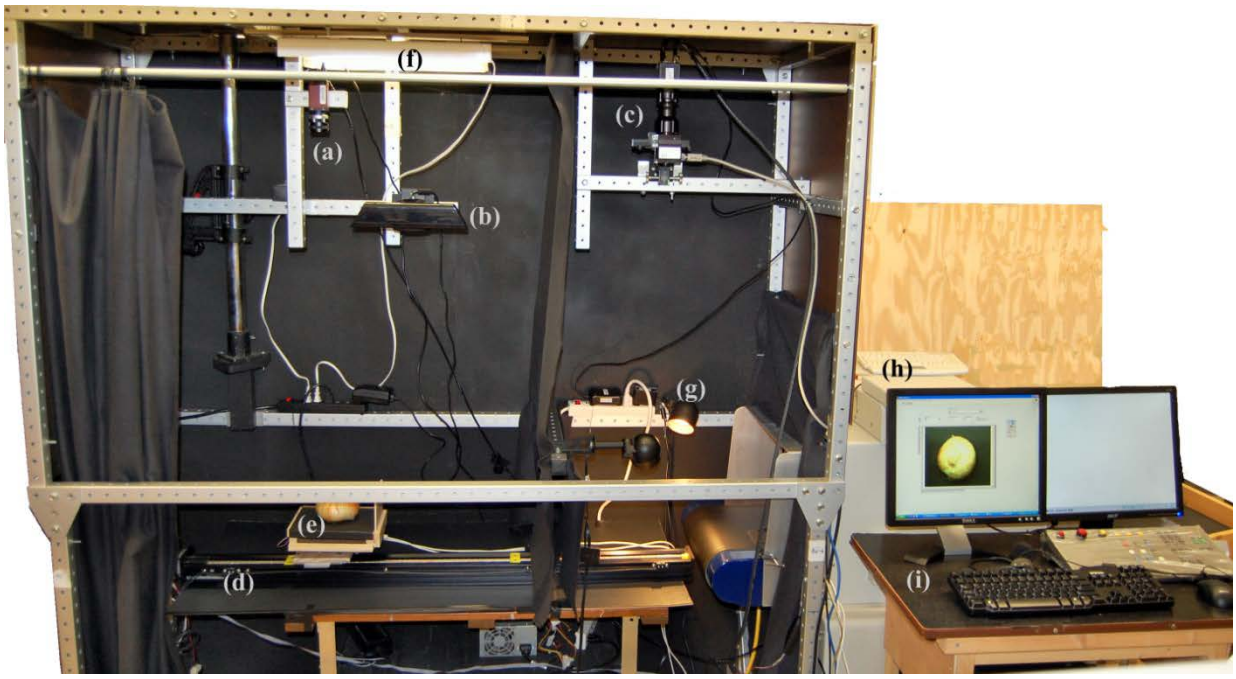

Figure 6.2. Key hardware components of the system and the front view of the system (front panels were temporally removed to show the interior layout of the system). (a) color camera, (b) RGB-Depth sensor, (c) hyperspectral imager, (d) linear slider, (e) onion holder, (f) fluorescent lamp, (g) halogen lamp, (h) X-ray scanner, (i) computer and monitors.

In this system, the spectral imaging system required white light with a continuous spectrum in the NIR region. But the light in the spectral range of 800-850 nm interferes with the operation of the Kinect sensor since the NIR emitter of the Kinect sensor uses the laser light at the same spectral region. Thus, instead of applying a universal lighting system to illuminate the whole conveying area, two illumination systems were built to provide lighting for the color and depth system and the NIR hyperspectral imaging system respectively. The lighting for the color and depth sensors was provided by two 18 inch cool-white fluorescent lamps (15 watt, 4200 K) with

built-in plastic diffusers. The fluorescent lamps were installed at the top of the chamber. The illumination system of the LCTF-based spectral imager includes two 12 Volt, 20 Watt halogen lamps, which were aligned at the two sides of the linear slider. The uniformity of the lighting was enhanced by using glass diffusers. Black curtains were installed inside the chamber to separate the two light chambers.

Figure 6.3 illustrates the design of the onion scanning stage. As shown in Figure 6.3 (1), the stage has a multi-layer structure. The bottom layer is the mounting base with the customized weighing device (Figure 6.3 (3.a)) on which data acquisition boards (Figure 6.3 (3.c) and (3.d)) were installed. The top layer is an onion holder. The frame of the onion holder was made from wooden bars. The top panel of the stage was made of a piece of 3 mm thick black card board for several reasons: (1) black paper provides a high contrast and uniform background for color and spectral images; (2) the flat panel provides a good background for depth image; and (3) the paper panel introduces very little background noise to X-ray images due to its low density. The middle layer connects the top onion holder and the bottom mounting base. A motorized linear actuator (Model L12-100-100-6-R, Firgelli, Victoria BC, Canada) was mounted on the platform, which was used as a robotic arm to push the onion holder from the stage to the conveyor belt of the X-ray scanner. The whole stage was mounted on a 60 inch long linear slider motorized by a NEMA 23 motor (Model MDrivePlus 23, Schneider Electric, CT, USA) with a programmable motion controller. The linear slider was placed on a custom wooden table whose height is adjustable.

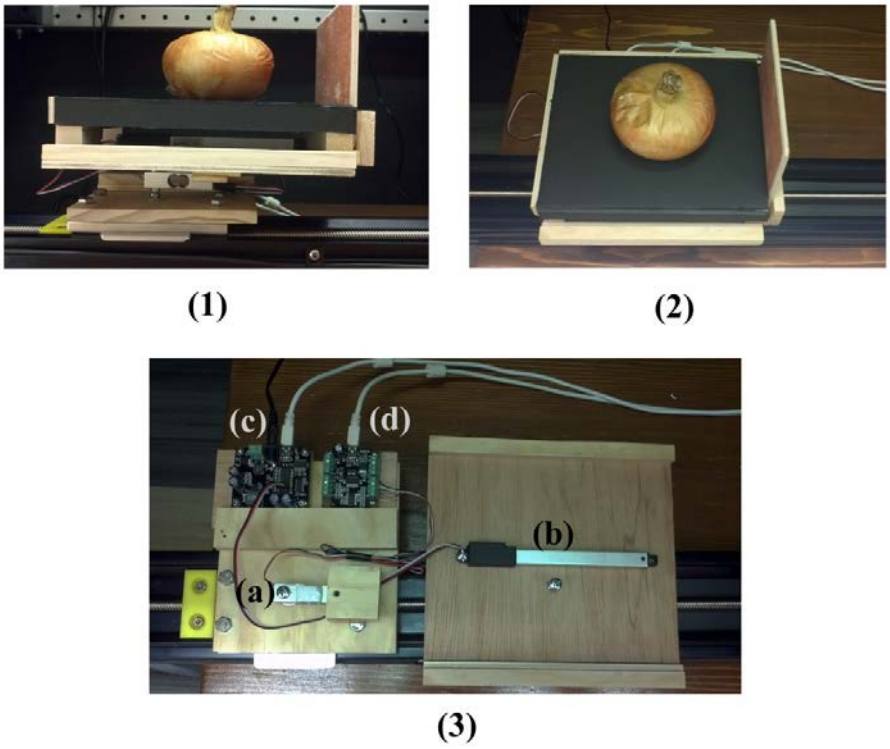

Figure 6.3. Pictures of the onion scanning stage: (1) side view; (2) top view; (3) sensors used in the stage (the stage was disassembled), including a micro load cell (a), linear actuator (b), DC motor controller for linear actuator (c), and Phidget Bridge controller (d).

The color camera was calibrated using a checker board pattern printed on letter-sized paper and a mini color checker card (Munsell mini ColorChecker, X-Rite, MI, USA). The procedure used for calibrating the Kinect sensor is described in Chapter 5. The LCTF spectral imaging unit of the system was calibrated following the method of Wang et al. (2012c). The custom weight sensor made from the micro load cell was validated using a 14 piece brass slotted weight set (Carolina Bio. Supply, NC, USA).

6.3.3 Program

A LabVIEW program was developed to control the process of scanning and collecting images. The program controls the motorized linear slider to deliver the onion to each desired position, and acquire multimodal images from the color camera, Kinect sensor, and spectral imager. The program also measures the weight information of an onion from the load cell integrated in the onion scanning stage. The program was written using LabVIEW graphical programming language (2012 sp1, National Instruments, TX, USA).

The GUI of the program (Figure 6.4) includes three sub-panels from left to right. The top panel on the left side provides an interface for operator to control the position of the scanning stage and measure the weight on the scanning stage. The bottom left panel was used to collect RGB and depth image of the onion. The third panel on the right side was designed for acquiring hyperspectral, multispectral, or monochromic images at the specified wavelength(s).

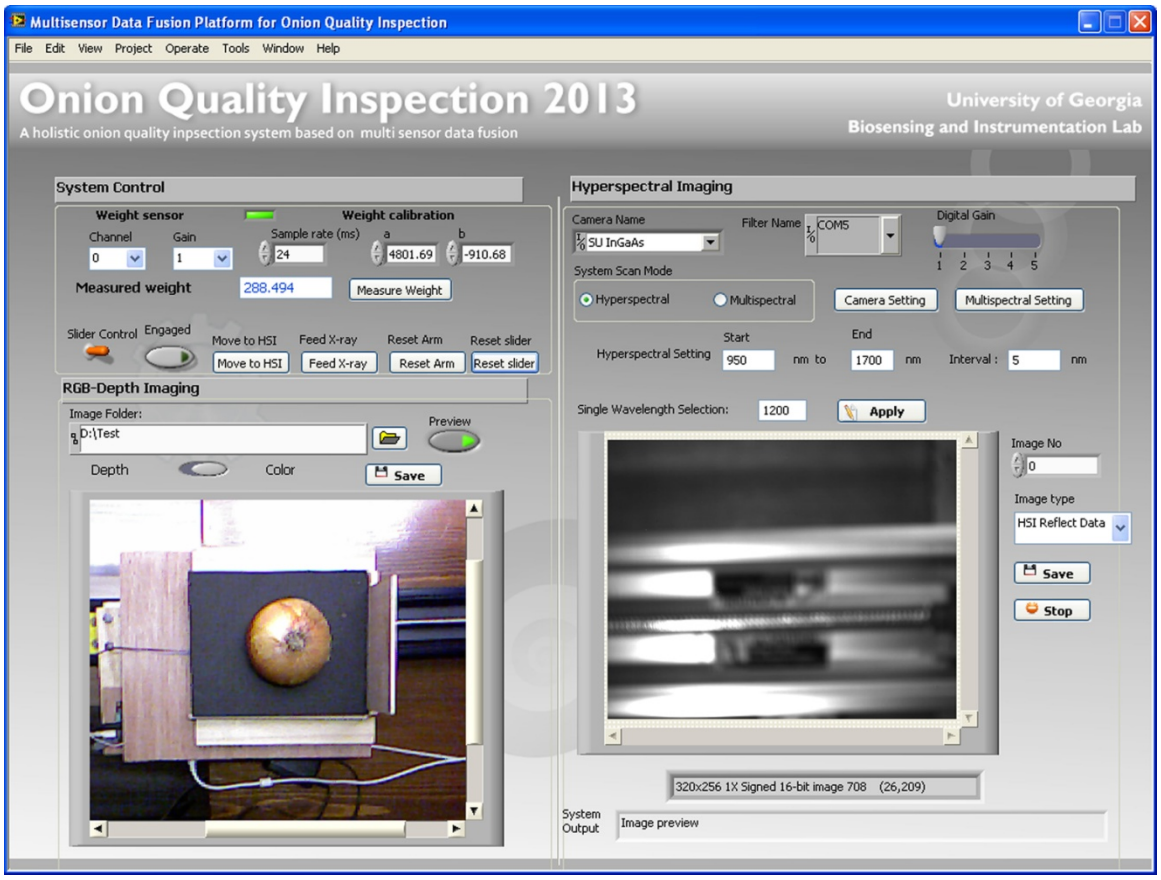

Figure 6.4. Main graphic user interface of the onion quality inspection system.

The program consists of multiple modules organized in a state machine model. The module for color images was developed using LabVIEW NI-DAQmx toolbox (National Instruments, TX, USA). The module for acquiring RGB-depth images was developed based on an open source LabVIEW wrapper (https://decibel.ni.com/content/docs/DOC-16978/) for an open source SDK for Kinect sensor (OpenNI, http://www.openni.org/), with open source drivers and middleware provided by PrimeSense (http://www.primesense.com). The module developed for acquiring hyperspectral images involved several sub-modules, that are introduced in detail in a previous work (Wang et al., 2012b). X-ray images were collected by the integrated software program provided by the manufacture (Autoclear, Fairfield, NJ, USA). Module for measuring

weight was developed using the drivers and LabVIEW application program interfaces (provided by Phidgets Inc.) of the Phidgets sensors. Module for controlling the motorized linear slider weight was developed based on the drivers and LabVIEW sub-VIs provided by Schneider Electric Inc.

6.4 Materials and Methods

A validation study was conducted to validate the sensing capability of this multisensor onion quality inspection system. Several key onion-quality parameters were evaluated using the system, including: weight, diameter, volume, density, and defect situation (with and without disease).

6.4.1 Plant materials and sample preparation

Sweet onions were purchased from local supermarkets in Athens, Georgia, USA in August of 2013. These onions were flat-globe shaped (Granex type). Since the onions were purchased from a supermarket, all of them had passed the commercial sorting conducted by onion packers and shippers. In the test, onions were manually inspected again, and bulbs from medium to colossal size without observable surface blemish or defects were selected. Selected onions were further divided into three groups for preparing three types of onion samples: healthy onions, onions with disease infection in outer scales, and onions with disease in internal scales. To prepare diseased onions under controlled conditions, inocula prepared from cultures of *Burkholderia cepacia* (*B. cepacia*) and *Pseudomonas viridiflava* (*P. viridiflava*) were used to produce bulbs with sour skin and bacterial streak and rot, respectively. Both pathogens were isolated from naturally diseased plants in the state of Georgia and cultured on potato dextrose agar medium. *B. cepacia* and *P. viridiflava* suspension were prepared by harvesting cultures from PDA and mixing them with sterile tap water. Pathogen suspensions (1.5-2 ml per onion)

were infiltrated into onions from the root cap area using a syringe with needle. To inject the *B. cepacia* suspension, the needle was pricked into the second or third scales of onion bulb with a 30-45 degree angle to the onion root cap. To inoculate onions with *P. viridiflava*, the needle was stabbed into the onion bulb perpendicular to the onion root cap so that the bacterial suspension was injected into the 4th scale or deeper.

In summary, three types of onion samples were prepared for this experiment: (1) 40 onions used as healthy samples (controls), which were stored in a refrigerator (5±1 $^{\circ}$C) for 2-3 weeks before the test; (2) 20 onions inoculated with *B. cepacia*, used as samples with sour skin; (3) 14 onions inoculated with *P. viridiflava*, used as samples with bacterial streak and rot. During the test, onions were stored individually in zip lock bags labeled by consecutive integer numbers. Onions inoculated with *B. cepacia* were incubated at 30±1 °C for 5-6 days and samples inoculated with *P. viridiflava* were incubated at 28±1 °C for 5-6 days before testing.

6.4.2 Experimental procedure

Before being scanned by the multisensor system, the physical parameters of onions (diameter, weight, and volume) were manually measured, and the measured values were used as the ground truth of the samples. The maximum equatorial diameter of each onion was measured by a digital caliper for three times and the average value was used. The weight of each onion was measured by a precision digital scale (accuracy of 0.01 gram) three times and averaged. The volume of each onion bulb was measured using the water displacement (WD) method (the detailed procedure for the WD test is described in section 5.3.2).

During scanning, each onion was placed on the onion holder mounted on the scanning stage of the system. The weight of the onion was measured by the custom weighing device, and the result was displayed on the GUI of the system and recorded in a text log file. The scanning stage

first moved to the initial position (right under the color camera) to take a color image of the onion. Then, based on the commands the operator sent from GUI, the scanning stage was moved to the preset positions to take RGB-D and hyperspectral images (950-1700 nm with spectral intervals of 5 nm), respectively. After being scanned by the hyperspectral imager, the onion holder was pushed onto the conveyor belt of the X-ray scanner by the micro robotic arm embedded inside the scanning stage to take an X-ray image. In the meanwhile, the scanning stage was reset to the initial position (under the color camera). In one complete scan, one color image, one RGB-D image, one hyperspectral image, and one X-ray image of the onion were collected. Since onions used in the test were flat-globe shaped, they were scanned at two orientations (neck facing up or root facing up) so that whole surface area of the onion could be examined.

After being scanned, onions were first cut open horizontally from the equatorial area and then were cut again from the neck to root direction, resulting in four separate pieces. The disease and defect level of the onion was evaluated based on their surface and internal appearance and then were graded into two classes: 0 (healthy) or 1 (defective).

6.4.3 Data processing and feature extraction

The maximum diameter and volume of onions were estimated using the depth image collected by the RGB-D sensor. Onion depth images were converted into point cloud images and rotated in 3-D space (X-Y-Z) to make the maximum projection on the X-Y plane to calculate the maximum diameter of onions. An onion point cloud image was later converted into a vortex image to estimate the volume of the onion using a linear regression model. The detailed algorithms for calculating diameter and volume of onion using depth image are introduced in section 5.3. Based on the measured weight and volume, the density of an onion was calculated.

The estimated diameter, volume, weight, and density of onions were compared to their corresponding reference values. Root mean squared error (RMSE) or root mean squared error of prediction (RMSEP) between the estimated parameters and the reference data were calculated to evaluate the accuracy of those measurements made by the proposed system and methods.

Hyperspectral images of onions were first converted into percentage images by applying flat field correction using the white reference hyperspectral image of a Spectralon reflectance panel and the dark hyperspectral image (collected when the optical entrance of the spectral imager was covered by a black cap). Then, images of onions at the wavelengths 1070 nm and 1400 nm were extracted and converted into log-ratio images ($\log_{10}\left(\frac{I_{1070nm}}{I_{1400nm}}\right)$), following the method introduced in Wang et al. (2012a). As discussed in Wang et al. (2012a), the generated log-ratio image of an onion can reflect the moisture distribution on the onion surface, in which a bright pixel indicates a high moisture percentage. When an onion is affected by a pathogen, onion flesh becomes decayed, and fluid is extracted from onion cells which changes the moisture distribution on the onion surface, particularly on the root and neck areas. Therefore, the intensity value and the texture pattern of the log-ratio image of the onion root and neck areas could provide a clue to identification of the infections. The sub-image of the onion neck or root area (100×100 pixels or 120×120 pixels, depending on the size of the onion image) was segmented from the log-ratio images. The maximum, mean, and minimum intensity values of the segmented image were calculated as the statistical features. The gray-level co-occurrence matrix (GLCM) of the image was calculated at 0^o, 45^o, 90^o, and 135^o angles. Based on the GLCM matrices, four textural features (contrast, correlation, energy, and homogeneity) of the onion log-ratio image were

calculated at each GLCM angle. Extracted intensity and textural features of all onion samples were saved into a text file in comma-separated values (CSV) format for later use.

X-ray images of onions were mainly used to extract features for detecting defects inside onions. At the first step, an onion X-ray grayscale image (160×160 pixels) was segmented from the X-ray image of the entire scene (including the onion and the onion holder). In the segmented X-ray image, the frames of the onion holder were removed, and the image only contained the area of the onion and the central area of the top panel of the onion holder. Since the top panel of the onion holder was made from lightweight card board of very low density, it was almost invisible to the X-ray scanner. Therefore, the segmented X-ray image mainly contained the information of the scanned onion bulb. The onion X-ray image was then filtered by a 3×3 pixel-wise adaptive Wiener filter (a low-pass smoothing filter) to reduce the noise. The 2% linear stretching was applied to increase the contrast of the onion X-ray image, which made 2% of the top and bottom intensity values at the image saturated and then mapped the rest of intensity values into the new intensity range linearly. A copy of the preprocessed onion X-ray grayscale image was then converted into a binary image using a threshold level of 0.9, in which the onion area was labeled as background (0) and the rest of area was labeled as foreground (1). The binary image was reversed to become a mask for the onion area. Morphological operations were then applied on the binary onion mask to fill the holes inside the region. All the foreground regions in the binary mask image were identified and the region with largest area size was used as the onion region while other regions were removed.

The identified onion mask was then applied to the preprocessed onion X-ray grayscale image to remove the background information. The maximum, mean, and minimum intensity values of the pixels in the onion region were calculated. The boundaries of the square area

containing the onion were identified to further extract the exact onion image from the X-ray image. The contrast, correlation, energy, and homogeneity of the extracted onion X-ray image were calculated based on GLCM matrices measured at 0^o, 45^o, 90^o, and 135^o angles. All image features extracted from onion X-ray images were saved into a CSV text file. All image processing and feature extraction operations (Figure 6.5) were conducted using custom programs developed in MATLAB 2012b.

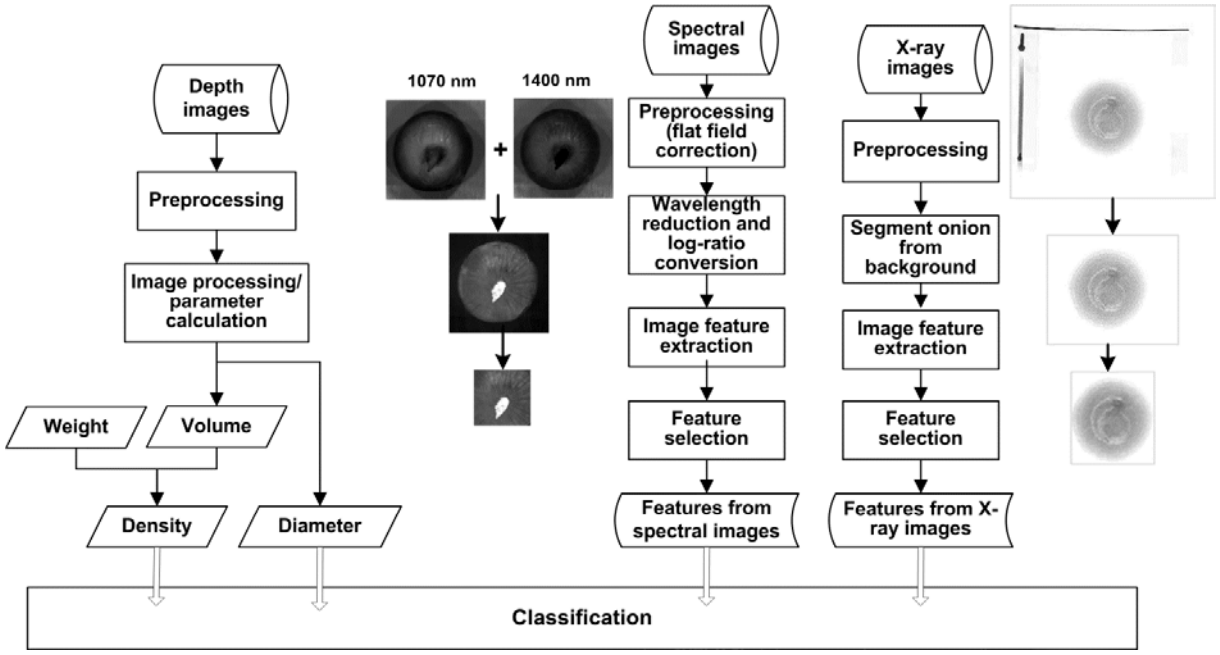

Figure 6.5. High-level flowchart of data processing and feature selections conducted on multimodal data collected in the validation experiment.

6.4.4 Feature selection and classification

The dataset of extracted image features were divided into a training dataset and a testing dataset. The training dataset included the image features of the first 20 onions in group 1 (onions

without any treatment), first six onions in group 2 (onions with bacterial streak and rot), and first 10 onions in group 3 (onions with sour skin). The remaining 38 onions were included in the testing dataset. The training dataset was used to select appropriate features and train classifiers, and the testing dataset was used as an independent validation and testing dataset in feature selection and classification.

Feature selections were conducted to reduce the dimensionality of the feature dataset for classification (Figure 6.5). Feature reduction and selection is crucial to the success for applications using this system since it involves large amounts of data in different domains. To achieve the optimal result, appropriate features should be extracted and selected, while features not contributing to classification should be avoided to reduce measurement and processing time and defying the curse of dimensionality.

The filtering feature selection method was applied to select features from the training feature datasets of X-ray and log-ratio images. For each of the datasets, t-tests (α=0.05) were conducted on each extracted feature to check the difference between the mean of the data of defective onions and the mean of the data of healthy onions. Features were first sorted based on the p-values of t-tests in an ascending order. Linear discriminant analysis (LDA) models were developed using the training dataset with incrementally increased numbers of features, and validated using the testing dataset. Misclassification errors (MCEs) of the LDA models were calculated to check the effect of including more features in the classifier. The optimal number of features was determined when the MCE of the classifier reached the maximum and later declined when the additional feature was included.

Image features extracted and selected from X-ray images, spectral images, and physical parameters of onions measured by the system were used together to build classifiers to

distinguish healthy onions from diseased onions. Out of four measured physical parameters of onions (weight, diameter, volume, and density), only the diameter and density were used in the classification models since the density of an onion is highly correlated with its weight and volume.

A number of classifiers were developed and tested in this work using different levels of fusion schemes (Figure 6.6). In the first scheme (Figure 6.6.a), image features selected from X-ray images and those selected from spectral log-ratio images were used to construct two classifiers, respectively. Three types of classifiers, namely, LDA, binary classification tree, and support vector machine (SVM), were tested and compared to identify an optimal "learner" for the problem. All classifiers were trained by the training dataset and tested using the independent testing dataset.

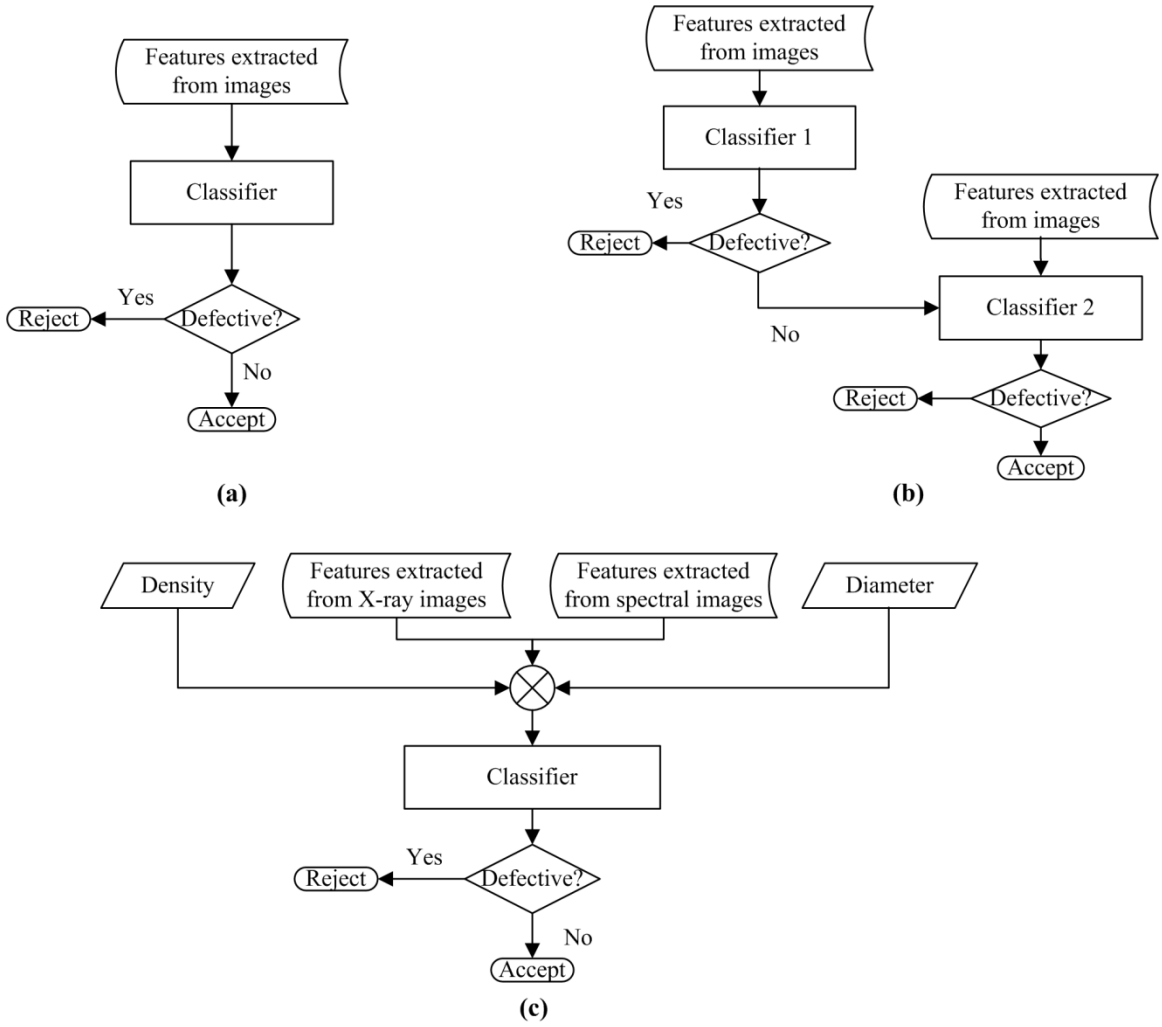

Figure 6.6. Classification schemes based on features extracted from multiple data sources. (a) Single classifier using features extracted from either X-ray or spectral images. (b) A cascade classifier combing two independent classifiers using X-ray and spectral image features. (c) Single classifier using all extracted features.

In the second scheme (Figure 6.6.b), two optimal classification models identified in the first scheme were constructed and combined in order to be used as one classifier. Using this cascade classifier, the items having passed inspections in the first classifier were further checked by the

second classifier. In this scheme, two cascade classifiers actually conducted a logical "OR" operation to detect all suspected diseased onions.

The third classification scheme (Figure 6.6.c) combined all aforementioned selected features and used them to train one single classifier. Since the dimensionality of the input feature changed, the classification of LDA, binary classification tree, and SVM were re-evaluated and compared using the training and testing datasets. The second and third classification schemes utilized the multimodal data collected by the system at decision and feature level, respectively. All feature selections and classification models were conducted with custom programs using the statistical and the machine learning toolboxes of MATLAB.

6.5 Results and Discussion

6.5.1 Examples of collected onion images

Based on the visual inspection on the onions being cut open, 31 out of 40 onions in the first group (without inoculation) were healthy and the other 9 onions had internal defects at different levels. Twelve out of 14 onions in the second group (inoculated with *P. viridiflava*) developed observable bacterial streak and rot, while two samples remained healthy. All 20 onions in the third group (inoculated with *B. cepacia*) developed different levels of sour skin. As observed in this validation experiment, onions inoculated in the second group (bacterial streak and rot) developed more internal decay than onions inoculated in the third group (sour skin) which had more intensive decay on the outer scales of onions.

Figure 6.7 demonstrates the multisource images of onions acquired using the multisensor inspection system and processed using the proposed algorithms, which includes one typical sample for each of the three types of onions tested in the validation test. The color images of

onions being cut open (pictures were taken manually using an independent color camera) were also included in the last column of the figure to show internal situations of the onions.

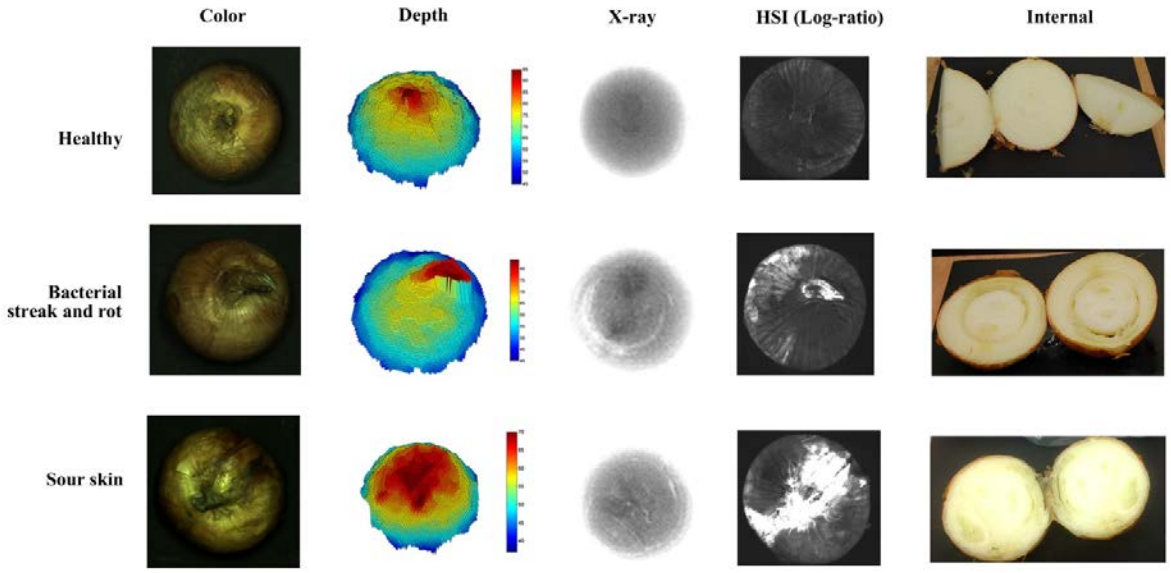

Figure 6.7. Examples of onion images acquired by the multisensor system and processed using the proposed algorithms. Images at each row belong to the same onion.

As shown in Figure 6.7, disease symptoms of onions with bacterial streak and rot or sour skin were shown in both X-ray and spectral log-ratio images. In X-ray images, the white areas and short lines indicate the internal voids and gaps inside the onion. The white (high intensity) spot in onion spectral log-ratio image reflects the high moisture content area on the surface and outer scales of the onion. Overall, onions with bacterial streak and rot showed more distinguishable textural patterns than those of onions with sour skin on the X-ray images, while disease symptoms shown on the spectral log-ratio images of sour skin onions were more obvious than those of bacterial streak and rot onions.

6.5.2 Measurement of onion physical parameters

Figure 6.8 shows the result of weight estimation of the 80 tested onions. It is shown that the system accurately measured the weight of onions, resulting in an average RMSE of 3.7 grams. This accuracy is lower than those of regular commercial benchtop precision balances, which usually have an accuracy of 0.001-0.1 gram. Since the accuracy of the micro load cell is only ±2.5 g, the relatively large error should be caused by the non-optimal design of the mechanical structure of the weighing device used in testing. The accuracy of the weight device can be further enhanced by improving the design of the custom weighing device. On the other hand, considering the average weight of the tested onions was about 400 grams, the relative error of weight measurement using this system was less than one percent, which is accurate enough for onion grading and packing.

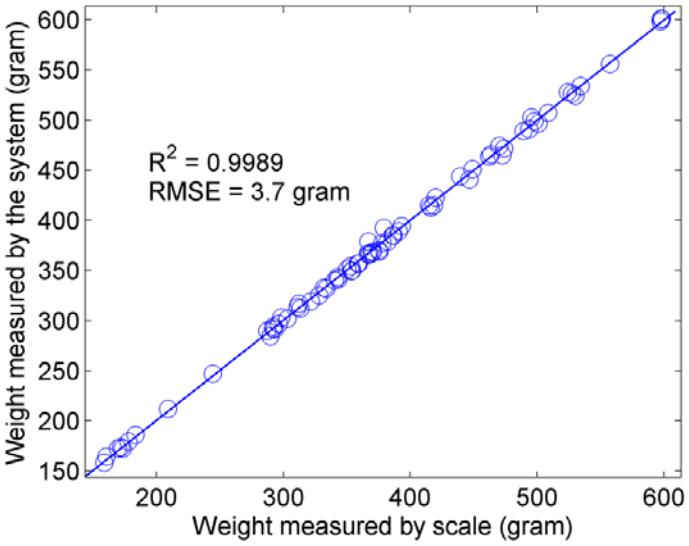

Figure 6.8. Comparison between the weight of onion samples measured using the proposed system and measured by a commercial digital balance.

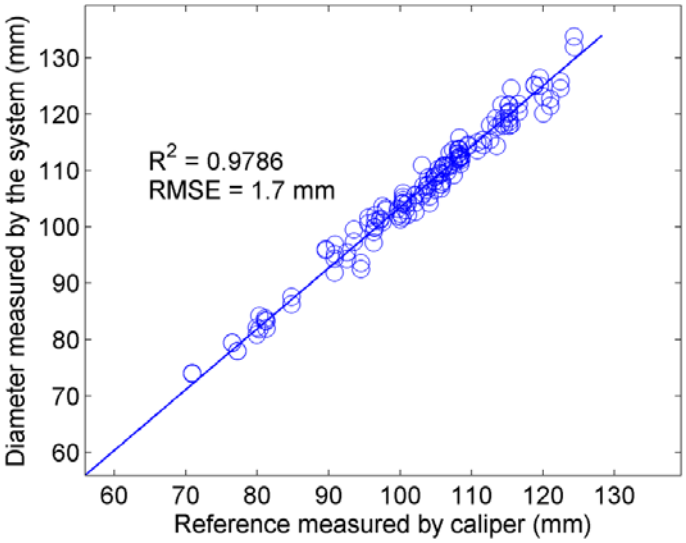

Figure 6.9. Comparison between the maximum diameter of onions estimated using the depth image and the maximum diameter measured by caliper.

The maximum diameter of onions estimated based on their depth images are listed in Figure 6.9. The estimated diameters of onions well matched (RMSE=1.7 mm) the reference values manually measured using the precision caliper. The accuracy achieved in here is comparable to the result of the test conducted in the previous chapter (Chapter 5), which confirmed that the proposed method using depth sensor is a reliable and accurate approach to measure the maximum diameter of onions.

The onion volume estimated using the depth image collected by the system showed an average error of 15.7 cm^3, compared to the volume measured using water displacement method (Figure 6.10). The overall accuracy of volume estimation was 96.9%, which is slightly higher than the accuracy achieved in the previous test discussed in Chapter 5. As discussed in Chapter

5, the accuracy is comparable to or higher than other reported studies of measuring the volume of fruits and vegetables.

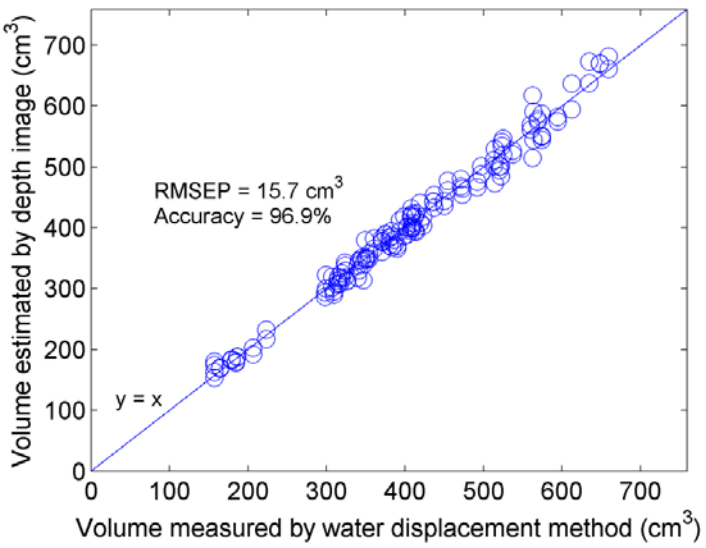

Figure 6.10. Results of onion volume estimated by the depth image collected by the onion quality inspection system.

Onion densities calculated from the volume and weight measured by the system were compared to their counterparts calculated using the reference values (weight measured by the digital scale and volume measured by the WD method) (Figure 6.11). Using the later value as the ground truth, the RMSE of the onion density estimated using the system was 0.03 gram/cm^3 and the average accuracy was 97.52%. It is known that the onion density is related to the dry matter content of the onion. Also, the density of a diseased onion could significantly change. Thus, the system capability to measure density nondestructively provides a useful factor for evaluating onion quality.

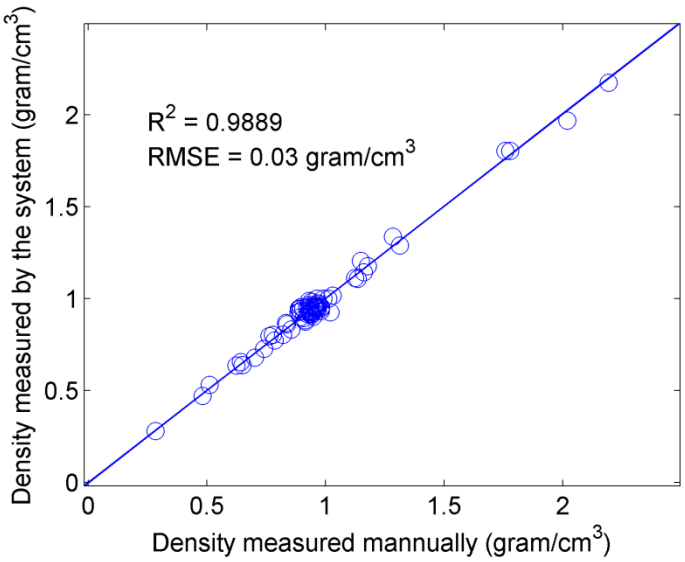

Figure 6.11. Comparison between the onion density values estimated by the system and the density values calculated based on the manually measured weight and volume.

6.5.3 Detection of defective onions

6.5.3.1 Classification using a single imaging sensor

Single classifiers using all image features (maximum intensity, mean intensity, minimum intensity, contrast, correlation, energy, homogeneity) extracted from the X-ray images or spectral images successfully distinguished about 60-70% of onions (Table 6.1). The highest classification rate (76.32%) was achieved by the SVM (Gaussian kernel, sigma=1.5) using spectral image features. For the classifiers using X-ray image features, the highest classification rate was accomplished by the classification tree (69.74%), which was slightly better than the classification rate (68.42%) of the SVM. Overall, false negative numbers were higher than false positive numbers, which means many defective onions (15 or more out of 44) were misclassified as healthy onions.

Table 6.1. Results of classification using single classifier based on all features extracted from X-ray images or from spectral log-ratio images of onions.

Data source	Classifier	Match	Mismatch			Classification Rate (%)
		Healthy	Defective	False positive	False negative	
X-ray image	LDA	25	25	7	19	65.79
	SVM	29	23	3	21	68.42
	Classification tree	24	29	8	15	69.74
Spectral log-ratio image	LDA	21	28	11	16	64.47
	SVM	29	29	3	15	76.32
	Classification tree	19	29	13	15	63.16

Figure 6.12 shows the results of feature selections for the six different types of classifiers listed in Table 6.1. For the LDA and SVM classifiers using X-ray image features, the misclassification rates significantly decreased when optimal features were selected, while no improvement was obtained by reducing the input features for the classification tree. For the classifiers built on the features of spectral images, feature selections reduced the misclassification rate at different levels for all classifiers. Overall, after feature reduction, SVM (Figure 6.12.c and Figure 6.12.d) accomplished higher classification rates than LDA and classification tree, and were selected for further data analysis.

The SVM using spectral image included all features extracted from onion log-ratio images except for the maximum intensity. This result is not consistent with a previous study (Wang et al., 2012a) in which the maximum intensity were identified as one of the most indicative log-ratio image features for distinguishing sour skin and healthy onions. The main reason for this difference is that in this study, positive (defective) samples included not only sour skin onions but also bacterial steak and rot and naturally defective onions. In log-ratio image, the maximum intensity indicates the highest moisture level on the onion surface (higher is brighter). Many of

internal defective samples tested in this study did not have distinct surface rot symptoms. Thus, the maximum values of log-ratio images of these onions were relatively low. On the other hand, some healthy onions tested in this study had very thin dry skins or were not covered by dry skin at certain spots, which resulted in large log-ratio values and a high maximum value of the log-ratio image. Thus, in this test the global maximum intensity value was not as indicative as other textural features such as the contrast and homogeneity.

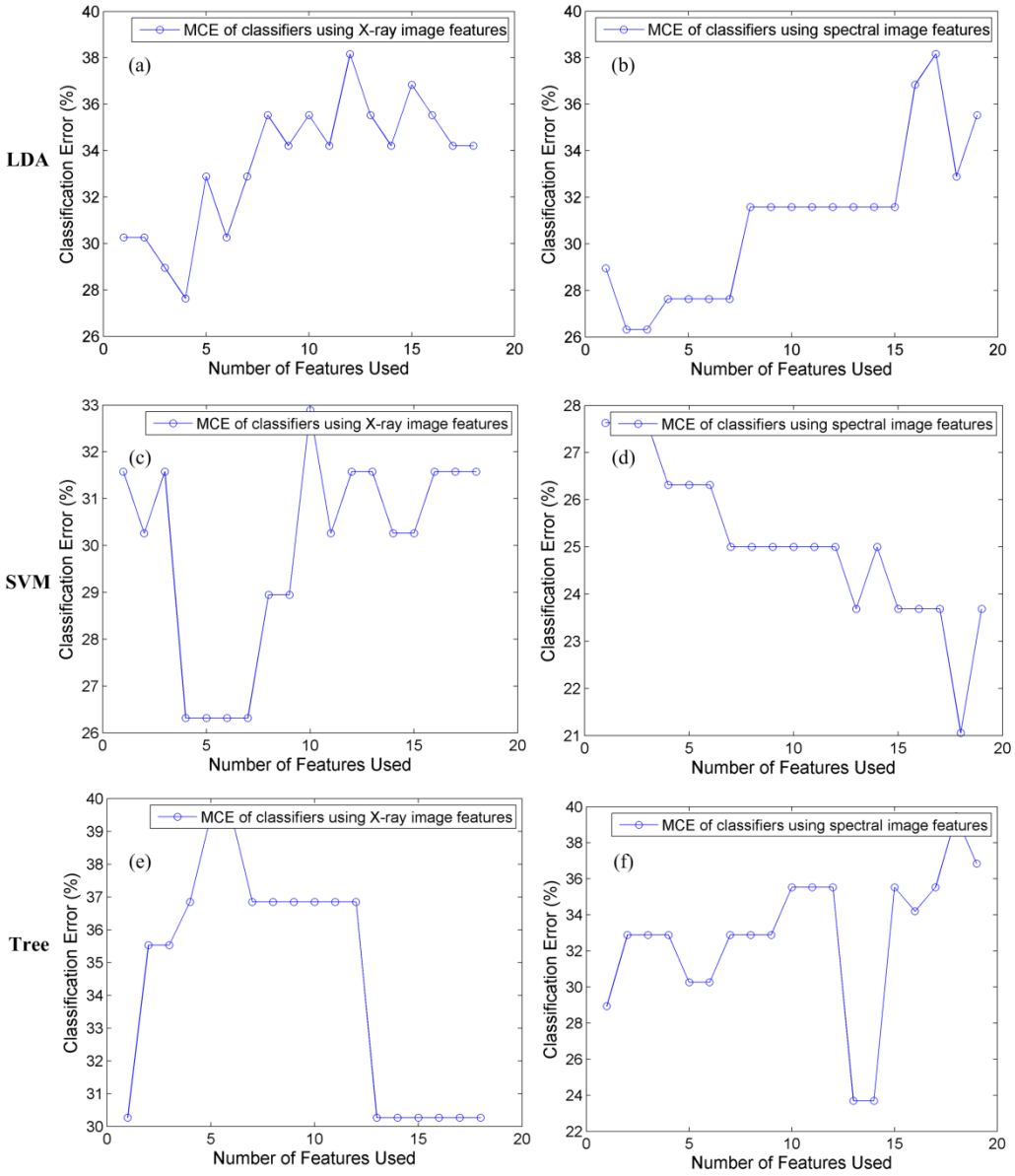

Figure 6.12. Results of feature selections using the filtering method, which shows the misclassification error (MCE) of LDA classifiers using features extracted from X-ray images (a) or extracted from spectral image (b), SVM classifiers using features extracted from X-ray images (c) or from spectral images (d), and classification trees using features extracted from X-ray images (e) or from spectral images (f).

The SVM classifier for onion X-ray images selected four textural features (Contrast at 45^o and 135^o, and Homogeneity at 45^o and 90^o). This selection is reasonable since the X-ray images of the onions with internal defects should have contrast and homogeneity values different from those of healthy onions. When onions flesh scales have internal voids or have decay caused by disease, the density values of those regions are often significantly reduced, which are shown as bright lines and regions in their X-ray images. As a result, the contrast of the onion X-ray image increases and the homogeneity decreases. Another observation is that the selected contrast and homogeneity features were mainly at diagonal orientations, which should be caused by the particular structure of onion scales. Since onion scales have ring patterns in X-ray images, those lines, arcs, and areas indicating defective onion flesh are easier to be detected at diagonal directions.

After feature selection, SVM classifiers using selected X-ray image features or spectral image features achieved 5.25% and 2.63% higher accuracy, respectively (Table 6.2). It is shown that the SVM using the selected features extracted from onion X-ray images ($SVM_{X\text{-}ray}$) detected all onions with bacterial streak and rot, but only identified 55% onions with sour skin. The SVM using the selected features extracted from onion spectral log-ratio images ($SVM_{spectral}$) misclassified one onion with bacterial streak and rot, and detected 85% of onions with sour skin. As for regular onions in the first group (without inoculation), $SVM_{X\text{-}ray}$ successfully detected 5 (out of 12) naturally defective onions, while $SVM_{spectral}$ did not identify any of them. As confirmed by cutting onions open in the experiment, defective onions in the first two groups mainly had higher levels of internal rot than the onions in the third group (sour skin), while the sour skin onions developed more intensive surface rot than those of other two groups. Thus, the results shown in Table 6.2 indicate that $SVM_{X\text{-}ray}$ was more capable of identifying onions with

internal defects, and $SVM_{spectral}$ performed better in distinguishing onions with surface rot from healthy onions.

Table 6.2. Results of classifications on the testing dataset using the single SVM based on selected features of onion X-ray images, the SVM using selected features of onion spectral images, and the cascade classifier combined both SVMs.

Classifier	Onion Group	Match		Mismatch		Accuracy (%)	Total Accuracy (%)
		Healthy	Defective	False positive	False negative		
SVM using X-ray image features	Regular	25	5	3	7	75.00	73.68
	Bacterial streak and rot	3	12	1	0	93.75	
	Sour skin	0	11	0	9	55.00	
SVM using spectral log-ratio image features	Regular	28	0	0	12	70.00	78.95
	Bacterial streak and rot	4	11	0	1	93.75	
	Sour skin	0	17	0	3	85.00	
Classifier with cascade SVMs	Regular	24	5	6	5	72.50	81.58
	Bacterial streak and rot	3	12	1	0	93.75	
	Sour skin	0	18	0	2	90.00	

The accuracy rate achieved by the $SVM_{X\text{-}ray}$ (73.68%) is much lower than the classification rates (about 90%) reported by Tollner et al. (2005) and Shahin et al. (2002). The main reason for this difference is that this study included a large number of sour skin samples that mainly had disease symptoms in external layers, while the studies of Tollner et al. (2005) and Shahin et al. (2002) were more focused on testing onions with internal diseases including center rot and neck rot. On the other hand, the performance of the $SVM_{X\text{-}ray}$ on the dataset of onions with inoculated internal diseases (Bacterial streak and rot) was comparable with the results of Tollner et al. (2005) and Shahin et al. (2002).

The overall accuracy of $SVM_{spectral}$ (78.95%) was also lower than the accuracy (87.14%) accomplished in a previous study (Wang et al., 2012a), in which an SVM was applied to distinguish sour skin and healthy onions. In fact, the performance of $SVM_{spectral}$ on two groups of diseased (inoculated) onions (85% and 93.75%) were comparable and even slightly better than the classifier reported in (Wang et al. (2012a)). The main reason that $SVM_{spectral}$ had a lower classification accuracy was that it missed all 12 positive onions in the first group - those defective onions passed HVI.

6.5.3.2 Classification based on sensor fusion

Using the cascade classifier combining $SVM_{X\text{-}ray}$ and $SVM_{spectral}$, the overall classification rate increased to 81.52% (Table 6.2). Particularly, compared to the relatively low rate of detecting defective onions by using $SVM_{X\text{-}ray}$ or $SVM_{spectral}$ individually (66.67%, 28 out of 42), the disease detection rate accomplished by the cascade classifier was significantly higher (83.33%, 35 out of 42). The result indicated that the $SVM_{X\text{-}ray}$ or $SVM_{spectral}$ had complementary capability to recognize the diseased onions that the other classifier failed to identify. On the other hand, the cascade classifier also had a higher false positive rate than those of using $SVM_{X\text{-}ray}$ or $SVM_{spectral}$ individually since this classification scheme considered all suspicious onions identified by either SVM as defective ones.

Table 6.3. Classification results for the testing dataset using the classifiers developed using feature-level data fusion.

Features used	Classifier	Match		Mismatch		Accuracy (%)
		Healthy	Defective	False positive	False negative	
Selected features of onion X-ray and spectral images	LDA	22	32	12	10	71.05
	SVM	28	32	6	10	78.95
	Tree	29	35	5	7	84.21
Diameter, density, and selected features of onion X-ray and spectral images	LDA	21	27	13	15	63.16
	SVM	28	34	6	8	81.58
	Tree	27	37	7	5	84.21

Table 6.3 shows the classification results of the testing dataset by using the LDA, SVM, and classification tree models developed using feature-level data fusion in which selected features were directly aggregated together and used as the input feature of the classifiers. Results showed that classification trees achieved higher classification rates (84.21%) than SVM and LDA models, which was also higher than the cascade SVM classifier using decision-level data fusion. The SVM using all selected features achieved the same classification rate with the cascade SVM classifier. As shown in the classification results, the inclusion of diameter and density in the SVM or classification tree models slightly increased the detection rates of defective onions.

In brief, the classification results of the validation test showed that image features extracted from the onion X-ray images and those extracted from spectral images are useful for the detection of disease infections in onions. X-ray and spectral images of onions could provide complementary clues for detecting defective onions. The classification rate of onions significantly improved when X-ray and spectral image features were combined at feature level

for classification, or the classifiers developed independently on the X-ray and spectral image data were cascaded at the decision level. The physical parameters measured by the system (diameter and density) also showed evidence of being useful in the detection of defective onions.

6.6 CONCLUSIONS

A novel multisensor machine vision system was designed for quality inspection of onions, utilizing color, 3-D depth, spectral, and X-ray imaging technologies. Selected imaging and sensor devices were integrated into one hardware platform. A software program was developed to control and synchronize hardware devices for data acquisition. The developed system can nondestructively acquire comprehensive information of onions in color, 3-D, spectral, and X-ray domains.

The proposed multisensor system has a greatly enhanced sensing capability than the conventional classification systems for fruits and vegetables. The validation experiment showed that the system accurately measured the weight (RMSE=3.7 grams), diameter (RMSE=1.7 mm), volume (accuracy=96.9%), and density (RMSE=0.03 gram/cm^3) of the tested onions. Classifiers using selected image features of the onion X-ray and spectral images were able to detect onions with either external or internal decay, or both. The X-ray imaging and spectral imaging demonstrated a complementary sensing capability in recognizing defective onions. When information collected from different types of sensors were fused at the decision level or at the feature level, the detection rates of defective onions were much higher than those classifiers using information extracted from a single image source.

To my knowledge, this prototype system is the first time that 3-D depth imaging, spectral imaging, and X-ray imaging technologies were integrated together for quality inspection of fruit and vegetables. The sensing capability of the system allows us to further apply this system to

measure additional onion quality factors, and to grade onions using more comprehensive criteria. This work made important progress towards the development of an automated and intelligent online onion inspection and grading system that can make accurate and fast classification decisions based on the information collected by multiple sensors. The system and methods presented in this chapter can be potentially extended to postharvest quality inspection of other agricultural products.

6.7 Acknowledgements

This work was funded by the USDA NIFA Specialty Crop Research Initiative (Award No. 2009-51181-06010). Authors also sincerely acknowledge Mr. Anthony Mason Dean, Mr. Paul Glatz, Ms. Delmaries Gonzalez, and Ms. Amber Leigh Stewart for their technical assist in this project.

CHAPTER 7

CONCLUSIONS, LIMITATIONS, AND FUTURE RESEARCH

7.1 SUMMARY AND CONCLUSIONS

This dissertation presents a series of research studies conducted to improve the automated postharvest quality inspection and grading of onions. First, optical properties of onion tissues were studied using spectroscopic methods to provide a better understanding of interactions between light and different types of onions. Then, imaging techniques with complementary sensing capabilities were selected to develop a multimodal system for conducting nondestructive quality inspection of onions. A hardware platform was built to integrate multiple types of imaging sensors into one system, and a software program was developed to integrate hardware devices, control the scanning process, and collect data. A number of methods were developed to apply machine vision and machine learning techniques to measure several key quality parameters of onions. At last, a comprehensive validation test was conducted to assess the performance of the proposed methods for measuring key quality factors of onions, and demonstrate the sensing capability of the developed system for onion quality inspection.

The work conducted in the first part (Chapter 3 and 4) measured the key optical properties of different cultivars of onions using a laser-based spectroscopic system (633 nm), and determined the light absorption and reduced scattering coefficients of healthy onions and onions with sour skin (*Burkholderia cepacia*) and neck rot (*Botrytis aclada*) in the spectral region of 550-1650 nm. Results of these studies lead to several useful findings and conclusions:

1) Onion tissues are scattering dominated (high-albedo) media in the spectral region of 550-

1300 nm. This finding indicates that it is possible to apply diffuse reflectance or back-scattering measurements to evaluate onion quality nondestructively since these techniques require the test object to be high-albedo material.

2) Onion dry skin and wet skin have significantly higher absorption and reduced scattering coefficients than onion flesh, and light can be significantly absorbed and scattered by onion outer skins. For the applications intended to measure the characteristics of onion flesh using optical methods, it is important to handle onion outer skins appropriately, such as removing the entire dry skin or displacing certain parts of the dry skin.

3) The light absorption coefficient of onion tissues is mainly associated with the pigment content in the visible spectral region and other chemical compounds (like water) in the NIR region, while the scattering coefficient of onion tissues is related to the cellular structure of onion cells. Different cultivars of onions could have significantly different light absorption and reduced scattering coefficients.

4) Optical characteristics (μ_a and μ_s') of healthy and diseased onions showed significant differences in both visible and NIR spectral regions. Both light scattering and absorption coefficients of onion tissues are potentially useful parameters for detecting diseased onions.

5) The transmittance measurement of an intact onion is not likely, since Monte Carlo simulations showed that the light at 633 nm lost 99% of its energy within 6 layers of onion tissues. The reflectance or interactance measurements could be more suitable for measuring intact onions.

6) Visible and NIR light has limited penetration capability in onions due to the relatively high light scattering and absorption of onion tissues. Imaging and sensing techniques in this spectral region mainly evaluate the situation of external layers of onions. Unless internal defects

exhibit symptoms on the surface of onions, other nondestructive sensing techniques with stronger penetration capability are needed to evaluate the quality of internal scales of onions.

In summary, the two studies conducted in the first part of this dissertation work provide quantitative evidences to understand the interactions between light and onion tissues, which give guidance to select appropriate optical techniques and design optical systems for quality inspection of onions. The optical properties of onion tissues measured in this study can be used to simulate light propagation in onion tissues using theoretical models and simulation tools for various other applications in the future.

The second part of this dissertation (Chapter 5 and 6) illustrates the design and implementation of a prototype system built with multiple sensors and demonstrates the sensing capability of the system in onion quality inspection. The developed multisensor machine vision system, utilizing color, depth imaging, spectral imaging, and X-ray imaging technologies, can acquire comprehensive information of onions in color, 3-D, spectral, and X-ray domains nondestructively. Moreover, a number of algorithms were developed to measure key quality factors of onions using the imaging/sensing technologies integrated in the system.

Compared to conventional classification systems for fruits and vegetables, the proposed system demonstrated a potential of a more versatile sensing capability. The novelty and key contributions of this part of work are:

1) In this study, the 3-D depth imaging, spectral imaging, and X-ray imaging technologies were integrated to conduct quality inspection of fruit and vegetables. Although each of these techniques has been investigated individually for quality inspection of fruits and vegetables previously, this research combined these technologies for the first time into a single sensing system, which led to a useful research platform for evaluating quality of onions and other fruits

and vegetables.

2) As demonstrated in this work, the consumer grade RGB-depth sensor included in the system accurately measured the size (diameter and volume) of onions. Consumer grade depth sensor was effective in collecting 3-D images of onions, with advantages of being invariant to the changes of lighting conditions and robust to the changes of the object orientation. Considering the low cost of the sensor, this technique leads to novel practical solutions to measure the size parameters of onions nondestructively, including diameter and volume. Particularly, the online measurement of volume has been a big challenge for onions. The successful measurement of onion volume using depth imaging provides an appealing new feature for online quality evaluation of onions. This study also demonstrated the feasibility of estimating the density of onions using a nondestructive approach.

3) The X-ray and NIR spectral imaging devices integrated in the system demonstrated complementary sensing capability in recognizing defective onions. Classifiers using image features extracted from X-ray and spectral images were able to detect onions with external and internal rot. When image features collected from both types of images were combined at the decision level or at the feature level, the detection rates of defective onions were greatly improved. This result proved the concept that using sensor fusion of multiple appropriately selected techniques can achieve a higher accuracy of onion disease detection than using any single sensor. Sensor fusion and data fusion are useful techniques for the quality inspection and grading of fruits and vegetables.

4) This work delivered a novel machine vision system that can acquire images from multiple sensors, and then developed multisensor data fusion algorithms for onion quality inspection. The validation experiment showed that the system accurately measured the weight,

diameter, volume, density of onions, and defective onions were distinguished from healthy onions. These external and intrinsic quality parameters of onions can be calculated simultaneously from the data collected by the system.

In conclusion, the developed multisensor system accomplished a strong sensing capability for quality inspection and grading of onions, which can nondestructively measure multiple key quality factors and evaluate onion quality holistically. As a prototype, the proposed system provides a solid base for the development of a fully automated and intelligent online inspection and grading system for onions in the future. Potentially, the system and methods presented in this dissertation can be also extended for postharvest quality inspection of other agricultural products.

7.2 LIMITATIONS

Due to the time limitation, this dissertation work mainly focused on developing a prototype and proving the concept of applying sensor fusion to conduct holistic quality inspection of onions. There are several noteworthy limitations of these studies:

1) Due to the limitations of the instruments, the optical properties of onion tissues in the spectral regions 400-550 nm and 1650-2500 nm were not measured.

2) The X-ray machine used in this study is a commercial line-scanner for regular inspection applications (hard X-ray). A custom X-ray imaging device with a lower energy level (soft X-ray) could acquire onion X-ray images with better contrast. Moreover, the X-ray images collected by the line-scanner are saved in an independent computer integrated in the X-ray machine. Thus, the machine vision system does not have the direct access to the X-ray data collected by the machine.

3) The proposed multisensor system and methods have not been tested with large numbers of samples directly collected from onion packinghouses. With a larger number of training

samples, the performance of the proposed classifiers could be improved.

4) Several devices used in the proposed multisensor system are research-oriented and are not optimal solutions for online classification. For instance, the weighing device made with the micro load cell could be more accurate. Moreover, the electronically tunable filter (the LCTF) and high profile color camera used in the system might be too expensive to be included in commercial classification systems for onions.

5) The cameras included in the proposed system (except for the X-ray scanner) can only observe the top half of the onion bulb in each scan. It would be better if the system can evaluate the entire onion within one scan.

6) The speed and automation level of the proposed system are not comparable to those of commercial classification lines for onions.

7.3 Future Research

Future studies could be conducted at the following aspects to further extend and improve this work:

1) Comprehensive computation models of onions can be constructed based on the measured optical properties to develop more in-depth understanding of the light-onion tissue interactions, such as the light propagation in intact onion bulbs.

2) The spectral sensing capability of the proposed system can be further enhanced at different aspects. First, line-scan hyperspectral imaging can be applied to improve the throughput of the system. Second, the spectral information of onions in the spectral region of 400-950 nm can be collected and used. Third, if all needed wavelengths are identified, multispectral imaging cameras should be used, which are often faster and cheaper than hyperspectral imaging devices.

3) Soft X-ray imaging can be applied to acquire onion X-ray images with high contrast,

which also provides a less radioactive operating environment for the system.

4) In addition to being used as a camera collecting 3-D images, the RGB-D sensor can be used as a motion sensor for other purposes, such as tracing the movement of the onion stage and monitoring the processing of the scanning. Moreover, the RGB-D sensor is a good mapping and localization tool for autonomous mobile robots navigation. It is possible to integrate the RGB-D sensor with robots for applications in onion storage rooms, such as automatically transporting onions and detecting diseased onions.

5) In addition to the quality factors evaluated in this study, other quality parameters of onions, such as shape, soluble solids content, and moisture content, can be evaluated.

6) The position of the onion neck and the orientation of the onion bulb can also be determined automatically using machine vision methods.

7) Special holders or rollers for onions can be designed to adjust the orientation of the onion during scanning. It is also necessary to develop a method to evaluate the whole surface area of the onion using as less imaging devices as possible.

8) Sensor/data fusion methods can be further studied and developed to make more accurate and versatile classification decisions based on the needs of specific applications. For instance, clean onions having passed the defect inspection can be further classified into multiple grades based on sugar content and pungency.

9) A real time online onion quality inspection system with multimodal sensors should be studied and developed in the future.

BIBLIOGRAPHY

Abbott, J.A., 1999. Quality measurement of fruits and vegetables. Postharvest Biology and Technology 15, 207-225.

Abhayawick, L., Laguerre, J.C., Tauzin, V., Duquenoy, A., 2002. Physical properties of three onion varieties as affected by the moisture content. Journal of Food Engineering 55, 253-262.

Altan, A., Oztop, M.H., McCarthy, K.L., McCarthy, M.J., 2011. Monitoring changes in feta cheese during brining by magnetic resonance imaging and NMR relaxometry. Journal of Food Engineering 107, 200-207.

Ariana, D., Guyer, D.E., Shrestha, B., 2006. Integrating multispectral reflectance and fluorescence imaging for defect detection on apples. Computers and Electronics in Agriculture 50, 148-161.

Baranowski, P., Lipecki, J., Mazurek, W., Walczak, R.T., 2008. Detection of watercore in 'Gloster' apples using thermography. Postharvest Biology and Technology 47, 358-366.

Baranowski, P., Mazurek, W., Witkowska-Walczak, B., Sławiński, C., 2009. Detection of early apple bruises using pulsed-phase thermography. Postharvest Biology and Technology 53, 91-100.

Barcelon, E.G., Tojo, S., Watanabe, K., 1999. X-ray Computed Tomography for Internal Quality Evaluation of Peaches. Journal of Agricultural Engineering Research 73, 323-330.

Birth, G.S., Dull, G.G., Renfroe, W.T., Kays, S.J., 1985. Nondestructive spectrophotometric determination of dry matter in onions. Journal of the American Society for Horticultural Science 110, 297-303.

Blasco, J., Aleixos, N., Moltó, E., 2003. Machine vision system for automatic quality grading of fruit. Biosystems Engineering 85, 415-423.

Blasco, J., Cubero, S., Mira, P., Molt, E., 2009. Development of a machine for the automatic sorting of pomegranate (Punica granatum) arils based on computer vision. Journal of Food Engineering 90, 27-34.

Block, E., 2010. Garlic and other alliums: The lore and the science. Royal Society of Chemistry, Burlington House, Piccadilly, London, UK.

Brandwein, B.J., 1965. The pigments in three cultivars of the common onion (Allium cepa). Journal of Food Science 30, 680-685.

Brewster, J.L., 2008. Onions and other vegetable alliums. CABI, Cambridge, MA, USA.

Brosnan, T., Sun, D.-W., 2004. Improving quality inspection of food products by computer vision—a review. Journal of Food Engineering 61, 3-16.

Bulanon, D.M., Burks, T.F., Alchanatis, V., 2009. Image fusion of visible and thermal images for fruit detection. Biosystems Engineering 103, 12-22.

Canessa, A., Chessa, M., Gibaldi, A., Sabatini, S.P., Solari, F., 2013. Calibrated depth and color cameras for accurate 3D interaction in a stereoscopic augmented reality environment. Journal of Visual Communication and Image Representation.

Chéné, Y., Rousseau, D., Lucidarme, P., Bertheloot, J., Caffier, V., Morel, P., Belin, É., Chapeau-Blondeau, F., 2012. On the use of depth camera for 3D phenotyping of entire plants. Computers and Electronics in Agriculture 82, 122-127.

Corzo-Martinez, M., Corzo, N., Villamiel, M., 2007. Biological properties of onions and garlic. Trends in Food Science & Technology 18, 609-625.

Cubeddu, R., D'Andrea, C., Pifferi, A., Taroni, P., Torricelli, A., Valentini, G., Ruiz-Altisent, M., Valero, C., Ortiz, C., Dover, C., Johnson, D., 2001. Time-resolved reflectance spectroscopy applied to the nondestructive monitoring of the internal optical properties in apples. Applied Spectroscopy 55, 1368-1374.

Cubero, S., Aleixos, N., Moltó, E., 2011. Advances in machine vision applications for automatic inspection and quality evaluation of fruits and vegetables. Food Bioprocess Technol 4, 487–504.

de Visser, C.L.M., van den Berg, W., 1998. A method to calculate the size distribution of onions and its use in an onion growth model. Scientia Horticulturae 77, 129-143.

Foskett, R.L., Peterson, C.E., 1950. Relation of dry matter content to storage quality in some onion varieties and hybrids. Proceedings of American Society for Horticultural Science 55, 314-318.

Fraser, D.G., Jordan, R.B., Künnemeyer, R., McGlone, V.A., 2003. Light distribution inside mandarin fruit during internal quality assessment by NIR spectroscopy. Postharvest Biology and Technology 27, 185-196.

Freedman, B., Shpunt, A., Machline, M., Arieli, Y., 2010. Depth mapping using projected patterns, Prime Sense Ltd., USA.

Fricke, T., Wachendorf, M., 2013. Combining ultrasonic sward height and spectral signatures to assess the biomass of legume–grass swards. Computers and Electronics in Agriculture 99, 236-247.

Gall, H., Muir, A., Fleming, J., Pohlmann, R., Gocke, L., Hossack, W., 1998. A ring sensor system for the determination of volume and axis measurements of irregular objects. Meas Sci Technol 9, 1809-1820.

Gitaitis, R., Nischwitz, C., 2006. Burkholderia, In: Gnanamanickam, S. (Ed.). Springer, Dordrecht, the Netherlands, pp. 645-670.

Gonzalez, M.E., Barrett, D.M., McCarthy, M.J., Vergeldt, F.J., Gerkema, E., Matser, A.M., Van As, H., 2010. ^{1}H-NMR Study of the Impact of High Pressure and Thermal Processing on Cell Membrane Integrity of Onions. Journal of Food Science 75, E417-E425.

Gowen, A.A., O'Donnell, C.P., Cullen, P.J., Downey, G., Frias, J.M., 2007. Hyperspectral imaging – an emerging process analytical tool for food quality and safety control. Trends in Food Science & Technology 18, 590-598.

Gowen, A.A., O'Donnell, C.P., Taghizadeh, M., Gaston, E., O'Gorman, A., Cullen, P.J., Frias, J.M., Esquerre, C., Downey, G., 2008. Hyperspectral imaging for the investigation of quality deterioration in sliced mushrooms (Agaricus bisporus) during storage. Sensing and Instrumentation for Food Quality and Safety 2, 133-143.

Gowen, A.A., Tiwari, B.K., Cullen, P.J., McDonnell, K., O'Donnell, C.P., 2010. Applications of thermal imaging in food quality and safety assessment. Trends in Food Science & Technology 21, 190-200.

Griffiths, G., Trueman, L., Crowther, T., Thomas, B., Smith, B., 2002. Onions--a global benefit to health. Phytotherapy research: PTR 16, 603–615.

Haff, R.P., Toyofuku, N., 2008. X-ray detection of defects and contaminants in the food industry. Sensing and Instrumentation for Food Quality and Safety 2, 262-273.

Hall, D.L., Llinas, J., 1997. An introduction to multisensor data fusion. Proceedings of the IEEE 85, 6-23.

Henningsson, M., Östergren, K., Sundberg, R., Dejmek, P., 2006. Sensor fusion as a tool to monitor dynamic dairy processes. Journal of Food Engineering 76, 154-162.

Henry, P., Krainin, M., Herbst, E., Ren, X., Fox, D., 2010. RGB-D mapping: Using depth cameras for dense 3D modeling of indoor environments.

Hole, C.C., Drew, R.L.K., Gray, D., 2000. Humidity and mechanical properties of onion skins. Postharvest Biology and Technology 19, 229-237.

Imou, K., Kaizu, Y., Morita, M., Yokoyama, S., 2006. Three-dimensional shape measurement of strawberries by volume intersection method. Transactions of the ASABE 49, 449-456.

Iraguen, V., Guesalaga, A., Agosin, E., 2006. A portable non-destructive volume meter for wine grape clusters. Meas Sci Technol 17, N92-N96.

Jastrzębska, A., Brudka, B., Szymański, T., Szłyk, E., 2003. Determination of phosphorus in food samples by X-ray fluorescence spectrometry and standard spectrophotometric method. Food Chemistry 83, 463-467.

Kasai, M., Lewis, A.R., Ayabe, S., Hatae, K., Fyfe, C.A., 2007. Quantitative NMR imaging study of the cooking of Japonica and Indica rice. Food Research International 40, 1020-1029.

Khoshelham, K., Elberink, S.O., 2012. Accuracy and resolution of kinect depth data for indoor mapping applications. 1437-1454.

Kim, A., Wilson, B.C., 2011. Measurement of ex vivo and in vivo tissue optical properties: Methods and theories, In: Welch, A.J., Gemert, M.J.C.E. (Eds.), Optical-Thermal Response of Laser-Irradiated Tissue, 2nd ed. Springer Netherlands, pp. 267-319.

Ko, M.-J., Cheigh, C.-I., Cho, S.-W., Chung, M.-S., 2011. Subcritical water extraction of flavonol quercetin from onion skin. Journal of Food Engineering 102, 327-333.

Kondo, N., 2010. Automation on fruit and vegetable grading system and food traceability. Trends in Food Science & Technology 21, 145-152.

Kondo, N., Ninomiya, K., Kamata, J., Chong, V.K., Monta, M., Ting, K.C., 2007. Eggplant grading system including rotary tray assisted machine vision whole fruit inspection. JOURNAL-JAPANESE SOCIETY OF AGRICULTURAL MACHINERY 69, 68.

Kotwaliwale, N., Weckler, P.R., Brusewitz, G.H., Kranzler, G.A., Maness, N.O., 2007. Non-destructive quality determination of pecans using soft X-rays. Postharvest Biology and Technology 45, 372-380.

Laurentini, A., 1994. The Visual Hull Concept for Silhouette-Based Image Understanding. Pattern Analysis and Machine Intelligence, IEEE Transactions 16, 150-162.

Lee, D.J., Xu, X., Eifert, J., Zhan, P., 2006. Area and volume measurements of objects with irregular shapes using multiple silhouettes. Optical Engineering 45, 027202-027202.

Li, C., Gitaitis, R., Tollner, B., Sumner, P., MacLean, D., 2009. Onion sour skin detection using a gas sensor array and support vector machine. Sensing and Instrumentation for Food Quality and Safety 3, 193-202.

Li, C., Heinemann, P., Sherry, R., 2007. Neural network and Bayesian network fusion models to fuse electronic nose and surface acoustic wave sensor data for apple defect detection. Sensors and Actuators B: Chemical 125, 301-310.

Li, C., Heinemann, P.H., 2007. ANN-integrated electronic nose and zNose system for apple quality evaluation. Transactions of the ASABE 50, 2285-2294.

Lorente, D., Aleixos, N., Gomez-Sanchis, J., Cubero, S., Garcia-Navarrete, O.L., Blasco, J., 2012. Recent Advances and Applications of Hyperspectral Imaging for Fruit and Vegetable Quality Assessment. Food Bioprocess Technol 5, 1121-1142.

Lorente, D., Blasco, J., Serrano, A.J., Soria-Olivas, E., Aleixos, N., Gomez-Sanchis, J., 2013. Comparison of ROC Feature Selection Method for the Detection of Decay in Citrus Fruit Using Hyperspectral Images. Food Bioprocess Technol 6, 3613-3619.

Lu, R., 2008. Quality evaluation of fruit by Hyperspectral imaging, In: Da-Wen, S. (Ed.), Computer Vision Technology for Food Quality Evaluation. Academic Press, Amsterdam, pp. 319-348.

Lu, R., Ariana, D.P., Cen, H., 2011. Optical absorption and scattering properties of normal and defective pickling cucumbers for 700–1000 nm. Sensing and Instrumentation for Food Quality and Safety 5, 51–56.

Lu, R., Cen, H., Huang, M., Ariana, D.P., 2010. Spectral absorption and scattering properties of normal and bruised apple tissue. Transactions of the ASABE 53, 263–269.

Lu, R., Peng, Y., 2007. Development of a multispectral imaging prototype for real-time detection of apple fruit firmness. Optical Engineering 46.

Mallor, C., Balcells, M., Mallor, F., Sales, E., 2011. Genetic variation for bulb size, soluble solids content and pungency in the Spanish sweet onion variety Fuentes de Ebro. Response to selection for low pungency. Plant Breeding 130, 55-59.

Marcone, M.F., Wang, S., Albabish, W., Nie, S., Somnarain, D., Hill, A., 2013. Diverse food-based applications of nuclear magnetic resonance (NMR) technology. Food Research International 51, 729-747.

Mark, G.L., Gitaitis, R.D., Lorbeer, J.W., 2002. Bacterial diseases of onion, In: Rabinowitch, H.D., Currah, L. (Eds.), Allium crop science: recent advances. CABI Pub., Wallingford, Oxfordshire, UK.

Mathanker, S.K., Weckler, P.R., Bowser, T.J., 2013. X-ray applications in food and agriculture: A review. Transactions of the ASABE 56, 1227-1239.

Maw, B.W., Hung, Y.C., Tollner, E.W., Smittle, D.A., Mullinix, B.G., 1996. Physical and mechanical properties of fresh and stored sweet onions. Transactions of the American Society of Agricultural Engineers 39, 633–637.

Mendoza, F., Lu, R., Ariana, D., Cen, H., Bailey, B., 2011. Integrated spectral and image analysis of hyperspectral scattering data for prediction of apple fruit firmness and soluble solids content. Postharvest Biology and Technology In Press, Corrected Proof.

Mendoza, F., Lu, R., Cen, H., 2012. Comparison and fusion of four nondestructive sensors for predicting apple fruit firmness and soluble solids content. Postharvest Biology and Technology 73, 89-98.

Mendoza, F., Verboven, P., Ho, Q.T., Kerckhofs, G., Wevers, M., Nicolaï, B., 2010. Multifractal properties of pore-size distribution in apple tissue using X-ray imaging. Journal of Food Engineering 99, 206-215.

Microsoft, 2010. Kinect.

Moreda, G.P., Ortiz-Cañavate, J., García-Ramos, F.J., Ruiz-Altisent, M., 2009. Non-destructive technologies for fruit and vegetable size determination – A review. Journal of Food Engineering 92, 119-136.

Mulayim, A.Y., Yilmaz, U., Atalay, V., 2003. Silhouette-based 3-D model reconstruction from multiple images. IEEE transactions on systems, man, and cybernetics. Part B, Cybernetics : a publication of the IEEE Systems, Man, and Cybernetics Society 33, 582-591.

Musse, M., Quellec, S., Cambert, M., Devaux, M.-F., Lahaye, M., Mariette, F., 2009. Monitoring the postharvest ripening of tomato fruit using quantitative MRI and NMR relaxometry. Postharvest Biology and Technology 53, 22-35.

Neethirajan, S., Jayas, D.S., White, N.D.G., 2007. Detection of sprouted wheat kernels using soft X-ray image analysis. Journal of Food Engineering 81, 509-513.

Nicolaï, B.M., Beullens, K., Bobelyn, E., Peirs, A., Saeys, W., Theron, K.I., Lammertyn, J., 2007. Nondestructive measurement of fruit and vegetable quality by means of NIR spectroscopy: A review. Postharvest Biology and Technology 46, 99-118.

Ninni, P.D., Martelli, F., Zaccanti, G., 2011. Intralipid: towards a diffusive reference standard for optical tissue phantoms. Phys Med Biol 56, 21–28.

Noda, T., Tsuda, S., Mori, M., Takigawa, S., Matsuura-Endo, C., Kim, S.-J., Hashimoto, N., Yamauchi, H., 2006. Determination of the phosphorus content in potato starch using an energy-dispersive X-ray fluorescence method. Food Chemistry 95, 632-637.

Noh, H.K., Peng, Y., Lu, R., 2007. Integration of hyperspectral reflectance and fluorescence imaging for assessing apple maturity. Transactions of the ASABE 50, 963-971.

Olafsdottir, G., Nesvadba, P., Di Natale, C., Careche, M., Oehlenschläger, J., Tryggvadóttir, S.a.V., Schubring, R., Kroeger, M., Heia, K., Esaiassen, M., Macagnano, A., Jørgensen, B.M., 2004. Multisensor for fish quality determination. Trends in Food Science & Technology 15, 86-93.

Park, B., Lee, S., Yoon, S.-C., Sundaram, J., Windham, W.R., Hinton Jr, A., Lawrence, K.C., 2011. AOTF hyperspectral microscopic imaging for foodborne pathogenic bacteria detection, Sensing for Agriculture and Food Quality and Safety III, April 26, 2011 - April 27, 2011.

SPIE, Orlando, FL, United states, pp. The Society of Photo-Optical Instrumentation Engineers (SPIE).

Pérez-Gregorio, R.M., García-Falcón, M.S., Simal-Gándara, J., Rodrigues, A.S., Almeida, D.P.F., 2010. Identification and quantification of flavonoids in traditional cultivars of red and white onions at harvest. Journal of Food Composition and Analysis 23, 592-598.

Pickering, J.W., Prahl, S.A., Wieringen, N.v., Beek, J.F., Sterenborg, H.J.C.M., Gemert, M.J.C.v., 1993. Double-integrating-sphere system for measuring the optical properties of tissue. Applied Optics 32, 399.

Prahl, S., 2011. Everything I think you should know about inverse adding-doubling.

Prahl, S.A., van Gemert, M.J.C., Welch, A.J., 1993a. Determining the optical properties of turbid media by using the adding–doubling method. Applied Optics 32, 559-568.

Prahl, S.A., van Gemert, M.J.C., Welch, A.J., 1993b. Determining the optical properties of turbid mediaby using the adding-doubling method. Applied Optics 32, 559.

Qin, J., Burks, T.F., Ritenour, M.A., Bonn, W.G., 2009. Detection of citrus canker using hyperspectral reflectance imaging with spectral information divergence. Journal of Food Engineering 93, 183-191.

Qin, J., Chao, K., Kim, M.S., 2011. Investigation of Raman chemical imaging for detection of lycopene changes in tomatoes during postharvest ripening. Journal of Food Engineering 107, 277-288.

Qin, J., Chao, K., Kim, M.S., Lu, R., Burks, T.F., 2013. Hyperspectral and multispectral imaging for evaluating food safety and quality. Journal of Food Engineering 118, 157-171.

Qin, J., Lu, R., 2007. Measurement of the absorption and scattering properties of turbid liquid foods using hyperspectral imaging. Applied Spectroscopy 61, 388–396.

Qin, J., Lu, R., 2008. Measurement of the optical properties of fruits and vegetables using spatially resolved hyperspectral diffuse reflectance imaging technique. Postharvest Biology and Technology 49, 355-365.

Qing, Z., Ji, B., Zude, M., 2008. Non destructive analyses of apple quality parameters by means of laser-induced backscattering imaging. Postharvest Biology and Technology 48, 215–222.

Rajkumar, P., Wang, N., Eimasry, G., Raghavan, G.S.V., Gariepy, Y., 2012. Studies on banana fruit quality and maturity stages using hyperspectral imaging. Journal of Food Engineering 108, 194-200.

Rodríguez Galdón, B., Tascón Rodríguez, C., Rodríguez Rodríguez, E.M., Díaz Romero, C., 2009. Fructans and major compounds in onion cultivars (Allium cepa). Journal of Food Composition and Analysis 22, 25-32.

Romano, G., Nagle, M., Argyropoulos, D., Müller, J., 2011. Laser light backscattering to monitor moisture content, soluble solid content and hardness of apple tissue during drying. Journal of Food Engineering 104, 657-662.

Ruiz-Altisent, M., Lleó, L., Riquelme, F., 2006. Instrumental quality assessment of peaches: Fusion of optical and mechanical parameters. Journal of Food Engineering 74, 490-499.

Saeys, W., Velazco-Roa, M.A., Thennadil, S.N., Ramon, H., Nicolai, B.M., 2008. Optical properties of apple skin and flesh in the wavelength range from 350 to 2200 nm. Applied Optics 47, 908-919.

Schwartz, H.F., 2011. Botrytis, downy mildew and purple blotch of onion.

Schwartz, H.F., Mohan, S.K., 2008a. Compendium of onion and garlic diseases and pests, 2nd ed. APS Press, American Phytopathological Society, St. Paul, Minn.

Schwartz, H.F., Mohan, S.K., 2008b. Compendium of Onion and Garlic Diseases and Pests APS Press, St Paul, Minn.

Shahin, M.A., Tollner, E.W., Gitaitis, R.D., Sumner, D.R., Maw, B.W., 2002. Classification of sweet onions based on internal defects using image processing and neural network techniques. Transactions of the American Society of Agricultural Engineers 45, 1613-1618.

Steinmetz, V., Sevila, F., Bellon-Maurel, V., 1999. A methodology for sensor fusion design: Application to fruit quality assessment. Journal of Agricultural Engineering Research 74, 21-31.

Sun, D.-W., 2010. Hyperspectral imaging for food quality analysis and control. Academic Press, London.

Takahama, U., Hirota, S., 2000. Deglucosidation of quercetin glucosides to the aglycone and formation of antifungal agents by peroxidase-dependent oxidation of quercetin on browning of onion scales. Plant and cell physiology 41, 1021-1029.

Tollner, E.W., Gitaitis, R.D., Seebold, K.W., Maw, B.W., 2005. Experiences with a food product X-ray inspection system for classifying onions. Applied Engineering in Agriculture 21, 907-912.

Tuchin, V., Viktorovich, 2007a. Tissue optics: light scattering methods and instruments for medical diagnosis. SPIE/International Society for Optical Engineering.

Tuchin, V.V., 2007b. Tissue optics: light scattering methods and instruments for medical diagnosis. SPIE/International Society for Optical Engineering.

U.S. Department of Agriculture, 1995. United States standards for grades of onions (other than Bermuda-Granex-Grano and Creole type). U.S. Department of Agriculture.

U.S. Department of Agriculture, 2011. U.S. onion statistics. United States Department of Agriculture, USDA Economics, Statistics and Market Information System

U.S. Department of Agriculture, 2013. Crop values 2012 summary. USDA, NASS, Feb 15, 2013, pp. 48-48.

United States Department of Agriculture, 2013. Crop Values 2012 Summary. USDA, NASS, Feb 15, 2013, pp. 48-48.

USDA, 1995. United States Standards for Grades of Onions (Other Than Bermuda-Granex-Grano and Creole Type). U.S. Department of Agriculture.

USDA, 2013. Crop Values 2012 Summary. National Agricultural Statistics Service of United States Department of Agriculture

Van Dyck, T., Verboven, P., Herremans, E., Defraeye, T., Van Campenhout, L., Wevers, M., Claes, J., Nicolaï, B., 2014. Characterisation of structural patterns in bread as evaluated by X-ray computer tomography. Journal of Food Engineering 123, 67-77.

van Staveren, H.J., Moes, C.J., van Marie, J., Prahl, S.a., van Gemert, M.J., 1991. Light scattering in Intralipid-10% in the wavelength range of 400-1100 nm. Applied optics 30, 4507–4514.

Veraverbeke, E.A., Verboven, P., Lammertyn, J., Cronje, P., De Baerdemaeker, J., Nicolaï, B.M., 2006. Thermographic surface quality evaluation of apple. Journal of Food Engineering 77, 162-168.

Wang, H., Li, C., Wang, M., 2013. Quantitative determination of onion internal quality using reflectance, interactance, and transmittance modes of hyperspectral imaging. Transactions of the ASABE 56, 1623-1635.

Wang, J., Nakano, K., Ohashi, S., Kubota, Y., Takizawa, K., Sasaki, Y., 2011. Detection of external insect infestations in jujube fruit using hyperspectral reflectance imaging. Biosystems Engineering 108, 345-351.

Wang, L., Jacques, S.L., Zheng, L., 1995. MCML--Monte Carlo modeling of light transport in multi-layered tissues. Computer methods and programs in biomedicine 47, 131-146.

Wang, L.V., Wu, H.-I., 2007. Biomedical optics: principles and imaging. Wiley-Interscience, Hoboken, New Jersey.

Wang, Q., Zhang, Q., 2013. Three-dimensional reconstruction of a dormant tree using RGB-D cameras, 2013 Annual International Meeting of the American Society of Agricultural and Biological Engineers, Kansas City, Missouri.

Wang, W., Li, C., Tollner, E.W., Gitaitis, R.D., Rains, G.C., 2012a. Shortwave infrared hyperspectral imaging for detecting sour skin (Burkholderia cepacia)-infected onions. Journal of Food Engineering 109, 38-48.

Wang, W., Li, C., Tollner, E.W., Rains, G.C., 2012b. Development of software for spectral imaging data acquisition using LabVIEW. Computers and Electronics in Agriculture 84, 68-75.

Wang, W., Li, C., Tollner, E.W., Rains, G.C., Gitaitis, R.D., 2012c. A liquid crystal tunable filter based shortwave infrared spectral imaging system: Calibration and characterization. Computers and Electronics in Agriculture 80, 135-144.

Wang, W., Li, C., Tollner, E.W., Rains, G.C., Gitaitis, R.D., 2012d. A liquid crystal tunable filter based shortwave Infrared spectral imaging system: Design and integration. Computers and Electronics in Agriculture 80, 126-134.

Wang, W., Paliwal, J., 2007. Near-infrared spectroscopy and imaging in food quality and safety. Sensing and Instrumentation for Food Quality and Safety 1, 193-207.

Williams, P., Norris, K., 2001. Near-infrared technology in the agricultural and food industries, 2nd ed. AACC Press, St. Paul, MN, USA.

Wu, D., Sun, D.-W., 2013. Advanced applications of hyperspectral imaging technology for food quality and safety analysis and assessment: A review — Part II: Applications. Innovative Food Science & Emerging Technologies 19, 15-28.

Yang, C.-C., Kim, M.S., Kang, S., Cho, B.-K., Chao, K., Lefcourt, A.M., Chan, D.E., 2012. Red to far-red multispectral fluorescence image fusion for detection of fecal contamination on apples. Journal of Food Engineering 108, 312-319.

Yang, C.C., Chao, K.L., Chen, Y.R., 2005. Development of multispectral image processing algorithms for identification of wholesome, septicemic, and inflammatory process chickens. Journal of Food Engineering 69, 225-234.

Zude, M., 2008. Optical monitoring of fresh and processed agricultural crops. Taylor & Francis, Boca Raton, FL, USA.